University of Valladolid

FACULTY OF SCIENCE

Bachelor in Mathematics

Face modelling and recognition

Student: Alejandro Barrio Mateos

Mentors: Francisco Javier Finat Codes
Eduardo Cuesta Montero

Date: 13 December 2023

Face modelling and recognition

Alejandro Barrio Mateos

Contents

List of Figures

To Javier for all the colacaos I owe you,
and because without your guidance this work would not have been possible;
my grandfather Abelardo,
for having been my sidekick for 22 wonderful years;
to my parents, José Antonio and Ascensión,
because everything I am today is thanks to you;
and to all my friends,
for being there whenever I need you.

Abstract

Face modelling and recognition is currently a booming area due to the multitude of applications that its use has for different modelling tools and software applications; from facial recognition for restricted access to work areas, finding and stopping criminals, gesture language for human-machine interaction; to other more playful purposes such as the use of filters in social networks or simulation and animation in multimedia content industries.

This project aims to understand the geometric and topological features related to the shape and deformations of the face inherent to the gestures of the human face using concepts of Differential Geometry and Curvature Flows. The simplest approach is to consider the human face as a piecewise smooth (PS) surface and segment it into regions according to the different curvatures of each region, dividing the face into elliptical, parabolic and hyperbolic regions for the underlying topological model of the 2-dimensional disc. This is crucial for understanding and reconstructing the different gestures a person can perform, which can be emulated computationally by using elastic models on which to propagate deformations.

Apart from this approach based on theoretical models (*top-down*), these tasks are most commonly carried out through strategies based on data collection for further processing. This strategy (*bottom-up*) allows theoretical models to be reconstructed from data. The automation uses techniques based on Machine Learning of the shape and its dynamics. This work also presents the methods for data capture and face recognition, exemplifying their use thanks to the implementation of the eigenfaces method.

Key words: Human face, PS-surfaces, curvatures, fundamental forms, curvature flows, Wilmore energy, SVD, PCA, LDA, eigenfaces.

Chapter 1

Introduction

The human face is a changing surface with a certain complexity. The characterisation of the geometry and its topological deformations for gestures is of great interest for the multimedia content industry (simulation and animation) or for non-verbal communication linked to gestures (human-robot interaction in Artificial Intelligence). Both aspects have been developed since the 1960s. From a geometrical point of view, the human face is a piecewise smooth surface that is characterised at each point by the total and mean curvatures. The evaluation of this data is carried out from an estimation of the tangential and normal data at each point. Differential Geometry of Curves and Surfaces provides the initial framework for relating intrinsic and extrinsic aspects.

Facial gestures are modelled as deformations of the original geometry with topological and kinematic aspects. The topological aspects are initially modelled in terms of a disc on which a differentiable structure is superimposed. Differential Shape Geometry uses results from Differential Geometry of Surfaces. The unified treatment with functional aspects motivates the development of an approach based on Banach spaces.

The deformations associated with gestures are described either continuously (using fields acting on functions) or discretely (associated with sparse configurations of "meaningful facts" such as isolated points and control segments). If we omit the most expressive elements (eyes and mouth), the face is topologically equivalent to a disk $\mathbb{D}^2$. The incorporation of these elements results in an underlying topological model given by a surface with three holes, which is topologically equivalent to the connected sum of three tori. The relative location of the control points provides the initial support for a triangular mesh that reconverts to quadrangular as a piecewise linear approximation to the local parameterisations of surfaces typical in Local Differential Geometry. The deformations are initially controlled in terms of energy functionals linked to the mean and total curvatures.

In this paper we focus especially on modelling problems, including the differential and statistical approaches, most frequently used to deal with face feature recognition and its evolution in spatio-temporal gestures. The two most commonly used strategies are labelled as: **top-down** (based on the use of theoretical models built from Differential Geometry and Algebraic Topology) and **bottom-up** (based on image data or scans providing point clouds to be clustered). Thus, Algebraic Topology provides the link between the ideal "soft" approach and the discrete (point cloud) approach using intermediate piecewise linear structures for clustering.

1.1 Structure of the memory

The work is divided into chapters. The first of these (which is in fact Chapter 2 of the report, since the first is the initial introductory chapter) is the one on **Differential Geometry of Surfaces**, where the basic mathematical foundations for modelling the face are presented, giving its general definition for varieties of any dimension, specifying a posteriori its specification in the case of surfaces. This is because a model based on appearances is adopted, considering the human face as a piecewise smooth surface, omitting the restrictions to which it would be subjected by the bony and muscular structures underlying it.

Just like any other surface, the human face can be decomposed into regions with total curvature of constant sign (positive or negative) separated by parabolic curves (eyebrows, corners of the lips, for example), which delimit elliptical regions from hyperbolic ones. In this chapter 3, entitled **Curvature maps**, the concepts and statements that allow this decomposition of the face to be given are introduced, seeing that from this it is possible both to characterise and reconstruct the face.

The use of models based on Differential Geometry of Surfaces and the characterisation of surfaces in terms of mean and total curvatures suggest the development of models based on Curvature Flows. This approach allows the Differential Geometry of the human face to be made compatible with the propagation processes associated with gesture generation. A simplified version based on the detection and subsequent coupling between different components of the face is used in this report. The components are characterised geometrically in terms of regions over which the sign of the total curvature is constant.

To perform the decomposition of the face into such regions (a process labelled "segmentation"), we assume that the control points are displaced according to elastic patterns along small pieces of integral curves that deform the mesh associated with the face surface. The extension associated with the propagation of the elastic impulses at each control point gives rise to overlaps and generation of conflict regions (points and curves) which are described as singularities of the Gaussian application which, to each point $p \in M$, associates its tangent space T_pM. This approach is the one adopted in Chapters 4 and 5.

The first of these, **Evolution of surfaces under curvature flows**, is based on the paper of the same name by Mumford et al. [31], where both the concept of Curvature Flows and their effect on the simplest singularities that can occur for applications between surfaces are presented, giving a practical example on the human face.

On the other hand, the Chapter called **Variational Approach** aims to give an alternative version of such modelling in terms of "characterisation of the sphericity" of the components that make up the face. In particular, it is the ideal starting point for the representation of gestures as it is done in animation, through Computational Geometry techniques for the analysis of surface variation. Alternatively, other flows from which geometric information can be extracted are also briefly presented.

Finally, Chapter 6 introduces the previously mentioned *Bottom-up strategies*. The main methods for data capture and face recognition are presented, giving as an example the functioning of the eigenfaces strategy, which has been implemented in Python through a Jupyter notebook (see Annex A.1).

To conclude, the final conclusions of the work are presented, as well as various challenges and alternative approaches that could not be developed in depth in the report due to the limitations of the length of the Final Degree Project.

Chapter 2

Differential Geometry of Surfaces

A search on the Internet for any model of a human face yields results analogous to the adjacent figure[1]: a surface with the most significant curvature changes in the area of the eyes, nose and mouth.

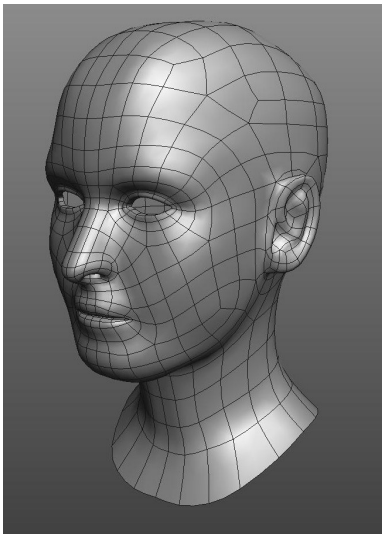

When we look closely at the static model, we see that it is a connected surface with no holes -unlike the real human face-, as this makes it easier to model. The holes in the nose, for example, are just concavities that simulate holes. Thanks to this simplification, we can make an effective representation from curves and surfaces, adapting the topological model of the 2-dimensional disc $mathbbD^2$.

However, in order to carry out the modelling in more detail, it is necessary to introduce basic notions that allow such a description to be given in the simplest possible terms compatible with the curved character of the support. Therefore, throughout this section we review classical results from Differential Geometry of Surfaces, from which a representation can be given based on real data collected from experimental data.

2.1 Basic notions

A human face is a surface contained in a cuboidal region of Cartesian space bounded by width, height and depth. Therefore, we will work in $\mathbb{R}^3$. To facilitate modelling, it is necessary to extend the initial framework of smooth surfaces to the PS (Piecewise Smooth) framework, or PL (Piecewise Linear) as an approximation to the PS framework.

[1]Imagen extraída de https://free3d.com/3d-model/head-basemesh-1383.html

The intuitive notion of smooth m-dimensional manifold M comes from the gluing of pieces called "charts" (U, φ), which are locally locally equivalent via local diffeomorphisms[2] to the Cartesian space $\mathbb{R}^m$. This construction allows to extend the Differential and Integral Calculus to the case of manifolds using the compatibility conditions on intersections of open ones, $U_i \cap U_j$, and the partitions of unity for the Integral Calculus. This description is adapted to PS-deformable models for the human face. The evaluation and control of deformations requires some kind of metric affecting the functions and control elements. For this purpose, we introduce the following notions:

Definition 2.1. *A **normed space** is a pair $(E, \|.\|)$ in which E is a vector space, and the map $\|.\| : E \to \mathbb{R}$ a **norm**. In case that its associated metric $d(e_1, e_2) = \|e_1 - e_2\|$ is complete, the pair defined above is called a **Banach space**.*

Definition 2.2. *Let X be a topological space. A C^k-**chart** on X is a pair (U, φ) where U is an open subset of X and φ is a homeomorphism of $U \subseteq X$ on an open subset of a Banach space. A C^k-**atlas** of X is a family of charts $\mathcal{A} = \{(U_i, \varphi_i)\}_{i \in I}$ such that:*

1. *$X = \cup_{i \in I} U_i$*
2. *Any two charts of $\mathcal{A}$ are compatible in the sense that the overlapping map between two of their members is a C^k-difeomorphism (the **overlapping map** of $(U_i, \varphi_i), (U_j, \varphi_j) \in \mathcal{A}$, with $U_i \cap U_j \neq \emptyset$, is $\varphi_{ji} = \varphi_j \circ \varphi_i^{-1}|_{\varphi_i(U_i \cap U_j)}$; being $\varphi_i(U_i \cap U_j)$ open and φ_{ji} a C^k-difeomorphism).*

Definition 2.3.

- *Two C^k-charts $\mathcal{A}_1$ y $\mathcal{A}_2$ are called C^k-**equivalent** if $\mathcal{A}_1 \cup \mathcal{A}_2$ is also a C^k-atlas (compatibility with the topologies underlying each atlas).*
- *An equivalence class of C^k-atlas in X is known as a C^k-**differentiable**, $\mathcal{D}$-structure for $k = \infty$.*
- *The union of C^k-atlas $\mathcal{A}_\mathcal{D} = \cup\{\mathcal{A} | \mathcal{A} \in \mathcal{D}\}$ is the **maximal atlas** of $\mathcal{D}$ and $(U, \varphi) \in \mathcal{A}_\mathcal{D}$ is a **local admissible chart**.*
- *If $\mathcal{A}$ is a C^k-atlas in S, the union of all atlases equivalent to $\mathcal{A}$ is the C^k-**structure**, **differentiable** in the case $k = \infty$, generated by $\mathcal{A}$.*
- *A **differentiable manifold** M is a pair $(X, \mathcal{D})$ in which X is a paracompact topological space[3] and $\mathcal{D}$ a C^k-differentiable structure over X.*

[2] A **diffeomorphism** is a differentiable homeomorphism (bijective and bicontinuous map) with differentiable inverse.

[3] A **paracompact** topological space is one in which every open covering admits a locally finite open refinement.

For the local study of manifolds, it is convenient to consider functions $f : M \to N$ between manifolds defined locally in U, V neighborhoods of $p \in M$ and $f(p) \in N$. Two such maps are equivalent in $p \in M$ if they coincide in the neighborhood $W = U \cap V$ of p. Thus, within the set of differentiable maps

$$\{f \mid f : U \to N, \text{for a neighborhood } U \text{ of } p \in M\},$$

we have the equivalence relation:

$$f \sim g \Leftrightarrow \exists W \text{neighborhood of } p \text{ such that } f|_W = g|_W$$

Definition 2.4. *An equivalence class of such a relation is called the* ***germ*** *of a map $M \to N$ around p. It is denoted from its representative $\bar{f}$; $\bar{f} : (M, p) \to N$ or $\bar{f} : (M, p) \to (N, q)$ if $\bar{f}(p) = q$. A germ of function is a differentiable germ $(M, p) \to \mathbb{R}$. The set of all function germs around $p \in M$ is denoted $\mathcal{O}_{M.p}$.*

2.2 Tangent bundle

To describe the surface S of a human face, we must characterise its geometric properties in terms of the geometry of curves and surfaces in a three-dimensional space. Facial gestures are modelled in terms of maps $f : S_1 \to S_2$ between surfaces. To do this, we must adapt the notions of differential calculus on curves and surfaces. This includes the study of tangent vectors to curves located on a surface, where such a vector has an intuitive correspondence to the idea of a "velocity vector".

Definition 2.5. *Let M be a manifold and consider $p \in M$. A* ***curve*** *on M is a map $c : I \to M$ of class C^1 of an interval $I \subset S \subset \mathbb{R}$ on M, such that $0 \in I$ and $c(0) = p$. Given two curves c_1 and c_2 in p, as well as (U, φ) an admissible chart where $p \in U$, we say that c_1 and c_2 are* ***tangent*** *in p with respect to φ if $(\varphi \circ c_1)'(0) = (\varphi \circ c_2)'(0)$.*

Two curves are tangent in (U, φ) if they have the same tangent vectors in that chart. This notion is **independent of the chosen chart** by virtue of the following result:

Proposition 2.1. *Let c_1 and c_2 be two curves in $p \in M$ and (U_1, φ_1), (U_2, φ_2) admissible charts. Then, c_1 and c_2 are tangent in p with respect to φ_1 if and only if they are tangent in p with respect to φ_2.*

Proof. If necessary, we take restrictions to assume $U_1 = U_2$. By virtue of the composite map theorem,

$$(\varphi_2 \circ c_1)'(0) = (\varphi_2 \circ c_2)'(0) \Leftrightarrow ((\varphi_2 \circ \varphi_1) \circ (\varphi_1 \circ c_1))'(0) = ((\varphi_2 \circ \varphi_1) \circ (\varphi_1 \circ c_2))'(0),$$

which is equivalent to $(\varphi_1 \circ c_1)'(0) = (\varphi_1 \circ c_2)'(0)$ □

As a consequence, it follows that the tangency at $p \in M$ is an equivalence relation between the curves at p. An equivalence class of these curves can be represented as $[c]_p$, where c is the representative of such a class.

Definition 2.6. *For a manifold M and considering $p \in M$, the **tangent space** to M in p is the set of equivalence classes of tangent curves in p:*

$$T_pM = \{[c]_p \mid c \text{ is a tangent curve at } p\}.$$

*For a subset $A \subset M$, $TM|_A = \sqcup_{p\in A} T_pM$. We call the **tangent bundle** of the manifold M to the 4-tuple (TM, π, M, F) where TM is the total space, $\pi : TM \to M$ is the natural projection on the base space M and $F = \mathbb{R}^m$ the generic fiber. The map $\pi_M : TM \to M$ defined as $\pi_M([c]_p) = p$ is the **projection of the total space** of M.*

It is also verified that there exists a covering $\mathcal{U} = (U_i)_{i\in I}$ by open U_i of M such that the local trivialisation $\pi^{-1}(U_i) \simeq_{C^infty} U_i \times \mathbb{R}^m$ (local equivalence between manifolds) is restricted to a (non-canonical) isomorphism of the fibre $T_pM := \pi^{-1}(p) \simeq_{\mathbb{R}} \{p\} \times \mathbb{R}^m$, with the generic fiber as vector spaces.

Given a C^1-map between manifolds, the tangent map is defined using the above notion:

Definition 2.7. *Let $f : M \to N$ be an map of class C^1. We define the **tangent** of f as $Tf : TM \to TN$, where $Tf([c]_p) = [f \circ c]_{f(p)}$.*

For the local study of manifolds, apart from this geometric definition (1), it will be convenient to consider the notion of tangent space in the algebraic (2) or analytic (3) framework. In both cases we must resort to the concept of germ of C^k-function presented previously. The aim of the different approaches to the problem is to model the first-order behaviour of C^k-functions on the manifold for $k = \infty$ (differentiable case), $k = \omega$ (analytic case) or $k = rational$ (algebraic case). The formalism is similar using the local ring structure for the set of germs of functions and modulus over such a ring for derivatives or differentials. In the smooth or differentiable case one has:

Definition 2.8. *The tangent space T_pM to the differentiable manifold M at point p is the real vector space of the derivatives of $\mathcal{O}_{M.p}$. A **derivation** of $\mathcal{O}_{M.p}$ is a linear map, $X : \mathcal{O}_{M,p}(p) \to \mathbb{R}$, which satisfies the product rule*

$$X(\bar{\phi} \cdot \bar{\varphi}) = X(\bar{\phi}) \cdot \bar{\varphi}(p) + \bar{\phi}(p) \cdot X(\bar{\varphi}).$$

In other words, the algebraic definition (2) introduces the cotangent fiber in terms of linear maps on the tangent space. Formally, it can be described as the space I^1/I^2 of initial forms, where I^i is the ideal whose lowest order term has degree i. In particular, this characterisation identifies the quotient with the space of (differentiable, analytic, algebraic) linear or first order functions. This approach is the most widely used in Algebraic Geometry and Analytic Geometry (AGAG).

From the analytical point of view (3), the derivation D of a function f at a point P only uses the values of the function at that point[4]. Substituting the function by its Taylor development, by virtue of Leibnitz's rule, we have that DQ depends only on its linear part. Therefore, Df depends only on the first order terms of f. As a consequence, once local coordinates have been fixed, the local representation of the tangent space of the map is redescribed in terms of the Jacobian matrix $Df = \frac{partial f_i}{partial x_i}$.

Definition 2.9. *A **tangent vector** on $p \in M$ is a correspondence that to each germ of a chart $\bar{h} : (M, p) \to (\mathbb{R}^n, 0)$ around p associates a vector $v \in \mathbb{R}^n$ with contact order ≥ 2 on $p \in M$. Thus, to the germ $v\bar{g} \circ \bar{h}$ corresponds to the vector $Dg_o \circ v$; g being a change of charts and Dg_0 the Jacobian matrix at the origin. If we denote as K_p the set of the germs of charts $\bar{h} : (M, p) \to (\mathbb{R}^n, 0)$ and $\mathcal{G}$ the set of invertible germs, the **tangent space** T_pM is equal to the set of maps $v : K_p \to \mathbb{R}$ such that $v(\bar{g} \circ \bar{h}) = Dg_0 \circ v(\bar{h})$, for all $\bar{g} \in \mathcal{G}$.*

Having presented the three definitions, we will give a brief demonstration of the equivalence between them. A more detailed demonstration can be found in [14]. Complementarily, in [30] it is shown that the preceding notions are equivalent to each other; for more details, see [51].

Proposition 2.2. *The three definitions of tangent space - geometric (1), algebraic (2) and analytic (3) - seen above are equivalent to each other.*

Proof.

(1) $\Rightarrow$ (3) Let γ be a curve in M such that $\gamma(0) = p$. Then, $D(f) = (f \circ \gamma)'(0)$ is a derivative point in p which depends only on the equivalence class of γ in T_pM.

(3) $\Rightarrow$ (1) Let f be a differentiable function with Taylor development centred at the point p given as $\sum_{i=1,...,n} c_i x^i$. Then, for any derivative at p, we obtain that $Df = c_1 Dx_1 + ... + c_n Dx_n$ thanks to Leibnitz's rule. Thus, D corresponds to the tangent vector $(Dx_1, ..., Dx_n)$.

(3) $\Rightarrow$ (2) Let D be the derivative at a point p. By Leibnitz's rule, replacing the function by its Taylor development, we see that $f \in I^1/I^2$. Therefore D is a linear map on $(I^1/I^2)^*$ (the dual of the cotangent space, the tangent space itself).

(2) $\Rightarrow$ (3) Let $l \in (I^1/I^2)^*$. It suffices to define the derivative at a point as $Df = l(f - f(p) + I^2)$. □

If we dispense with the musculoskeletal structure of the skull, a more easily visualised characterisation of a simplified topological model (without holes) of the human face in terms of visual appearances is as follows:

[4]See e.g. [10]. The map presented in Definition 2.8 is a linear map on the local ring of regular functions which verifies the Leibnitz rule.

The surface $S \subset \mathbb{R}^3$ of the human face is obtained by gluing local charts (U, φ) for S. The tangent plane at each point $p = varphi(u, v) \in S$ provides a first-order approximation. It is described in terms of the subspace generated by the partial derivatives of the coordinate curves, $\varphi_u(u, v)$ and $\varphi_v(u, v)$, at each point. The tangent bundle is the disjoint union of the tangent spaces at each point on the surface.

2.3 Vector bundle

In addition to the tangent space T_pM, the other key element to consider for the local modelling of the surface is given by the normal vector at each point[5]. The use of normal vectors to model the changing geometry of complex objects is a technique frequently used in Computer Graphics; in particular, it allows the radiometric information (e.g. colour and illumination) contained in 3D space to be reprojected. This method, which is based on the manipulation of normal vectors to achieve this effect, is known as **bump mapping**.

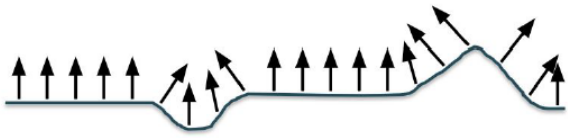

Figure 2.1: Normal vectors of a surface with irregularities. **Source:** [22]

Figure 2.2: Emulation of irregularities by use of bump mapping. **Source:** [22]

In more formal terms, the manipulation of the normal vectors modifies the vector bundle of the surface by deformations and, consequently, the type of immersion in $\mathbb{R}^3$. The mathematical idea behind bump mapping is to introduce and superimpose radiometric distributions (greyscale intensity, colour, textures, radiance...) on the surface S and control their variation in terms of the vector bundle. One advantage is the lower computational cost of the tangential representation. This idea is clearly seen thanks to Figures 2.1 and 2.2.

Definition 2.10. *Given an immersion $f : S \to \mathbb{R}^3$ of a surface S, the **normal space** at each point is the quotient $T_p\mathbb{R}^3 \mid_S$ times the subspace T_pS. The gluing of all of them gives the normal space to the manifold, known as **vector bundle**; $\mathcal{N}_f$.*

These quotients are pasted into the vector bundle using the local S-charts as a submanifold of $\mathbb{R}^3$, yielding the aforementioned $\mathcal{N}_f$ bundle at the f-immersion, which is also denoted as $\mathcal{N}_{S/\mathbb{R}^3}$. The joint handling of tangent and normal information is carried out in terms of sections characterised as follows.

[5]If the surface is immersed in spaces of dimension greater than three, the **normal subspace** is considered instead of simply the normal vector.

Definition 2.11. *Let $U \subset M$ be an open of M and F be an f-dimensional vector space.*

- *The cartesian product $U \times E$ is the **total space** of a **trivial bundle** with **base space** U and **projection map** $U \times F \to U$. This bundle has f linearly independent sections, corresponding to the elements of a basis of the fibre F.*
- *A **local section** $s : U \to \pi^{-1}(U)$ is a C^k-map such that $\pi \circ s = 1_U$ (map identity). In particular, the map $U \to U \times \{0\}$ is the **null section**.*
- *For each base point $u \in U$, $\pi^{-1}(u) \simeq \{u\} \times E$ (non-canonical isomorphism, since they depend on the base point) is the **fibre** of u.*

Observation. *The vector bundle to the surface representing the human face has rank 1 (being the quotient space $S/\mathbb{R}^3$), which facilitates the description of propagation models.*

The comparison between faces or the tracking of facial expressions is done using overlapping structures, given by maps between bundles. Therefore, it is necessary that we develop such terminology. A **morphism between fibres** $\xi_1 = (E_1, \pi_1, B_1, F_1)$ and $\xi_2 = (E_2, \pi_2, B_2, F_2)$ is essentially an map that carries fibres of ξ_1 into fibres of ξ_2 ; more formally, a pair of maps $F : E_1 \to E_2$ and $f : B_1 \to B_2$ such that $f\pi_2 \circ F = f \circ \pi_1$. Using local trivialisations, this is described in terms of the homomorphisms that apply one fibre to another, the set of these being designated $L(F, F')$. We start with the simplest case corresponding to trivial bundles.

Definition 2.12. *Let $U_1 \times F_1$ and $U_2 \times F_2$ be vector bundles and $f : U_1 \to U_2$ be a C^k-map. Any linear map between fibres gives rise to a C^r-**map between bundles**. varphi : $U_1 \times F_1 \to U_2 \times F_2$. This local description is extended to the global case using charts and the vector space $L(F_1, F_2)$ of linear maps between fibres, giving rise to the notion of **homomorphism between vector bundles** (F, f).*

- *If the fibration is injective (resp. surjective) for any $b_1 \in B_1$, one has a **monomorphism** (resp. **epimorphism**) of vector bundles.*
- *If it is an isomorphism at a point we obtain a **local isomorphism between bundles**, being **global** in case it occurs for any base point $b_1 \in B_1$.*

The isomorphism module classification provides the basic types of bundles on a manifold M.

Isomorphisms provide a theoretical criterion for the recognition of the human face in terms of multiple data represented by vectors and parameters (associated with radiometric conditions, e.g.). The simplest models for deformations (related to gesture generation) use regular maps (monomorphisms vs epimorphisms) between bundles.

The computational management is carried out using eigenvalue techniques associated with the basic structures of tangential or normal type. The structural model for the latter is described using the Gauss map on the surface, which gives the normal vector to the surface at each point. A more detailed analysis is presented in Section 2.8.

2.4 The face as a union of submanifolds

The human face does not have a simple structure as a differentiable surface. A typical example of a manifold with different behaviours for the total curvature is the $\mathbb{T}^2$ torus, in which two circumferences (parabolic curves) separate elliptic and hyperbolic components. In the case of the human face, the presence of parabolic curves (in the eyebrows, e.g.) or receding edges (at the ends of the corners of the lips, e.g.) motivate a "segmentation" as a disjoint union of components with total curvature of constant sign. In this way, the face is composed of smaller manifolds that we join into a larger one. The decomposition of the face into components is formalised in terms of the notion of submanifold.

Definition 2.13. *A **submanifold** of a manifold M is a subset $B \subset M$, with manifold structure compatible with the differentiable structure of M; that is, for every $b \in B$, there exists an admissible local chart (U, φ) in M with $b \in U$ such that $\varphi : U \to E \times F$ y $\varphi(U \cap B) = \varphi(U) \cap (E \times \{0\})$.*

To facilitate comparison between manifolds and manifolds, it is necessary to have characterization criteria that minimize the use of charts. Submersions and immersions provide characterization criteria for manifolds. The **Implicit Function Theorem** is the key to the local forms of a submersion and immersion as regular maps; that is, whose differential has maximum rank. This Theorem allows us to give a local expression of the regularity in terms of linear projections or linear subspaces. Detailed demonstrations of these characterizations can be found in [1].

Definition 2.14. *Let M, N be manifolds and $f : M \to N$ of class C^k, with $k \geq 1$. The map f is **regular** on $p \in M$ if its dfierential has maximum rank equal to the minimum of $m = dim(M)$ and $n = dim(N)$. The simplest case corresponds to functions $N = \mathbb{R}$.*

- *A point $q\mathbb{R}$ is a **regular value** of f if, for each $p \in f^{-1}(\{q\})$, the differential $d_p f$ is surjective. We denote by $\mathcal{R}_f$ the set of regular values of f. Note that $(N \backslash f(M)) \subset \mathcal{R}_f \subset N$-.*
- *If, for every $p \in S$, $T_f M$ is surjective, f is said to be a **submersion** in S. Therefore, $q \in \mathcal{R}_f$ iff f is a submersion in $f^{-1}(\{q\})$. In the case where $T_p f$ is not surjective, $p \in M$ is a **critical point** and $q = f(p) \in N$ a **critical value** of f.*

As an example, the map of the height of the sphere on the straight line has two critical points which are called North and South pole, respectively.

Theorem 2.1 (Submersion Theorem)**.** *Let $f : M \to N$ be of class C^∞ and $q \in \mathcal{R}_f$. Then, the level set $f^{-1}(q) = \{p \in M \mid f(p) = q\}$ is a closed submanifold of M with tangent space $T_p f^{-1}(q) = \ker T_p f$.*

Proof.

If $f^{-1}(q) = f^{-1}(q) = \emptyset$, the theorem holds.

Otherwise, for $p \in f^{-1}(q)$ we can find charts (U, φ) and (V, ψ) such that $p \in U$, $f(U) \subset V$, $\varphi : U \to U' \times V'$, $\varphi(p) = (0, 0)$, $\psi : V \to V'$ and $f_{\varphi\psi} : U' \times V \to V'$ is the projection onto the second component; by virtue of the Implicit Function Theorem. Since $\varphi(U \cap f^{-1}(q)) = f^{-1}_{varphi\psi}(0) = U' \times \{0\}$, we obtain that $f^{-1}(q)$ is submanifold.

Finally, since $f_{\varphi\psi}$ is the projection onto the second component, where $U' \subset E$ and $V' \subset F$, we have that $T_u(f^{-1}_{\varphi\psi}(0)) = T_u U' = E = \ker(T_u f_{\varphi\psi})$ for $u \in U'$, which is the local version of the final part of the statement. □

Recall that a linear map $f : V \to W$ between vector spaces is **suryective** (resp. **injective**) if $\ker(f) = 0$ (resp. $\operatorname{coker}(f) = W/f(V) = 0$). The conditions of being injective or surinjective are dual to each other. Consequently, the local conditions of immersion and submersion for manifolds (or of monomorphism and epimorphism between bundles) are also dual to each other. However, the global characterization of an immersion (locally dual of submersion) is not as straightforward.

Definition 2.15. *A map $f : M \to N$ of class C^k, $k \geq 1$ is an **immersion** in p if the differential $d_p T f$ is injective. It is a global immersion if it is a local immersion for any $p \in M$.*

Theorem 2.2 (Immersion Theorem)**.**

For a map $f : M \to N$ of class C^r, $r \geq 1$, are equivalent:

1. *f is an immersion in p;*
2. *There are charts (U, φ) and (V, ψ) with $p \in U$, $f(U) \subset V$, $\varphi : U \to U'$, $\psi : V \to U' \times V'$ and $\varphi(p) = 0$ such that $f_{\varphi\psi} : U' \to U' \times V'$ is the inclusion $u \to (u, 0)$;*
3. *There is a neighborhood U of m such that $f(U)$ is a submanifold of N and $f|_U$ a diffeomorphism of U onto $f(U)$.*

Proof.

(1) $\Leftrightarrow$ (2) is given by the local immersion theorem.

(2) $\Rightarrow$ (3) Again, thanks to the local submersion theorem, we can choose U and V such that $f(U)$ is a submanifold of V. Moreover, since $V \subset N$ is open, $f(U)$ is a submanifold in N. We obtain the remaining implication thanks to the definition of submanifold. □

Definition 2.16. *If $f : M \to N$ is an injective immersion, $f(M)$ is an **immersed submanifold** of N.*

The next objective is to characterize under what conditions the immersed submanifold is a differentiable manifold. An immersed submanifold can either have normal crossings (normal tangents at a point, as in the case of ordinary nodes, e.g.) or present a "pathological behavior at infinity" (like spirals or smooth fractal models, e.g.). To avoid these problems in the classical geometric framework, the conditions of being injective and proper are added. In the functional framework developed in this paper, a more topological formulation is adopted.

Definition 2.17. *An immersion $f : M \to N$ which is a homeomorphism in $f(M)$ whose topology is the inherited topology of N, is called* ***embedding****.*

Therefore, if $f : M \to N$ is an embedding, $f(M)$ is a manifold of N. In particular, thanks to the following theorem we can guarantee the conditions under which an immersion is an embedding (less restrictive than the fact that the map is proper). The proof of this result consists in applying in a straightforward way the definition of subspace topology (see [1] for more details).

Theorem 2.3. *An injective immersion that is an open or closed map in its image is an embedding.*

Finally, as a counterpart to the concept of tangency already seen above, we will give a first introduction to the idea of **transversality**, which can be considered as the notion "opposite". We say that two manifolds M_1 and M_2 of N are transversal in $p_i n M_1 \cap M_2$ if their tangent spaces, T_pM_1 and T_pM_2, generate the tangent space T_pN of N at p. The manifolds are transverse if this condition is verified for any point $p_i n M_1 \cap M_2$. In particular, two tangent curves in space are not transverse (even if they have linearly independent tangent at each intersection point). The following definition extends this intuitive idea to the relative case:

Definition 2.18. *A map $f : M \to N$ of class C^k, $k \geq 1$, is called* ***transverse*** *to the submanifold P of N (represented as $f \pitchfork P$) if $f^{-1}(P) = \emptyset$; or if the following holds for all $m \in f^{-1}(P)$:*

T1 *$(T_m f)(T_m M) + T_{f(m)}P = T_{f(m)}N$, and*

T2 *The inverse image of $T_{f(m)}P$, $(T_m f)^{-1}(T_{f(m)}P)$, splits into $T_m M$.*

Theorem 2.4 (Transversal Mapping Theorem)**.** *Let $f : M \to N$ be a map of class C^∞ and W be a submanifold of N. If $f \pitchfork W$, then $f^{-1}(W)$ is a of M and $T_p(f^{-1}(W)) = (T_p f)^{-1}(T_{f(p)}W)$ for all $p \in f^{-1}(W)$. If W has finite codimension[6] in N, then $codim(f^{-1}(W)) = codim(W)$.*

This theorem, whose detailed proof can be found in [1], is a global version of the Submersion Theorem already seen, which turns out to be the same for the case where W is a point.

[6] Given a submanifold B of a manifold M, its **codimension** is that of the quotient space with respect to the tangent space of the manifold in which it is immersed; $\mathrm{codim}(B) = \dim(M) - \dim(B)$. This definition is analogous to that used for vector spaces.

2.5 Vector fields

In order to be able to work in a global and simpler way with the vector and tangent bundles, we will resort to the notion of vector fields. These will allow us to study later the deformations of the face for the expression of facial gestures. The support for the propagation processes (for gesture filling or modeling) and the constraints associated with the face structure (local elastic-type models), is given by the curvature maps of the face. Therefore, the characterization of facial gestures is more natural if it is formulated in geometrical terms.

Definition 2.19. *Let M be a manifold. A **vector field** on M is a local section $s : U \to TU = U \times \mathbb{R}^m$ of the tangent bundle $\tau_M = (TM, \pi, M, \mathbb{R}^m)$ of M. The set of all vector fields in M of class C^k is denoted $\mathcal{X}^k(M)$, or $\mathcal{X}^\infty(M)$ in the case C^∞. This set has a $\mathcal{O}_X$-module structure over the ring of C^k-regular functions over X.*

Therefore, a vector field X over a manifold M is a C^k-map

$$X : M \xrightarrow{T} M \quad \text{such that} \quad X(p) \in T_pM, \quad \forall m \in M.$$

In other words, it uniquely maps to each point of M a vector based on that point. In the analytic framework (local convergence for serial developments at each point), we can represent each field as $X = \sum_i x_i \frac{\partial}{\partial x_i}$. Again, let us look at these concepts with a focus on the case at hand.

> Given a surface S, a vector field on it is a map $X : S \to \mathbb{R}^3$ which to each point $p \in S$ maps a vector $X(p) \in \mathbb{R}^3$. The tangent bundle is generated by the tangent vector fields $X(p) \in T_pS$ for $p \in S$. The vector bundle is generated by the fields $X(p)$ such that $langleX(p), v\rangle = 0; \forall v \in T_pS$.

Vector fields in **dynamical systems** provide the simplest examples for describing a time-varying evolution. The **flows** are the "packets" of local solutions associated with the fields. To analyze such evolution, it is necessary to consider the idea of **flow boxes**.

Definition 2.20. *Let M be a manifold and $X \in \mathcal{X}^k(M), k \geq 1$. A **flow box** of X in $p \in M$ is a triple (U_0, a, F) where:*

1. *$U_0 \subset M$ is open, $p \in U_0$ and $a \in \mathbb{R}_+ \cup \{\infty\}$;*
2. *$F : U_0 \times I_a \to M$ is of class C^k, where $I_a = (-a, a)$;*
3. *For each $u \in U_0$, $c_u : I_a \to M$ defined as $c_u(t) = F(u, t)$ is an integral curve of X at point u;*
4. *$F_t : U_0 \to M$ defined as $F_t(u) = F(u, t)$ satisfies that, for $t \in I_a$, $F_t(U_0)$ is open and F_t is a C^k-difeomorphism in its image.*

This can be seen in a simpler way if we consider that the flow is the extension to the case of manifolds of the Ordinary Differential Equations (ODE) with prefixed initial conditions verifying Lipschitz-type constraints, corresponding to the polynomial bound on the variation of the tangent vector at each point.

$$h'(t) = \Delta h(t),$$

$$h(0) = u.$$

Thus, the **linear flow** or **flow box** associated to the vector field X, is the uniparametric family of maps that are solutions of the previously stated problem:

$$\{h_t : U \to U \ \mid \ h_t(u) := e^{tA}u\} \quad \text{where} \quad t \in I \subset \mathbb{R}.$$

The existence and uniqueness theorem of ODEs justifies the introduced notion of local flows over surfaces and its extension to the global case.

2.6 Vector fields as differential operators

In addition to the dynamic approach presented above, we can also study vector fields from an algebraic point of view, which provides a unification with Algebraic and Analytic Geometries, as well as with the functional approach and its applications. Our first objective is the adaptation to (maps between) manifolds in a simple way. One motivation is linked to the classical idea of infinitesimal displacements as deformations of a flow box. To concretise this idea, we will introduce the following concepts:

Definition 2.21.

1. *Let $\varphi : M \to N$ be a map of class C^k between manifolds and $f \in C^k(N, \mathbb{R})$. We define the **inverse image** or **pull-back image** of f by φ as $\varphi^* f = f \circ \varphi \in C^r(M, \mathbb{R})$.*

2. *If f is a C^k-difeomorphism and $X \in \mathcal{X}^k(M)$, the **direct image** or **push-forward** of X by varphi is defined as $\varphi_* X = T\varphi \circ X \circ \varphi^{-1} \in \mathcal{X}^k(N)$.*

Both notions can be easily interchanged, simply by considering the inverse map between manifolds (going from φ to φ^{-1}), i.e., defining $\varphi_* = (\varphi^{-1})^*$; analogous in the remaining case. Therefore, the direct image of a function f over M is $\varphi_* f = f \circ \varphi^{-1}$ and the inverse image of a vector field Y over N is $\varphi^* Y = (T\varphi)^{-1} \circ Y \circ \varphi$.

However, to perform this comparison between manifolds we initially impose that φ is a diffeomorphism (because of the definition of direct image). Later we relate objects present in two different manifolds using more general conditions.

Definition 2.22. *Let $\varphi : M \to N$ be a map of class C^k between manifolds. The vector fields $X \in \mathcal{X}^{k-1}(M)$ and $Y \in \mathcal{X}^{k-1}(N)$ are said to be **φ -related** ($X \sim_\varphi Y$) if $T\varphi \circ X = Y \circ \varphi$.*

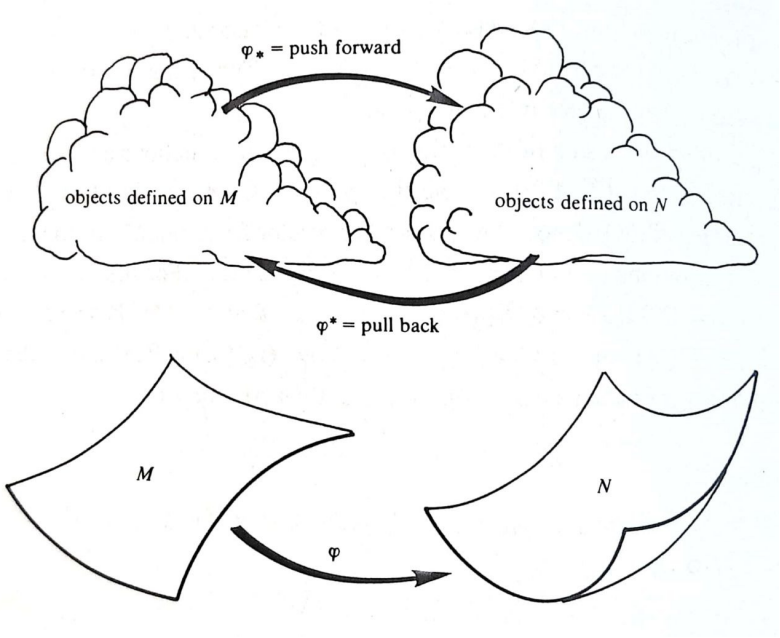

Figure 2.3: *Push-forward* and *pull-back*. **Source:** [1]

Next, we study how vector fields act on functions in terms of the directional derivative. Let $f : M \to \mathbb{R}$, so $Tf : TM \to T\mathbb{R} = \mathbb{R} \times \mathbb{R}$. We know that the tangent vector to $\mathbb{R}$ at $\lambda \in \mathbb{R}$ can be expressed as (λ, μ), so Tf acting on a vector $v \in T_pM$ can be written as:

$$Tf \cdot v = (f(p), df(p) \cdot v).$$

Thus, for every $p \in M$, $df(p) \in T_p^*M$. Therefore, df is a section of the dual T^*M of the tangent bundle which is called a **co-vector field** or a **1-form**.

Definition 2.23. *The 1-form $df : M \to T^*M$ defined in this way is called the **differential** of f.*

To facilitate the understanding of this idea, we adapt it to the case of 2-dimensional manifolds.

Given a surface S and the function $f : S \to \mathbb{R}$, the differential of the latter is extracted from that obtained by the associated differentiable function of $\mathbb{R}^2$ on $\mathbb{R}$. Specifically, given a curve $\alpha : (-epsilon, \epsilon) \to S$ which satisfies $\alpha(0) = p$ and $\alpha'(0) = v$, the differential is computed as

$$df_p(v) = \frac{d}{dt}|_{t=0} f(\alpha(t)).$$

Using the above notions, we introduce the concept of the derivative of a function through a vector field:

Definition 2.24. *Let $f \in C^k(M, \mathbb{R})$ and $X \in \mathcal{X}^{k-1}(M), k \geq 1$. We define the* ***Lie derivative*** *or* ***directional derivative*** *of f along X as*

$$\mathcal{L}_X f \equiv X[f] = df \cdot X = \sum_i \frac{\partial f}{\partial x_i} X_i \in \mathcal{X}^{k-2}(M).$$

Similarly, we can define the same concept applied from one vector field to another, which we formulate in terms of Functional Analysis to facilitate its extension to more general cases.

Definition 2.25. *Let M be a manifold over a Banach space C^infty and $X, Y \in \mathcal{X}(M)$. We define the* ***Lie derivative*** *of Y with respect to X, also called the* ***Lie bracket*** *of X and Y, as:*

$$[X, Y] = XY - YX.$$

The Lie bracket is an antisymmetric inner product on T_pM verifying the Jacobi identity (see below). Thanks to this operation, we can define a structure on the space of vector fields as follows.

Proposition 2.3. *The vector space $\mathcal{X}(M)$ of vector fields over M with the Lie bracket operation $[\ ,\ ]$ on $\mathcal{X}(M)$ has structure of* ***Lie algebra****; that is,*

(i) $[\ ,\ ]$ *is bilinear with respect to $\mathbb{R}$;*

(ii) $[X, X] = 0$ *for all $X \in \mathcal{X}(M)$;*

(iii) ***Jacobi's identity:***

$$[X, [Y, Z]] + [Y, [Z, X]] + [Z, [X, Y]] = 0 \text{ for all } X, Y, Z \in \mathcal{X}(M).$$

Proof. All three properties can be proved directly from the above definition of a Lie bracket. As an example, we will give the proof that Jacobi's identity (iii) is satisfied, for which we only need to develop each term:

$$[X, [Y, Z]] = XYZ - XZY - YZX + ZYX,$$

$$[Y, [Z, X]] = YZX - YXZ - ZXY + XZY,$$

$$[Z, [X, Y]] = ZXY - ZYX - XYZ + YXZ.$$

Adding the above expressions means that the terms cancel each other out. □

2.7 Tensors

A tensor of type (r, s) in Linear Algebra is a combination of products of s vectors and r co-vectors with coefficients belonging to the base field. The algebrization based on vector fields and their duals (differential forms), as well as the local triviality conditions for the tangent and cotangent bundles, allows the tensors to be extended to the geometric framework. Thanks to them, models based on s trajectories, subject to r constraints with varying coefficients, can also be expressed in a natural way. These models are ubiquitous in all areas of scientific and technological knowledge.

Tensor fields are linear combinations of formal products of scalar, vector and co-vector fields. From the global point of view, they correspond to sections of bundles constructed on the smooth basis manifold M or its natural extensions to Banach spaces B (or even to possibly singular manifolds X). This construction is performed locally on each fibre of the tangent bundle and the data is "glued" using "**transition functions**" (lifting to the fibre of the change of chart operations on the basis).

Before giving the definition for manifolds, we will introduce the notion of tensor in vector spaces in order to make the extension to manifolds more comprehensible. For this, we consider $L^k(E_1, ..., E_k; F)$ to designate the vector space of continuous k-multilinear maps of $E_1 \times ... \times E_k$ on F. The special case $E^* \equiv L(E; \mathbb{R})$ is the dual space of E.

Definition 2.26. *Given a vector space E, the elements of*

$$T^r_s(E) = L^{r+s}(E^*, ..., E^*, E, ..., E; \mathbb{R}),$$

*(r copies of E^* and s copies of E) are called **tensors of** E, **contravariants of order** r **and covariants of order** s; or simply of **type** (r, s).*

Definition 2.27. *Given two elements $t_1 \in T^{r_1}_{s_1}(E)$ and $t_2 \in T^{r_2}_{s_2}(E)$, their **tensor product** is $t_1 \times t_2 \in T^{r_1+r_2}_{s_1+s_2}(E)$, which is defined as:*

$$(t_1 \otimes t_2)(\beta^1, ..., \beta^{r_1}, \gamma^1, ..., \gamma^{r_2}, f_1, ..., f_{s_1}, g_1, ..., g_{s_2}) =$$

$$= t_1(\beta^1, ..., \beta^{r_1}, f_1, ..., f_{s_1}) t_2(\gamma^1, ..., \gamma^{r_2}, g_1, ..., g_{s_2}),$$

where $\beta^i, \gamma^j \in E^*$ y $f_k, g_l \in E$.

The preceding description is extended to a vector space over an arbitrary field $\mathbb{F}$ by replacing $\mathbb{R}$ by $\mathbb{F}$, giving rise to the space of $\mathbb{F}$-evaluated tensors of type (r, s); $T^r_s(E; \mathbb{F})$. In this case, the tensor product requires a bilinear form in the evaluation space for its definition. In the case $\mathbb{F} = \mathbb{R}$, the tensor product is associative, bilinear and continuous; but not commutative. By convention, we designate $T^1_1(E) = L(E; E)$ and $T^0_0(E; F) = F$. The local construction is also extended to the algebraic case, replacing the vector spaces over a field by moduli over a base ring.

Having seen these concepts applied to vector spaces, we seek to define them analogously to the case of manifolds using tensor bundles, whose sections are tensors of type (r, s). The local construction is easily extended to the global case by gluing local data via the corresponding transition functions. The naturalness of this construction is associated with the use of direct and inverse images.

Definition 2.28. *Let M be a manifold and $\tau_M : TM \to M$ be its tangent bundle. We denote by $T^r_s(M) = T^r_s(TM)$ the* ***bundle of contravariant tensors of order*** *r* ***and covariants of order*** *s, or simply of* ***type*** *(r, s). We identify $T^1_0(M) = TM$ and the null section of $T^r_s(M)$ as M. $T^0_1(M)$ is the* ***cotangent bundle*** *of M. The* ***k-forms*** *are the sections of the k outer power (vector outer product) $\Lambda^k T^*M$, which is also denoted as Ω^k_M. The direct sum of the exterior powers is denoted as τ^*_M with its structural projection $T^*M \xrightarrow{M}$, or as $\Omega^*_M := \oplus^m_{k=0}\Omega^r_M$.*

Recall that an arbitrary C^k-section s of a bundle maps each basis point $b \in U \subset M$ to a vector $s(b)$ on the bundle above it, where the mapping is of class C^k. For the bundle $T^r_s(M)$, the image for a section is called **tensor**. Given a vector bundle $\pi : E \to B$, the C^infty sections are denoted as $\Gamma^infty(\pi)$ or $\Gamma^infty(\pi)$.

Definition 2.29. *A* ***tensor field of type*** *(r, s) on a smooth manifold M, is a C^infty-section of $T^r_s(M)$. We denote by $\mathcal{T}^r_s(M)$ the set $\Gamma^infty(T^r_s(M))$ together with its (infinite dimensional) real vector space structure. A* ***covector*** *or* ***one-differential form*** *is an element of $\mathcal{X}(M) = \mathcal{T}^0_1(M)$.*

We can also extend the concept of tensor product presented previously to other algebraic structures over arbitrary fields, modules over rings or finite-dimensional algebras. In particular, we denote by $\mathcal{F}(M)$ the set of maps of M in $\mathbb{R}$ of class C^infty (the standard local manifold structure used in $\mathbb{R}$) together with its structure as a module over a regular local ring in the algebraic case, commonly used in Algebraic or Analytic Geometry.

Definition 2.30. *Given $f \in \mathcal{F}(M)$ and $t \in \mathcal{T}^r_s(M)$, let $ft : M \to T^r_s(M)$ be defined as $ft(m) = f(m)t(m)$. If $X_i \in \mathcal{X}^(M)$ $(i = 1, ..., s)$, $\alpha^j \in \mathcal{X}^*(M)$ $(j = 1, ..., r)$, and $t' \in \mathcal{T}^{r'}_{s'}(M)$; we define*

$$t(\alpha^1, ..., \alpha^r, X_1, ..., X_s) : M \to \mathbb{R} \text{ by } t(\alpha^1, ..., X_s)(m) = t(m)(\alpha^1(m), ..., X_s(m)),$$

and

$$t \otimes t' : M \to T^{r+r'}_{s+s'}(M) \text{ by } (t \otimes t') = t(m) \otimes t'(m).$$

2.8 Gauss-Weingarten map

The object of study of this paper is the differential geometry of the human face as a piecewise smooth surface. The **Intrinsic Geometry** of a surface only takes into account the properties associated with the tangent bundle and the corresponding operations (duality, products) introduced in the previous section; while the **Extrinsic Geometry** of a surface also takes into account the properties related to the immersion in the ambient space. Deformations allow to connect both aspects in any dimension.

To fix ideas, and as we have mentioned previously, we will focus on dimension 2 manifolds (**surfaces**) which we will denote as S, with a greater emphasis on the extrinsic aspects of it. In particular, we ignore three-dimensional aspects such as the underlying bone and muscle structure.

If we consider the normal vector N to S, the directional derivative that we have defined in Section 2.6 allows us to study the evolution of this normal vector in the ambient space. The extrinsic analysis of the normal map is the key to properly understand the evolution of the different components that make up the face when it performs gestures.

The most significant elements for the analysis of facial gestures are concentrated around the mouth and eyes. The support for the initial information is the tangent bundle, while its spatio-temporal evolution is analysed in terms of the vector bundle. In particular, given a vector field X (which could represent the constraints of the corners of the lips), $LX \equiv \mathcal{L}_X N$ measures the variation of the tangent plane with respect to the normal vector of the X direction.

Definition 2.31. *The endomorphism on the tangent space $L\colon T_pS \to T_pS$ given above is called the* ***shape operator*** *or the* ***Weingarten map****.*

Proposition 2.4. *The operator L is self-adjoint; that is,*

$$\langle LX, Y\rangle = \langle X, LY\rangle; \forall X, Y \in T_pS.$$

Proof. By the Leibnitz rule, $X\langle N, Y\rangle = \langle \mathcal{L}_X N, Y\rangle + \langle N, L_X Y\rangle$.

Thus,

$$X\langle N, Y\rangle = \langle \mathcal{L}_X N, Y\rangle + \langle N, \mathcal{L}_X Y\rangle \Rightarrow \langle \mathcal{L}_X N, Y\rangle = X\langle N, Y\rangle - \langle N, \mathcal{L}_X Y\rangle = -\langle N, \mathcal{L}_X Y\rangle$$

$$Y\langle X, N\rangle = \langle \mathcal{L}_Y X, N\rangle + \langle X, \mathcal{L}_Y N\rangle \Rightarrow \langle X, \mathcal{L}_Y N\rangle = Y\langle X, N\rangle - \langle \mathcal{L}_Y X, N\rangle = -\langle \mathcal{L}_Y X, N\rangle,$$

where the terms $\langle X, N\rangle$ and $\langle N, Y\rangle$ are null since N is the normal vector and $X, Y \in T_pS$ (their inner product is zero). Thanks to this, it is possible to substitute:

$$\langle LX, Y\rangle - \langle X, LY\rangle = \langle \mathcal{L}_X N, Y\rangle - \langle X, \mathcal{L}_Y N\rangle = -\langle N, \mathcal{L}_X Y\rangle + \langle \mathcal{L}_Y X, N\rangle =$$

$$= -\langle N, \mathcal{L}_X Y\rangle + \langle N, \mathcal{L}_Y X\rangle = \langle N, \mathcal{L}_Y X - \mathcal{L}_X Y\rangle = \langle N, [X, Y]\rangle = 0,$$

the inner product being a symmetric bilinear form and $[X, Y] \in T_pS$. □

2.9 Moving references for a surface

While the shape operator we have defined allows us to study the evolution of the vector normal to the surface, for gesture control greater precision is required to facilitate the location of the most significant elements on the surface of the human face. The moving references associated with the surface coordinate curves are the key to locating and tracking gestures. Except for some very simple cases, there is no "natural" parametrization for a surface. In addition, the integral curves associated with the different propagation processes provide more dynamically appropriate parametrizations. We start by recalling some basic notions.

Definition 2.32. *Given a surface S (locally) in parametric form as*

$$r : \mathbb{R}^2 \to \mathbb{R}^3 \ / \ r(u,v) = (r_1(u,v), r_2(u,v), r_3(u,v)) \ , \ r \in C^\infty,$$

which is the generalisation of Monge's approach based on the projection onto the coordinate planes, its ***linearisation*** *is $d_p r : T_p\mathbb{R}^2 \to T_p\mathbb{R}^3$ and is given from the Jacobian $Jr = \frac{\partial(r_1,r_2,r_3)}{\partial(u,v)}$. The* ***coordinate curves*** *on S are $r(u_0, v)$ y $r(u, v_0)$.*

Although these concepts are analogous to those already seen in Section 2.2, their application to dimension 2 manifolds allows us to locate ourselves within a surface. In particular, the coordinates of the 'salient features' or most significant facts for facial gestures are represented in terms of intersections of parametric curves.

The moving references in the case of curves in space or twisted curves are described in terms of the **Frénet-Serret intrinsic frame**. Although this description is given in terms of the arc length (intrinsic parameter), it does not depend on the chosen coordinate system. This facilitates localisation at any point on the curve. In the case of surfaces, the moving reference is given by the **tangent plane** T_pS and the **normal vector** N.

This new reference makes localisation easier, as it only uses the orthonormal basis of the tangent plane and the normal vector to indicate any point on the surface in terms of location and orientation. Recall that the orientation of a surface at a point is determined by the normal vector at that point.

Definition 2.33. *The* ***Gauss map*** *of a chart is defined by taking the unit normal vector at each point, resulting in*

$$N : U \to \mathbb{S}^2 \ / \ N(p) = \frac{r_u \times r_v}{||r_u \times r_v||}.$$

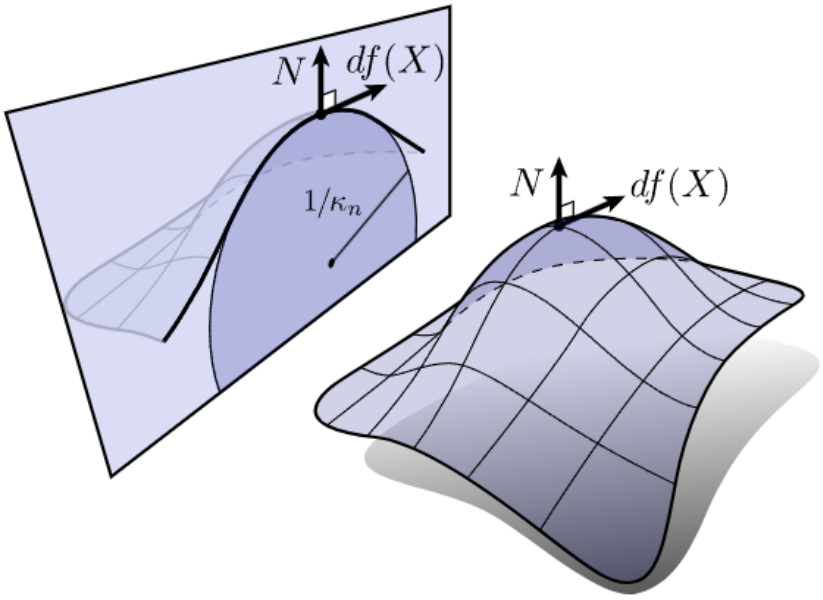

Figure 2.4: Moving reference on a surface. **Source:** [18]

The Gauss map can always be defined locally and assigns to each point on the surface a point on the sphere, which allows the corresponding element of the normal bundle to be obtained. Orientable surfaces have two possible Gauss maps, corresponding to the two possible choices for the direction of the normal vectors. However, non-orientable surfaces (such as the Möbius strip or the Klein bottle) do not have a consistent way of choosing a direction for the normal vectors that is globally compatible (all the changes of chart with positive determinant for the Jacobian matrix). Therefore, non-orientable surfaces do not have a Gaussian map.

Definition 2.34. *A surface S is **orientable** if there exists a differentiable map $N : S \to \mathbb{S}^2$ such that $N(p)$ is the unique unit vector normal to S at p.*

The Gauss map can only be defined globally for a surface in case it is orientable, i.e. when the transport of the orientation along any closed path is consistent at the completion of a cycle. Moreover, it allows to define in an equivalent way the Gauss-Weingarten map presented in the previous section.

Definition 2.35. *The differential of the Gauss map $dN : T_pS \to T_{N(p)}mathbbS^2$ induces the Weingarten endomorphism L: $T_pS \to T_pS$.*

Chapter 3

Curvature maps

This chapter focuses on the characterisation and reconstruction of surfaces by pasting local invariant data. The key is the characterisation of a surface (except for rigid motions) by the mean and total curvatures. To calculate this data, we use the concepts introduced in the previous chapter that allow us to calculate the invariants of a surface. This process focuses on the characterisation of the different types of **curvature**. Intuitively, this can be described as the "quantity" by which a geometric object within an euclidean space deviates from being a linear subspace. The formalisation of this idea makes it possible to classify the regions of the face according to their curvature. It should be noted that the main references for the writing of this chapter have been [16] and [27].

In this chapter we assume, unless otherwise stated, that we are working with a surface S parametrized locally by $r(u, v)$ where $r : D \to S$, D being a domain of the cartesian plane $\mathbb{R}^2$.

Definition 3.1. *Given a surface S and $X, Y \in T_pS$, we define the **k-th fundamental form** as $\langle L^{k-1}X, Y\rangle$; $k \in \mathbb{N}$.*

Each of these bilinear forms has a different associated quadratic form (representing a metric), although we usually restrict ourselves to the first two fundamental forms. The higher order ones are not considered for the moment, although they are of great interest. By way of example, it suffices to consider the third fundamental form $(III) = \langle L^2X, Y\rangle$ (of great use in Chapter 5), which expresses the "variation of the form" and depends linearly on the previous ones.

3.1 First fundamental form

Definition 3.2. *Given a surface S, its **first fundamental form** is defined as:*

$$(I) \equiv \langle r_u, r_v\rangle = \begin{pmatrix} r_u \cdot r_u & r_u \cdot r_v \\ r_v \cdot r_u & r_v \cdot r_v \end{pmatrix} = \begin{pmatrix} E & F \\ F & G \end{pmatrix}.$$

This definition is consistent with the approach developed in Section 2.2, as T_pS is generated by the tangent vectors to the curves r_u and r_v. Therefore, as can be seen in Figure 3.1, the first fundamental form describes the behaviour of pairs of vectors in the tangent plane and is the key to introduce metrics on the surface.

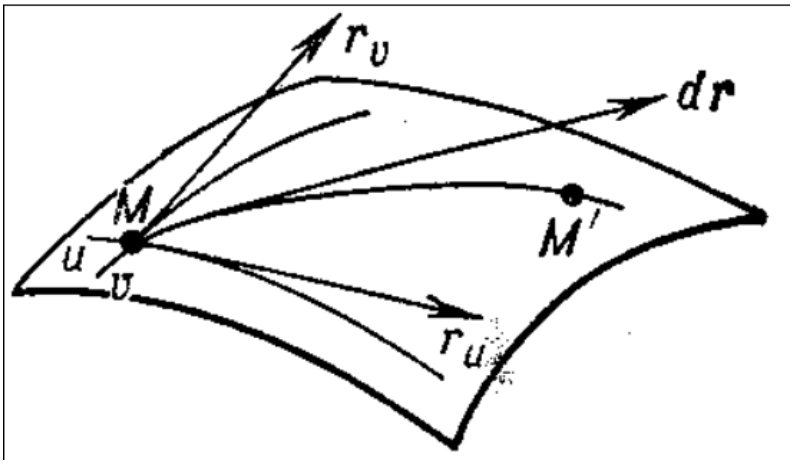

Figure 3.1: Interpretation of the first fundamental form. **Source:** [21]

Definition 3.3. *For any $X, Y \in T_pS$, we define its **scalar product** as:*

$$\langle X, Y\rangle = \begin{pmatrix} X_1 & X_2 \end{pmatrix} (I) \begin{pmatrix} Y_1 \\ Y_2 \end{pmatrix} = X_1Y_1E + (X_1Y_2 + X_2Y_1)F + Y_1Y_2G.$$

Thus, (I) defines a symmetric bilinear inner product on S whose associated quadratic form is the metric of the surface. Intuitively, (I) expresses the distance between affixes (points of the complex plane). This product also allows us to define the length of a curve on a surface.

Definition 3.4. *The **length of a curve** γ on a surface S is:*

$$l(\gamma) = \int_I ||\gamma'(t)||\, dt = \int_I ||r_u u'(t) + r_v v'(t)||\, dt = \int_I \sqrt{Eu'(t)^2 + 2Fu'(t)v'(t) + Gv'(t)^2}\, dt.$$

These local definitions extend to any connected surface:

Lemma 3.1. *If S is a connected surface of class C^1; then, each pair of points can be joined by a (piecewise smooth) **rectifiable curve**.*

Proof.

We consider $p, q \in S$. Since S is connected, $\exists\sigma(t)$ continuous curve, with $t \in [0, 1]$ of extremes $\sigma(0) = p$ and $\sigma(1) = q$. Thus, since $[0, 1]$ is compact, so too is $\mathrm{Im}(\sigma)$.

Therefore, there exists a finite number of arcs $\sigma_i(t)$ such that

$$t_i \leq t \leq t_{i+1}, i \in \{1, ..., n\}, t_1 = 0 \text{ y } t_n = 1;$$

as well as coordinate environments that satisfy $\mathrm{Im}(\sigma_i) \subset W_i$. We consider in W_i the points $\sigma(t_i) = (u_i, v_i)$ y $\sigma(t_{i+1}) = (u_{i+1}, v_{i+1})$. The curve γ_i is defined by:

$$u = u_i + \frac{t - t_i}{t_{i+1} - t_i}(u_{i+1} - u_i), v = v_i + \frac{t - t_i}{t_{i+1} - t_i}(v_{i+1} - v_i),$$

for $t_i \leq t \leq t_{i+1} (1 \leq i \leq n)$ and $\gamma = \gamma_n \circ ... \circ \gamma_1$. Therefore, γ is a rectifiable (piecewise smooth) curve with extremes $\gamma(0) = p$ and $\gamma(1) = q$. □

By virtue of the preceding description, we can define a **metric** on S by considering $\Gamma(p, q)$ as the set of rectifiable curves of S with extremes p and q; $\rho(p, q) = \inf_{\gamma \in \Gamma(p,q)}(l(\gamma))$. These paths of minimum length are the **geodesics**.

Definition 3.5. *Given two points $p, q \in S$, the path of minimum length joining them $\rho(p, q) = \inf_{\gamma \in \Gamma(p,q)}(l(\gamma))$ is called **geodesic**.*

Using the above notions, it is possible to extend well known concepts for metric spaces to surfaces.

Definition 3.6. *Given two surfaces (S_1, g) and (S_2, h) where g, h are respective metrics on S_1 and S_2; we will say that $f : (S_1, g) \to (S_2, h)$ is a **local isometry** on $p \in S_1$ if there exists an environment U of $p \in S_1$ such that:*

$$g(p', q) = h(f(p'), f(q)); \forall p', q \in U$$

*being usual to consider $p' = p$. The isometry is **global** if it holds $\forall p \in S_1$.*

In other words, an isometry between surfaces is a map that preserves distances on surfaces. This notion is a particular case of the notion of isometry for metric spaces adapted to surfaces. If we consider the linearisation $df : TS_1 \to TS_2$, the above definition can be reformulated in terms of the first fundamental form as:

$$I_1(X, Y) = I_2(df(X), df(Y)); \forall X, Y \in TS_1,$$

where I_1 and I_2 are the corresponding fundamental forms of S_1 and S_2.

These prior notions extend naturally to the approach introduced in Section 2.9, introducing the notion of the area of a surface.

Definition 3.7. *Given a region $D \subset S$, we can calculate its **area** as:*

$$A(D) = \int \int_D ||r_u \times r_v|| \, dudv.$$

The definition of area is invariant by local diffeomorphisms. In fact, an analogous formulation can be given in terms of the first fundamental form, if we consider that:

$$|I| = \begin{vmatrix} E & F \\ F & G \end{vmatrix} = \begin{vmatrix} r_u r_u & r_u r_v \\ r_v r_u & r_v r_v \end{vmatrix} = ||r_u||^2 ||r_v||^2 - |r_u r_v|^2 = ||r_u \times r_v||,$$

which ensures that the prior definition is positive definite and allows it to be rewritten in terms intrinsic to the surface itself:

$$A(D) = \int\int_D \sqrt{EG - F^2}\, dudv = \int_D dA.$$

Definition 3.8. *The* ***surface area element*** *is* $dA = \frac{r_u \times r_v}{||r_u \times r_v||}$.

Just as we have seen metric-preserving applications, there is the analogous concept for area-preserving applications, such as the Archimedean mapping or the Lambert projection, which can be seen in more detail in [25] and [55].

Definition 3.9. *Given two surfaces* S_1 *and* S_2*, we will say that* $f : S_1 \to S_2$ *is an* ***isoareal mapping*** *or area-preserving if:*

$$\begin{vmatrix} I_1(X_1, X_1) & I_1(X_1, X_2) \\ I_1(X_1, X_2) & I_1(X_2, X_2) \end{vmatrix} = \begin{vmatrix} I_2(Y_1, Y_1) & I_2(Y_1, Y_2) \\ I_2(Y_1, Y_2) & I_2(Y_2, Y_2) \end{vmatrix},$$

$\forall X_1, X_2 \in TS_1$ *where* $Y_i = df X_i$*;* $i \in \{1, 2\}$.

Observation. *While this definition is given for surfaces, it can be generalised to Riemannian varieties of any arbitrary dimension using the determinant:*

$$|(I_1(X_i, X_j))_{1 \leq i,j \leq n}| = |(I_2(Y_i, Y_j))_{1 \leq i,j \leq n}|.$$

This type of mappings are called ***unimodular****, having specific names depending on the dimension of the variety (isoareal for dimension 2, isovolumetric for dimension 3, etc.).*

Having established the notions of distance and area, it will also be convenient to explain the definition of the angle formed by two curves on a surface. To do this, we consider two regular curves c_1 and c_2 of S with a common point p. These curves are parametrized respectively by $(u_1(t), v_1(t))$ and $(u_2(t), v_2(t))$, with tangent vectors $t_1(p) = (u_1'(t), v_1'(t))$ y $t_2(p) = (u_2'(t), v_2'(t))$.

Definition 3.10. *The angle formed by* c_1 *and* c_2 *is that of their tangent vectors at that point, which is also expressed in terms of* (I)*:*

$$\cos(\alpha) = \frac{t_1 t_2}{||t_1||||t_2||} = \frac{Eu_1'u_2' + 2F(u_1'v_2' + v_1'u_2') + Gv_1'v_2'}{\sqrt{Eu_1'^2 + 2Fu_1'v_1' + Gv_1'^2}\sqrt{Eu_2'^2 + 2Fu_2'v_2' + Gv_2'^2}}.$$

Observation. *For coordinate curves on* S *(*$v = cte.$ *or* $u = cte.$*), the expression for the angle they form simplifies to:*

$$\cos(\alpha) = \frac{Fu_1'v_2'}{\sqrt{Eu_1'^2}\sqrt{Gv_2'^2}} = \frac{F}{\sqrt{EG}},$$

and we obtain that, if $F = 0$*, the curves are orthogonal at that point.*

Definition 3.11. *A mapping between surfaces S_1, S_2 is called **conformal** if it preserves angles. In terms of the first fundamental form, this can be expressed as:*

$$\frac{I_1(X_1, X_2)}{||X_1||||X_2||} = \frac{I_2(Y_1, Y_2)}{||Y_1||||Y_2||},$$

$\forall X_1, X_2 \in TS_1$ *where* $Y_i = df X_i$*;* $i \in \{1, 2\}$.

The best known conformal maps are the Mercator projection or the Möbius transformations. For more details on these examples, please consult [25], [44] or [55].

Conformal applications are very useful for representing facial gestures because, when a face is deformed to perform any kind of gesture, the geometry of the surface changes from Euclidean to Conformal. As these transitions are elastic, the face returns to its original state together with its conformal geometry thanks to this conservation of angles. This approach is developed in more depth in section 5.2.

3.2 Second fundamental form

The second fundamental form, also known as **shape tensor**, is a quadratic form of the tangent plane of a smooth surface in $\mathbb{R}^3$. Together with (I), it allows one to define invariants of the surface in terms of its principal curvatures.

We will assume that S is an orientable surface, $N : S \to \mathbb{S}^2$, and we recall that there is a field of unit normal vectors $n = \frac{r_u \times r_v}{||r_u \times r_v||}$ (the vector bundle).

Definition 3.12. *The **second fundamental form** of S in the basis of T_pS is:*

$$(II) \equiv \langle Lr_u, r_v \rangle = \begin{pmatrix} r_{uu} \cdot n & r_{uv} \cdot n \\ r_{uv} \cdot n & r_{vv} \cdot n \end{pmatrix} = \begin{pmatrix} e & f \\ f & g \end{pmatrix} \equiv \begin{pmatrix} L & M \\ M & N \end{pmatrix},$$

and is usually represented as $Ldu^2 + 2Mdudv + Ndv^2$.

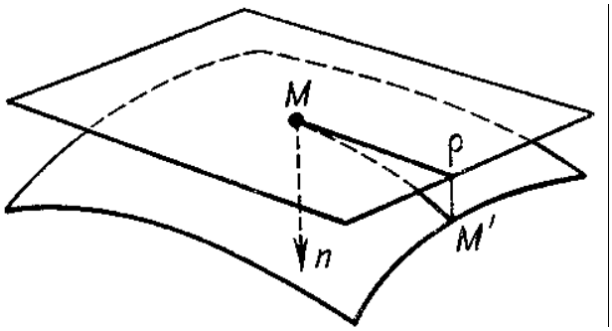

Figure 3.2: Interpretation of the second fundamental form. **Source:** [21]

We can see that its coefficients are the projections of the second derivative on the normal line, so its meaning refers to the variation in the tangent plane of the normal vector, as shown in the Figure 3.2.

Going back to what was exposed in Section 2.8, we recall that the differential $dN : T_pS \to T_{N(p)}\mathbb{S}^2$ induces the Weingarten endomorphism L: $T_pS \to T_pS$, since $T_pS = T_{N(p)}\mathbb{S}^2$ as both are perpendicular to the normal vector. For the sake of clarity, from now on we will denote the Weingarten endomorphism as d_pN in order to specify the point at which it is defined, and we will designate its matrix as K.

Proposition 3.1. *$\forall p \in S$, the linear endomorphism $d_pN : T_pS \to T_pS$ is self-adjoining.*

This result is simply a particular case of the approach seen in Section 2.8. However, this reformulation of the proposition together with its corresponding proof, carried out using a concrete parametrization of both the surface and the tangent space (see [16]), allows us to associate to this self-adjoint linear application a quadratic form. The quadratic form corresponding to d_pN is $(II); \forall p \in S$.

More formally, $(II) = -d_pN$. Thus, $(II)(v) = -\langle d_pN(v), v\rangle$; which is the directional derivative of the normal vector along a vector field (in this case v).

Definition 3.13. *Let c be a regular curve in S passing through $p \in S$, κ be the curvature of c at p, and $\cos(\theta) = \langle n, N(p)\rangle$, where n is the normal vector to c. The value $\kappa_n = \kappa\cos(\theta)$ is called the* ***normal curvature*** *of c at p.*

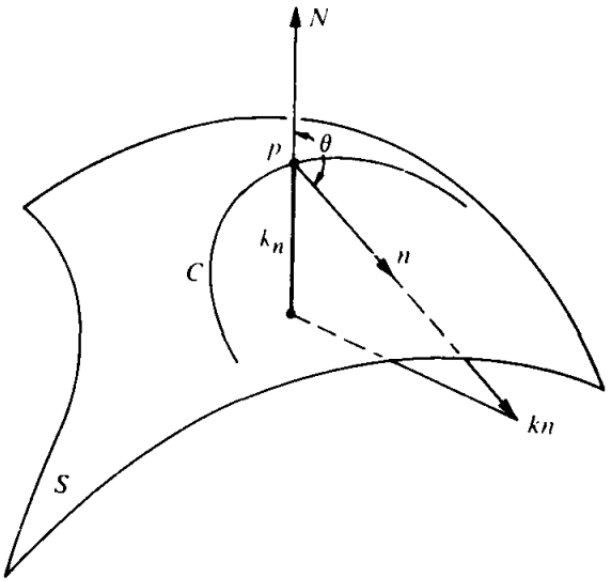

Figure 3.3: Geometric interpretation of normal curvature. **Source:** [16]

In other words, κ_n is the length of the projection of the vector κn onto the normal to the surface at p, whose sign is given by the orientation $N(p)$ of S.

Proposition 3.2 (Meusnier)**.** *All the curves contained in S that have at a given point $p \in S$ the same tangent line, have at this point the same normal curvature.*

Proof. Let $c \subset S$ be a regular curve parametrized by the arc length (p.b.a.) $\alpha(s)$ with $\alpha(0) = p$. If we denote as $N(s)$ the constraint of the normal vector $N(p)$ to the curve $\alpha(s)$, we have that $\langle N(s), \alpha'(s)\rangle = 0$, so that $\langle N(s), \alpha''(s)\rangle = -\langle N'(s), \alpha'(s)\rangle$. Thus,

$$(II)(\alpha'(0)) = -\langle d_p N(\alpha'(0)), \alpha'(0)\rangle = -\langle N'(0), \alpha'(0)\rangle = \langle N(0), \alpha''(0)\rangle = \langle N, \kappa n\rangle = \kappa_n(p)$$

□

The result facilitates a geometric interpretation of the second fundamental form since, for a unit normal vector $v \in T_pS$, its value is equal to the normal curvature of a regular curve passing through p and tangent to that vector. Therefore, we can speak of the normal curvature along a direction in p, which is maintained along the **normal section** of S in p (the intersection of the surface with the plane containing v and $N(p)$), since all the curves passing through that point will have the same normal curvature there.

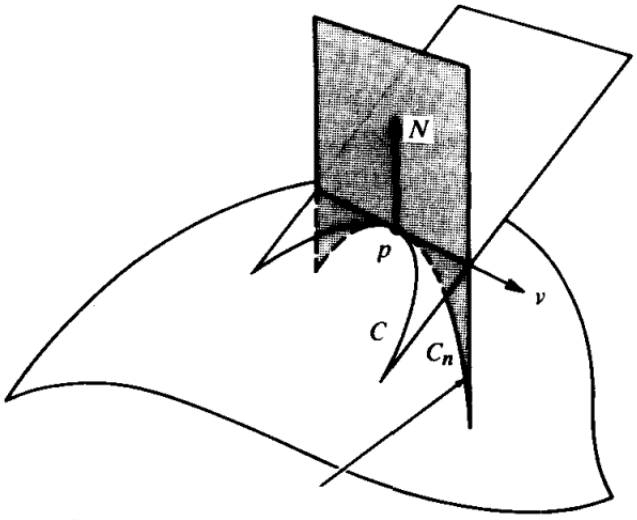

Figure 3.4: Geometric interpretation of Meusnier's Proposition. **Source:** [16]

We can give an alternative formulation of these concepts in terms of osculating circles[1], as Banchoff proves in [7].

Proposition 3.3 (Meusnier alternative)**.** *All the curves of a surface that pass through the same point and have the same tangent to it, have the same normal curvature at that point and the osculating circles form a sphere (**Meusnier's sphere**).*

[1] An **osculating circle** is that which best approximates the curvature of a curve at a specific point on the curve.

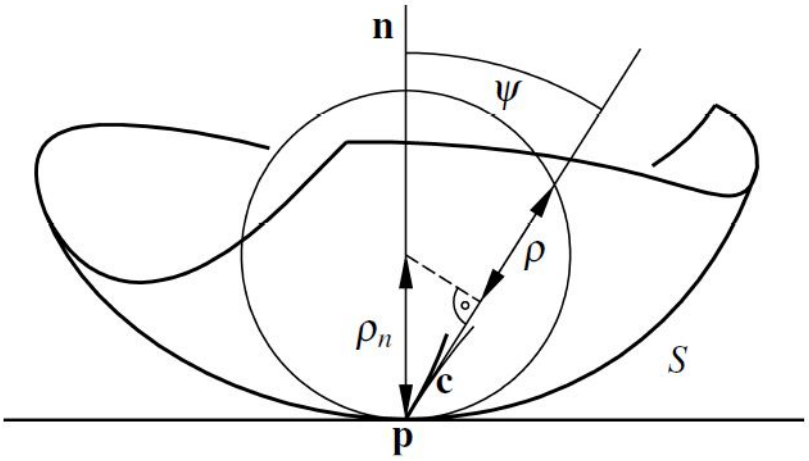

Figure 3.5: Interpretation of Meusnier's Proposition as an osculating circle. **Source:** [45]

3.3 Principal curvatures

Definition 3.14. *The **normal curvature** in a direction w is defined as $\kappa_w = \frac{II(w,w)}{I(w,w)}$.*

Since the application d_pN is self-adjoint, for each $p \in S$ there exists an orthonormal basis $\{e_1, e_2\}$ of T_pS where $d_pN(e_1) = \kappa_1 e_1$ and $d_pN(e_2) = \kappa_2 e_2$, where κ_1 and κ_2 are the maximum and minimum eigenvalues of (II) restricted to the unit circle of T_pS; i.e., the extreme values of the normal curvature at p. The proof of this result can be found in [16].

Definition 3.15. *The values κ_1 and κ_2, which are the respective maximum and minimum normal curvatures, are called the **principal curvatures** in p and their corresponding directions d_1, d_2 are the **principal directions** in p.*

The knowledge of these values allows us to calculate in a simple way the normal curvature along a given direction of T_pS. In fact, considering $v \in T_pS$ with $|v| = 1$, since we are using an orthonormal basis of T_pS,

$$v = e_1 \cos(\theta) + e_2 \sin(\theta),$$

being θ the angle from e_1 to v according to the orientation of T_pS.

Proposition 3.4 (Euler's formula)**.**

$$\kappa_n = \kappa_1 \cos^2(\theta) + \kappa_2 \sin^2(\theta).$$

Proof.

$$\kappa_n = (II)(v) = -\langle d_pN(v), v\rangle = -\langle d_pN(e_1\cos(\theta) + e_2\sin(\theta)), e_1\cos(\theta) + e_2\sin(\theta)\rangle =$$

$$= \langle e_1\kappa_1\cos(\theta) + e_2\kappa_2\sin(\theta)), e_1\cos(\theta) + e_2\sin(\theta)\rangle = \kappa_1\cos^2(\theta) + \kappa_2\sin^2(\theta)$$

□

This result allows to link with the approach provided by the alternative Meusnier's Proposition (3.3), defining a new concept that allows to study a surface in greater detail [26].

Definition 3.16. *Given a surface S, its **focal surface**, also called **surface of centres** or **evolute**, is the one formed by the centres of the osculating circles. Since there are two principal curvatures, there are two focal surfaces in each direction normal to the surface, whose points are of the form:*

$$b_1(p) = p + \frac{N}{\kappa_1}, \qquad b_2(p) = p + \frac{N}{\kappa_2}; \qquad \forall p \in S.$$

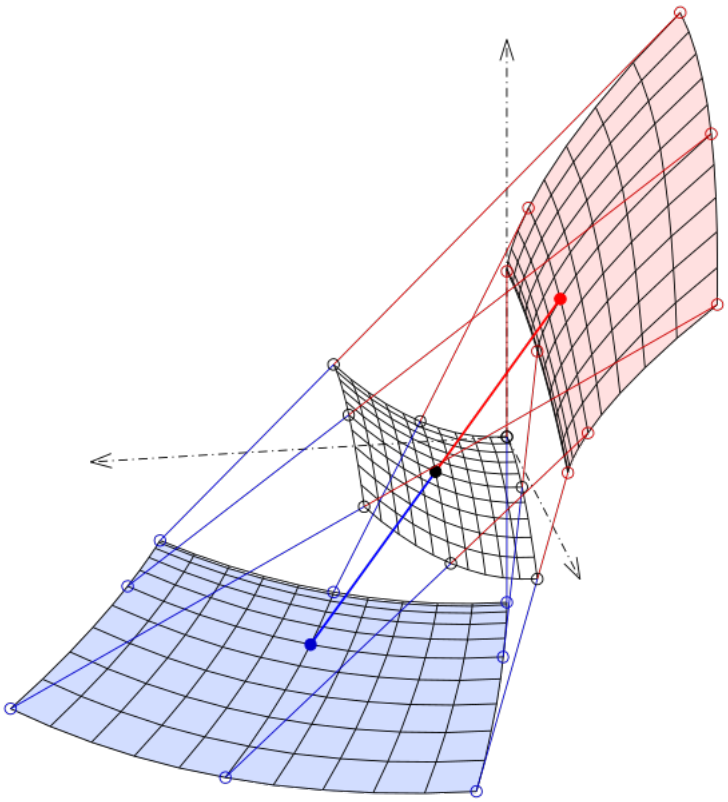

Figure 3.6: Focal surfaces of a hyperbolic paraboloid. **Source:** Ag2gaeh

Let us calculate these principal curvatures. Since d_pN is a linear application with associated matrix K, its algebraic invariants are determined in terms of its trace and its determinant.

$$|\lambda I - K| = (\lambda - \kappa_1)(\lambda - \kappa_2) = \lambda^2 - (\kappa_1 + \kappa_2)\lambda + \kappa_1\kappa_2 = \lambda^2 - \mathrm{tr}(K)\lambda + |K|.$$

If the orientation of the surface is changed to the opposite orientation, the determinant does not change (as it is key that the dimension is even), but the trace changes sign.

Definition 3.17.

- *The **mean curvature** is half of the trace of the Gauss map which, in terms of the principal curvatures, is written as:*

$$H \equiv \kappa_m = \frac{1}{2}\operatorname{tr}(K) = \frac{1}{2}(\kappa_1 + \kappa_2).$$

- *The **total curvature**, also known as the **Gaussian curvature**, is the determinant of the Gauss map which, in terms of the principal curvatures, is written:*

$$\mathbf{K} \equiv \kappa_t = |K| = \kappa_1\kappa_2.$$

  This value allows to give a classification of the points of a surface:

  1. ***Elliptical** if $\mathbf{K}(p) > 0$.*
  2. ***Hyperbolic** if $\mathbf{K}(p) < 0$.*
  3. ***Parabolic** if $\mathbf{K}(p) = 0$; which is either because $\kappa_1 = 0$ (**blue parabolic point**), or because $\kappa_2 = 0$ (**red parabolic point**).*

By virtue of the **Mean Value Theorem**, regions of elliptic points are separated by parabolic curves from regions of hyperbolic points. In the human face, this is evident when considering the transition of curvature that exists, for example, when moving from the forehead to the eye socket area, with the eyebrows being the transition region between the two areas.

Definition 3.18. *A point is **umbilic** or **umbilical** if all normal curvatures coincide (all directions are principal); $\kappa_1(p) = \kappa_2(p)$. A point is called **plane** if it is simultaneously umbilical and parabolic; $\kappa_1(p) = \kappa_2(p) = 0$.*

This classification is completed by a final type of points. However, in order to define them, the following concept must first be introduced:

Definition 3.19. ***Lines of curvature** are curves that are always tangent to a principal direction. In particular, they are the integral curves for the principal direction fields.*

By definition, we see that through each non-umbilical point pass two lines of curvature corresponding to each of the principal curvatures.

Definition 3.20. *A **ridge point** is a point where one of the principal curvatures has an extreme value (maximum or minimum) along its corresponding line of curvature. As with parabolic points, we distinguish between **red** and **blue** points depending on whether they refer to κ_1 or κ_2, respectively.*

In other words, a ridge point is a point where the surface has a higher order contact with one of the osculating spheres (this is a good approximation of the variety in such areas). Moreover, in umbilic points the colour of the ridges changes, so they serve to delimit regions in a similar way as parabolic points do.

After having seen the different classifications in which we can classify each point of a surface, we will return to the idea presented in the Definition 3.16 to make this distinction from an alternative point of view.

Proposition 3.5. *Given a surface S,*

- *S always has two different focal surfaces for its non-umbilical points; whereas in the umbilical points both evolutes coincide.*
- *If it has a ridge, the focal surface will have a cusp.*
- *For the case of points with zero total curvature, one of the focal surfaces will have a point at infinity corresponding to the principal curvature that is null.*

Proof of these results, immediate from the definitions themselves, can be found in texts such as [41]. Some of these cases can be seen in Figure 3.7.

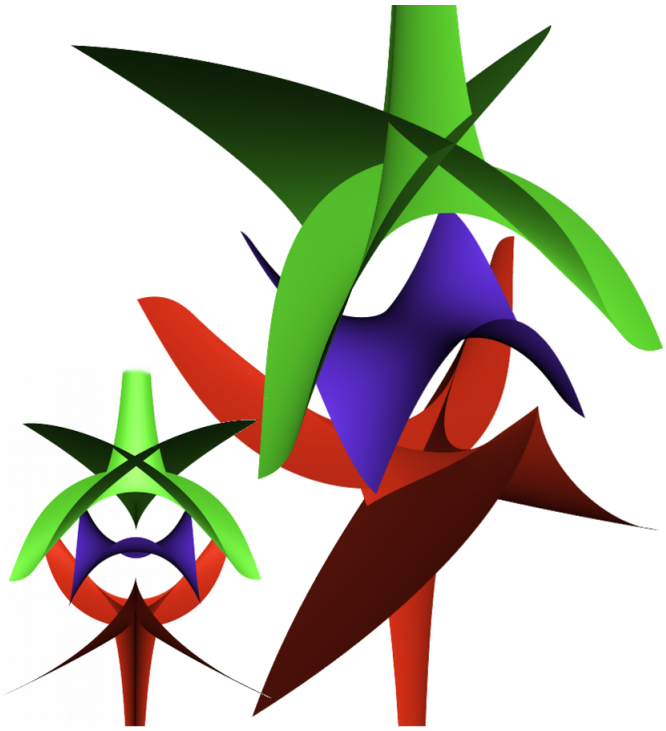

Figure 3.7: Focal surfaces of a monkey saddle. **Source:** Rocchini

3.4 Local expression of principal curvatures

All the concepts presented in the preceding sections depend on the chosen parameterization, which is not efficient when dealing with general situations. Therefore, throughout this section, the matrix of the Weingarten map is given in terms of the first two fundamental forms, relating intrinsic elements to others that depend on the chosen parameterization.

Recall that if $r(u,v) : U \subset \mathbb{R}^2 \to S$ is a local parametrization in a neighborhood of $p_0 = r(u_0, v_0)$, the normal vector with respect to that parametrization is $N \circ r = \frac{r_u \times r_v}{||r_u \times r_v||}$, which determines the local orientation in S. Thus, the coefficients of the differential application of the linear endomorphism given by the Gauss map d_pN, can be given in local terms (according to the parametrization) as:

$$(II) = \langle LX, Y\rangle = \begin{pmatrix} L & M \\ M & N \end{pmatrix} = \begin{pmatrix} -d_pN(r_u)\cdot r_u & -d_pN(r_u)\cdot r_v \\ -d_pN(r_u)\cdot r_v & -d_pN(r_v)\cdot r_v \end{pmatrix}.$$

Using that $(N \circ r)r_u = 0$ and $(N \circ r)r_v = 0$, we can rewrite:

$$L = (N \circ r)r_{uu}, \quad M = (N \circ r)r_{uv}, \quad N = (N \circ r)r_{vv}.$$

Using the matrix K of d_pN, it holds

$$K \begin{pmatrix} r_u \\ r_v \end{pmatrix} = \begin{pmatrix} a_{11} & a_{12} \\ a_{21} & a_{22} \end{pmatrix} \begin{pmatrix} r_u \\ r_v \end{pmatrix} = \begin{pmatrix} a_{11}r_u + a_{12}r_v \\ a_{21}r_u + a_{22}r_v \end{pmatrix}.$$

Obtaining then:

$$-L = (a_{11}r_u + a_{12}r_v)r_u = a_{11}E + a_{12}F, \quad -M = (a_{11}r_u + a_{12}r_v)r_v = a_{11}F + a_{12}G$$

$$-M = (a_{21}r_u + a_{22}r_v)r_u = a_{21}E + a_{22}F, \quad -N = (a_{21}r_u + a_{22}r_v)r_v = a_{21}F + a_{22}G$$

which is rewritten in matrix terms as;

$$\begin{pmatrix} a_{11} & a_{12} \\ a_{21} & a_{22} \end{pmatrix} \begin{pmatrix} E & F \\ F & G \end{pmatrix} = -\begin{pmatrix} L & M \\ M & N \end{pmatrix} = -\begin{pmatrix} e & f \\ f & g \end{pmatrix}$$

From the above expression we obtain the **shape operator**:

$$\begin{pmatrix} a_{11} & a_{12} \\ a_{21} & a_{22} \end{pmatrix} = -\begin{pmatrix} e & f \\ f & g \end{pmatrix} \begin{pmatrix} E & F \\ F & G \end{pmatrix}^{-1} \text{ by } \begin{pmatrix} E & F \\ F & G \end{pmatrix}^{-1} = \frac{1}{EG - F^2} \begin{pmatrix} G & -F \\ -F & E \end{pmatrix}^{-1}$$

which gives us the so-called **Weingarten equations**:

$$a_{11} = \frac{fF - eG}{EG - F^2}, \quad a_{12} = \frac{eF - fE}{EG - F^2}, \quad a_{21} = \frac{gF - fG}{EG - F^2}, \quad a_{22} = \frac{fF - gE}{EG - F^2}.$$

Thanks to this expression, we obtain an alternative representation of the principal curvatures defined in the previous section, whose equivalence in the definition is based on the fact that we are dealing with a change of parametrization:

$$H = \frac{1}{2}\operatorname{tr}(K) = \frac{1}{2}(a_{11} + a_{22}) = \frac{eG - 2fF + gE}{2(EG - F^2)},$$
$$\mathbf{K} = |K| = a_{11}a_{22} - a_{12}a_{21} = \frac{eg - f^2}{EG - F^2}.$$

3.5 Surface characterisation

Given a surface S, we have a regular parametrization with a reference $\{r_u, r_v, N\}$. To give its spatial evolution, we derive with respect to u and v, obtaining the vectors that determine it. This is the underlying idea behind the Christoffel symbols.

The **Christoffel symbols** are coefficients that express the variation in T_pS with respect to its base $\{r_u, r_v\}$ (deformation of the support). They are the analogue of the Frénet-Serret formulae for surfaces, since they assign to each point of the surface a frame to study the derivatives of its vectors. We can then write

$$r_{uu} = \Gamma^1_{11} r_u + \Gamma^2_{11} r_v + A_{11} N,$$
$$r_{uv} = \Gamma^1_{12} r_u + \Gamma^2_{12} r_v + A_{12} N,$$
$$r_{vu} = \Gamma^1_{21} r_u + \Gamma^2_{21} r_v + A_{21} N,$$
$$r_{vv} = \Gamma^1_{22} r_u + \Gamma^2_{22} r_v + A_{22} N,$$

where the propagation of the normal (extrinsic) vector can be expressed, by calculating the inner product of these relations with N, as:

$$A_{11} = \langle r_{uu}, N\rangle = e, \quad A_{12} = \langle r_{uv}, N\rangle = f, \quad A_{22} = \langle r_{vv}, N\rangle = g.$$

Moreover, N is expressed in terms of the tangent vectors as:

$$N_u = a_{11} r_u + a_{12} r_v,$$
$$N_v = a_{21} r_u + a_{22} r_v,$$

where the above coefficients are defined by the Weingarten equations.

Definition 3.21. *The coefficients Γ^k_{ij} $(i, j, k \in \{1, 2\})$ expressed above are known as the Christoffel symbols of the parametrization r, the four formulae where they have been presented being known as the **Gauss equations**. Since $r_{uv} = r_{vu}$, we obtain that $\Gamma^k_{ij} = \Gamma^k_{ji}$, so the Christoffel coefficients are symmetric (there are 6 in total).*

In matrix terms, the Gauss equations simplify as:

$$\begin{pmatrix} r_{uu} \\ r_{uv} \\ r_{vv} \end{pmatrix} = \begin{pmatrix} \Gamma^1_{11} & \Gamma^2_{11} & e \\ \Gamma^1_{12} & \Gamma^2_{12} & f \\ \Gamma^1_{22} & \Gamma^2_{22} & g \end{pmatrix} \begin{pmatrix} r_u \\ r_v \\ N \end{pmatrix}.$$

Obtaining Christoffel symbols

1. Calculate the expressions of the coefficients of the first fundamental form:

$$r_{uu}\cdot r_u=\frac{1}{2}E_u,\quad r_{uv}\cdot r_u=\frac{1}{2}E_v,\quad r_{uv}\cdot r_v=\frac{1}{2}G_u,\quad r_{vv}\cdot r_v=\frac{1}{2}G_v,$$

$$r_{uu}\cdot r_v=F_u-r_{uv}\cdot r_u=F_u-\frac{1}{2}E_v,\quad r_{vv}\cdot r_u=F_v-r_{uv}\cdot r_v=F_u-\frac{1}{2}G_u.$$

2. From the Gauss formulae, we obtain:

$$r_{uu}\cdot r_u=\Gamma^1_{11}E+\Gamma^2_{11}F,\quad r_{uu}\cdot r_v=\Gamma^1_{11}F+\Gamma^2_{11}G,$$

$$r_{uv}\cdot r_u=\Gamma^1_{12}E+\Gamma^2_{12}F,\quad r_{uu}\cdot r_v=\Gamma^1_{12}F+\Gamma^2_{12}G,$$

$$r_{vv}\cdot r_u=\Gamma^1_{22}E+\Gamma^2_{22}F,\quad r_{vv}\cdot r_v=\Gamma^1_{22}F+\Gamma^2_{22}G.$$

3. Substitute the values from step 1 into the formulae from the previous step, giving the following three subsystems:

$$\begin{pmatrix}E & F\\ F & G\end{pmatrix}\begin{pmatrix}\Gamma^1_{11}\\ \Gamma^2_{11}\end{pmatrix}=\begin{pmatrix}\frac{1}{2}E_u\\ F_u-\frac{1}{2}E_v\end{pmatrix}\qquad\begin{pmatrix}E & F\\ F & G\end{pmatrix}\begin{pmatrix}\Gamma^1_{12}\\ \Gamma^2_{12}\end{pmatrix}=\begin{pmatrix}\frac{1}{2}E_v\\ \frac{1}{2}G_u\end{pmatrix},$$

$$\begin{pmatrix}E & F\\ F & G\end{pmatrix}\begin{pmatrix}\Gamma^1_{22}\\ \Gamma^2_{22}\end{pmatrix}=\begin{pmatrix}F_v-\frac{1}{2}G_u\\ \frac{1}{2}G_v\end{pmatrix}$$

The resulting formulas for the Christoffel symbols are condensed in the following matrix equation, where only the coefficients of the first fundamental form are shown:

$$\begin{pmatrix}\Gamma^1_{11} & \Gamma^1_{12} & \Gamma^2_{22}\\ \Gamma^2_{11} & \Gamma^2_{12} & \Gamma^2_{22}\end{pmatrix}=\begin{pmatrix}E & F\\ F & G\end{pmatrix}^{-1}\begin{pmatrix}\frac{1}{2}E_u & \frac{1}{2}E_v & F_v-\frac{1}{2}G_u\\ F_u-\frac{1}{2}E_v & \frac{1}{2}G_u & \frac{1}{2}G_v\end{pmatrix}.$$

As we have just seen, the expressions of the derivatives of r_u, r_v, N with respect to the basis $\{r_u, r_v, N\}$ depend only on the coefficients of the first two fundamental forms of the surface. One way to relate these coefficients is to consider the expressions:

$$(r_{uu})_v-(r_{uv})_u=0,\quad (r_{vv})_u-(r_{vu})_v=0,\quad N_{uv}-N_{vu}=0.$$

Expressed in terms of the Gauss and Weingarten equations, these relationships are written as:

$$A_ir_u+B_ir_v+C_iN=0,$$

where $A_i, B_i, C_i (i=1,2,3)$ are functions of the coefficients of the first two fundamental forms and their derivatives. Moreover, since the basis vectors are linearly independent, all the coefficients A_i, B_i, C_i must cancel, giving rise to the nine relations:

$$A_i=0,\quad B_i=0,\quad ,C_i=0,\quad i=1,2,3.$$

Proposition 3.6. *The coefficients of the first fundamental form of a surface S can be obtained from the total curvature of the surface and the Christoffel symbols:*

$$E\mathbf{K} = (\Gamma^2_{11})_v - (\Gamma^2_{12})_u + \Gamma^1_{11}\Gamma^2_{12} + \Gamma^2_{11}\Gamma^2_{22} - \Gamma^1_{12}\Gamma^2_{11} - (\Gamma^2_{12})^2,$$

$$F\mathbf{K} = (\Gamma^1_{12})_u - (\Gamma^1_{11})_v + \Gamma^2_{12}\Gamma^1_{12} - \Gamma^2_{11}\Gamma^1_{22} = (\Gamma^2_{12})_v - (\Gamma^2_{22})_u + \Gamma^1_{12}\Gamma^2_{12} - \Gamma^1_{22}\Gamma^2_{11},$$

$$G\mathbf{K} = (\Gamma^1_{22})_u - (\Gamma^1_{12})_v + \Gamma^1_{22}\Gamma^1_{11} + \Gamma^2_{22}\Gamma^1_{12} - \Gamma^2_{12}\Gamma^1_{22} - (\Gamma^1_{12})^2.$$

Proof. We will only prove the first formula, known as **Gauss' formula**, the other two relations being proved in an analogous way. Considering the expression $(r_{uu})_v - (r_{uv})_u = 0$, it can be rewritten in terms of the Gauss equations as:

$$\Gamma^1_{11}r_{uv} + \Gamma^2_{11}r_{vv} + eN_v + (\Gamma^1_{11})_v r_u + (\Gamma^2_{11})_v r_v + e_v N = \Gamma^1_{12}r_{uu} + \Gamma^2_{12}r_{vu} + fN_u + (\Gamma^1_{12})_u r_u + (\Gamma^2_{12})_u r_v + f_u N$$

which can be simplified from the equation of the coefficients of r_v and, again, the Gauss equations:

$$\Gamma^1_{11}\Gamma^2_{12} + \Gamma^2_{11}\Gamma^2_{22} + ea_2 2 + (\Gamma^2_{11})_v = \Gamma^1_{12}\Gamma^2_{11} + (\Gamma^2_{12})^2 + fa_1 2 + (\Gamma^2_{12})_u$$

where, thanks to the Weingarten equations, we obtain:

$$(\Gamma^2_{11})_v - (\Gamma^2_{12})_u + \Gamma^1_{11}\Gamma^2_{12} + \Gamma^2_{11}\Gamma^2_{22} - \Gamma^1_{12}\Gamma^2_{11} - (\Gamma^2_{12})^2 = E\frac{eg - f^2}{EG - F^2} = E\mathbf{K}$$

□

Thanks to this result we have the proof of the following theorem that characterises surfaces in terms of their Gaussian curvature. In particular, two surfaces are equivalent by a rigid motion (see Section 5.2) iff their fundamental forms are related by a transformation.

Theorem 3.1 (Gauss' Theorema Egregium)**.**
The Gaussian curvature of a regular surface is invariant by local isometries.

Proof. Given two surfaces $S, \tilde{S}$ and a local isometry $f : S \to \tilde{S}$ between them, we know that their parametrizations can be expressed as $r(u, v)$ and $\tilde{r}(u, v) = f \circ r(u, v)$, so both have the same first fundamental form. Therefore, thanks to the previously calculated expressions, they also have the same Gaussian curvature. □

Observation. *The reciprocal is not always true. Indeed, given two surfaces with the same Gaussian curvature at all points, there may not be an isometry that preserves it. However, there does exist a diffeomorphism which preserves this total curvature [16].*

The initial description of Gaussian curvature is based on the embedding of a surface in space. However, it does not depend on the embedding but only on the metric structure of the surface itself (first fundamental form). This idea motivates the geometry of the first fundamental form to be known as **Intrinsic Geometry**, since it can be developed without reference to the space in which the surface is contained.

3.6 Surface reconstruction

Returning to the formulae presented in Proposition 3.6, the second of these can be proved in the same way, but substituting in the analogous expression of

$$(r_{uu})_v - (r_{uv})_u = 0$$

the coefficients of r_u instead of those of r_v. The analogous procedure using the coefficients of N results in:

$$e_v - f_u = e\Gamma^1_{12} + f(\Gamma^2_{12} - \Gamma^1_{11}) - g\Gamma^2_{11}.$$

Proceeding in the same way on $(r_{vv})_u - (r_{vu})_v = 0$, we also obtain the expression:

$$f_v - g_u = e\Gamma^1_{22} + f(\Gamma^2_{22} - \Gamma^1_{12}) - g\Gamma^2_{12}.$$

Both equations usually occur simultaneously, as shown in the following result.

Proposition 3.7 (Mainardi-Peterson-Codazzi equations)**.**

$$e_v - f_u = e\Gamma^1_{12} + f(\Gamma^2_{12} - \Gamma^1_{11}) - g\Gamma^2_{11},$$

$$f_v - g_u = e\Gamma^1_{22} + f(\Gamma^2_{22} - \Gamma^1_{12}) - g\Gamma^2_{12}.$$

Definition 3.22. *The Gauss formula together with the Mainardi-Peterson-Codazzi equations are known as the* ***compatibility equations****.*

The name compatibility equations arises from the fact that the knowledge of the fundamental first and second forms locally determines a surface, so that its reconstruction is possible. This would be indicated more precisely in the following theorem.

Theorem 3.2 (Bonnet)**.**

Let $E, F, G, e, f, g : V \to \mathbb{R}$ be differentiable functions, being V an open of $\mathbb{R}^2$, such that $E, G, EG - F^2 > 0$ in V. From these, we construct the Christoffel symbols Γ^k_{ij} as obtained in the previous section, and $\mathbf{K} = \frac{eg-f^2}{EG-F^2}$. Then, if all these functions satisfy the compatibility equations, for every $v_0 \in V$ there exists an open $V' \subset V$ with $v_0 \in V'$ and a local chart $x' : V' \to x(V')$ such that E, F, G, e, f, g are the coefficients of its first and second fundamental form, respectively.

Moreover, if V' is connected and there exists a local chart $y' : V' \to y(V')$ with the same conditions, then there exists a direct move $F : \mathbb{R}^3 \to \mathbb{R}^3$ such that $y = F \circ x$.

This result is a consequence of the existence and uniqueness theorem for systems of Partial Differential Equations (PDEs), its precise proof being given in [16].

Chapter 4

Surface evolution under curvature flows

In the previous chapter we have presented a precise definition of the concept of curvature, as well as the results that allow us to characterise and reconstruct surfaces, which allows us to give a static reconstruction of the surface of the face in terms of Differential Geometry of Surfaces. However, the human face is not a fixed surface; on the contrary. Humans make a large number of facial gestures that express emotions or moods and are essential for non-verbal communication. In the topological framework they are described by different deformations of the surface. Therefore, our next step will be the reconstruction and analysis of facial gesture over time. For this purpose, we resort to the evolution of curvature map values in terms of flows.

This chapter builds on the homonymous paper presented by Mumford et al. in [31], as it introduces the basic concepts in simple terminology, as well as their immediate application to the analysis of the human face. If a topological approach were to be adopted, it would be necessary to introduce the basic concepts of **Singularities Theory** of germs of maps between manifolds, as can be seen in [5] or [11] for the most basic aspects. While such an approach fits several of the concepts presented in this document, the classification of (multi-)germs of singularities requires additional elements of **Lie group actions** on **jetspaces**[1]. The development of this formalism requires an extension of the length of the memory; therefore, a more simplified geometric approach has been preferred.

The evolution of singularities over time is initially approached in terms of "slices" of the space of universal deformations of "basic types" of (germs of) functions or, more generally, maps. This theory was first developed for germs of functions in the late 1950s and early 1960s by René Thom and popularised in the following decade by Chirstopher Zeeman and is called **Catastrophe Theory**.

[1]Intuitively, the k-**jet** of a function at a point is the truncated Taylor polynomial in order k; the k-jet of a map $f \in C^r(n,p)$ is given by the k-jets of its p-components.

The classification of application germ singularities was carried out simultaneously by the English (led by J.Mather and C.T.C.Wall) and Russian (led by V.I.Arnold) schools in [6]. The extension of this approach to multi-germs is applicable to the analysis of facial gestures, using the correspondences between universal deformations and appearance-based gestural models. For example, in Figure 4.1 we can see how the two transitions presented would correspond to the animation of closing and opening the mouth (lip movement corresponding to one of Thom's catastrophes).

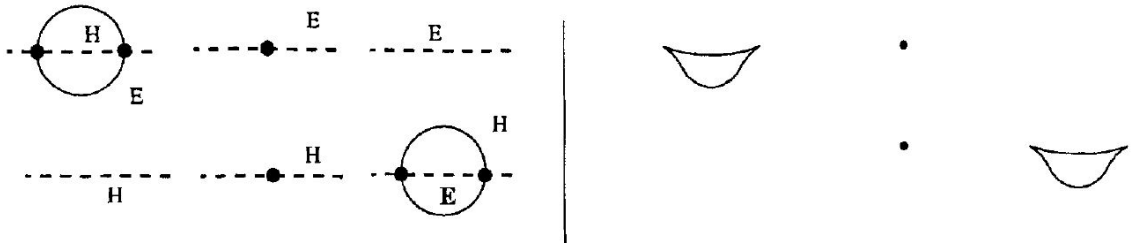

Figure 4.1: Cusp catastrophe transition for curvatures with same sign **Source:** [12]

A more detailed analysis of these elements can be found in the articles by Bruce et al. [12] and [13], which focus on the study of ridges or parabolic curves for evolving surfaces. This analysis is somewhat more detailed than the one we will give in this chapter, as it is done in terms of height functions, bifurcation sets and focal surfaces.

4.1 Curvature Flows

Having defined curvature as an extrinsic invariant of the surface, the next step will be to study its evolution over time. This study will make it possible to model the variation in the curvature of the face when a facial gesture is made, maintaining the description of the given human face and adapting it to the deformations it undergoes. For this purpose, the concept of **flows** presented in Section 2.5 is used, adapting it to the geometry of the face as a smooth surface (class C^infty) in pieces.

In addition to analysing the evolution of the surface over time, a flow can also be considered as a smoothing process for experimentally captured discrete information. The flow-based approach allows estimating the main features of the surface that facilitate a simpler description by decreasing the computational complexity of discrete models. This approach is adopted by Mumford et al. in [31], where they look for "ideal" flows, in the sense of not incorporating new features that were not in the original surface.

To adapt to the notation used in that article, in this chapter we will represent the surface explicitly instead of the parametric form, by means of the Monge representation $z = f(x, y)$. This allows us to give an equivalent formulation of the different concepts presented in the previous chapter, which can be obtained immediately after the proper change of variables.

Proposition 4.1. *(Formulae using Monge representation)*

$$E = 1 + f_x^2, \quad F = f_x f_y, \quad G = 1 + f_y^2, \quad EG - F^2 = 1 + f_x^2 + f_y^2,$$

$$e = \frac{f_{xx}}{\sqrt{1 + f_x^2 + f_y^2}}, \quad f = \frac{f_{xy}}{\sqrt{1 + f_x^2 + f_y^2}}, \quad g = \frac{f_{yy}}{\sqrt{1 + f_x^2 + f_y^2}}, \quad N = \frac{(-f_x, -f_y, 1)}{\sqrt{1 + f_x^2 + f_y^2}},$$

$$H = \frac{(1 + f_x^2) f_{yy} - 2 f_x f_y f_{xy} + (1 + f_y^2) f_{xx}}{2(1 + f_x^2 + f_y^2)^{3/2}}, \quad \mathbf{K} = \frac{f_{xx} f_{yy} - f^2 xy}{(1 + f_x^2 + f_y^2)^2}, \quad \Gamma_{ij}^k = \frac{z_{ij} z_k}{1 + z_1^2 + z_2^2}.$$

From now on, we will describe locally piecewise smooth surfaces using "patches", which are described in terms of Taylor developments of order 5 for each PS-surface. The intrinsic characterisation is performed using the principal curvatures, which in this case are easily computed in terms of the Hessian of the Monge form. This approach significantly simplifies the second order term of the development:

$$z = f(x, y) = \frac{1}{2}(\kappa_1 x^2 + \kappa_2 y^2) + \frac{1}{3!} \sum_{j=0}^{3} \binom{3}{j} b_j x^{3-j} y^j +$$

$$+ \frac{1}{4!} \sum_{j=0}^{4} \binom{4}{j} b_j x^{4-j} y^j + \frac{1}{5!} \sum_{j=0}^{5} \binom{5}{j} b_j x^{5-j} y^j + O((x, y)^5),$$

where Landau's large O refers to the higher degree terms. After a suitable translation and rotation, any point on the surface can be represented in this way. Therefore, it is sufficient to focus on a small area around the origin, which is where the development is considered.

We can then begin with the study of the evolution of the surface. To do so, we consider the uniparametric family of surfaces $\{S_t\}$ parametrized by t, which is often referred to as "time" or "scale". Locally, such a family can be represented in Monge form as:

$$S_t = \{(x, y, z) \ \mid \ z = F(x, y, t)\}$$

At time t, we deform the surface S_t along the normal direction N_t of each point at a rate of β:

$$\frac{dS_t}{dt} = \beta N_t$$

expressed in terms of a first order approximation. From Monge's notation, this equation becomes:

$$S_{t+\Delta t} - S_t = (\Delta x, \Delta y, \Delta z) = \beta \frac{(-F_x, -F_y, 1)}{\sqrt{1 + F_x^2 + F_y^2}} \Delta \cdot t + O(\Delta t)$$

where $\Delta z = \Delta F = F_x \Delta x + F_y \Delta y + F_t \Delta t + O(\Delta t)$. Thus, when $\Delta t \to 0$,

$$F_t = \left(\frac{\beta \Delta t}{\sqrt{1 + F_x^2 + F_y^2}} - F_x \Delta x - F_y \Delta y \right) / \Delta t + O(\Delta t)/\Delta t = \beta \sqrt{1 + F_x^2 + F_y^2}.$$

If we assume that the initial surface S_0 is described in Monge form as $z = f(x, y)$, we obtain the initial value problem:

$$F_t(x, y, t) = \beta \cdot \sqrt{1 + F_x^2 + F_y^2},$$
$$F(x, y, 0) = f(x, y).$$

For a small t, we can approximate the solution as:

$$F(x, y, t) = F(x, y, 0) + F_t(x, y, 0) \cdot t + O(t) = f(x, y) + \beta \cdot \sqrt{1 + f_x^2 + f_y^2} \cdot t + O(t).$$

This approximation is valid for the problem presented in this document, as facial gestures are most of the time performed in little more than a second, so the time in which the deformation occurs is small enough for this approximation of the solution to be adequate.

Definition 4.1. *The approximation of the solution to the deformation process described above is known as* ***curvature flow*** *if the term β is replaced by one of the curvatures (principal, mean or total). In particular, the most relevant ones are:*

- ***Mean curvature flow****:*

$$F(x, y, t) = f(x, y) + H(x, y) \cdot \sqrt{1 + f_x^2 + f_y^2} \cdot t + O(t)$$

- ***Principal curvature flow****:*

$$F(x, y, t) = f(x, y) + K_i(x, y) \cdot \sqrt{1 + f_x^2 + f_y^2} \cdot t + O(t),$$

  being called K_i flow for each of the respective cases, where $K_i(x, y)$ is a function associated to the principal curvatures.

The main difficulty in solving this problem is that the equation to be solved is a non-linear parabolic Partial Differential Equation (PDE). Even assuming that the surface is smooth, the deformation of the given family of surfaces could give rise to singularities. In particular, the principal curvatures are non-differentiable functions at the umbilic points, so these points will become singularities under the principal curvature flows.

The existence and uniqueness of such solutions is a non-trivial problem, since it involves the search for **viscosity solutions** for PDEs. Therefore, we will only outline here the main idea justifying the existence and uniqueness of such solutions, and the concrete details can be found in [17].

In order to give the existence and uniqueness of solutions in cases such as the equation presented, it is sufficient to apply Theorem 6.8 of [17], concerning the global existence of solutions for degenerate elliptic geometric equations. This theorem can be applied if we consider the uniparametric family of surfaces $\{S_t\}$ as level surfaces of a given function u, $S_t = \{(x, y, z) \mid u(t, x, y, z) = 0\}$, which we know thanks to the proposition 3.3 (Meusnier's alternative formulation).

4.1.1 Good flows vs. Bad flows

A "good" flow must always simplify a surface. This means that, as t increases (over time), no new features or singularities are generated; quite the contrary. This monotonic descent of the main significant facts of the surface allows to give a hierarchical representation of the surface.

For the two dimensional case (plane curves), we take the flow

$$\frac{dC_t}{dt} = \kappa N_t,$$

where $C_t = \{(x, y) \mid y = F(x, t)\}$ is a family of curves, κ the curvature and N_t the normal direction of C_t. Analogous to the analysis performed in the case of the family of uniparametric surfaces, we obtain that this flow leads to the equation

$$F_t = \frac{F_{xx}}{1 + F_x^2}$$

As an example, if we consider the curve $y = x^4$, which has a double inflection point at the origin, we see that:

$$F(x, t) = x^4 + 12x^2t + O(x^4, tx^2),$$
$$\frac{\partial^2 F}{\partial x^2} = 0 \Leftrightarrow 12(x^2 + 2t) + O(t, x^2) = 0.$$

from which we see that, for this simplification, there are two inflection points if $t < 0$; while for $t > 0$ there are none. Therefore, the flow does not generate inflection points, but eliminates them. Likewise, neither does it generate "vertices" (points where the curvature takes extreme values). We can then say that, for this case, the chosen flow is **good**.

The three-dimensional case, which is the one we are interested in, has an analogous treatment. The only difference is that in this case the singularities that may arise are parabolic points, crests, umbilical points and Gaussian cusps (points where the curve defined by the Gauss map presents a cusp).

4.2 Local effect of curvature flows

Having defined what a flow is and, more specifically, what we consider to be a good flow, we will analyse the effect of the flows presented on the singularities already defined in the previous chapter: parabolic points, ridges and umbilical points. When we refer to the "**loops**" of these, we mean the propagation of this singularity over time (since, for example, the temporal sequence of a gesture is based on deforming the surface to eventually return to the initial position of the surface).

It should be noted that this study will be carried out locally and will focus on generic surfaces. Therefore, the characteristics appear and change in a **stable** way (the pattern on the basis of which the characteristics of the surface are altered is not modified in the event of slight perturbations). However, in the case of surfaces of revolution such a treatment would not be valid, since the symmetries that characterise them would be affected.

4.2.1 On parabolic points

Generally, and without going into further detail, for a uniparametric family of surfaces, parabolic curves can only be created through the transition called A_3 [12]. At the moment it occurs, there exists (locally) a single parabolic point, which can disappear or become a parabolic loop.

The set of red parabolic points (those at which $\kappa_2 = 0$) of S_0 around the origin satisfy:

$$0 = f_{xx}f_{yy} - f_{xy}^2 = \kappa_1(b_2x + b_3y) + (\frac{1}{2}\kappa_1 c_2 + b_0b_2 - b_1^2)x^2 +$$

$$+(\kappa_1 c_3 + b_0b_3 - b_1b_2)xy + (\frac{1}{2}\kappa_1 c_4 + b_1b_3 - b^2)y^2 + O((x,y)^2).$$

In case a red parabolic loop is created, there should be a moment when the transition A_3 takes place at some point on the surface. In order to make the study easier, we assume that this moment is $t = 0$ and the origin is an isolated red parabolic point in S_0 (the analysis would be analogous if it were of blue type). Therefore, $b_2 = b_3 = 0$ and the above relation is reduced to the quadratic form only

$$Q(x,y) = (\frac{1}{2}\kappa_1 c_2 - b_1^2)x^2 + \kappa_1 c_3 xy + \frac{1}{2}\kappa_1 c_4 y^2,$$

which is positive definite, or negative definite, around the origin.

Let us look at the influence that the flows presented in the previous section can have:

- **Mean curvature flows:** Since we already know the value of the flow, we only have to substitute in this expression the flow considered by the mean curvature and take the approximation of the explicit representation given previously. Thanks to this, we obtain that the parabolic set of S_t is given by:

$$0 = F_{xx}F_{yy} - F_{xy}^2 = (\frac{1}{2}\kappa_1(c_2 + c_4) + O(x,y))t + O(t) +$$

$$+(\frac{1}{2}\kappa_1 c_2 - b_1^2)x^2 + \kappa_1 c_3 xy + \frac{1}{2}\kappa_1 c_4 y^2 + O((x,y)^2).$$

  For a given t, we see that the set of parabolic points satisfies:

$$t = -\frac{Q(x,y)}{\frac{1}{2}\kappa_1(c_2 + c_4)} + O((x,y)^2)$$

  n this case, the sign of the quadratic form depends on that of $\kappa_1 c_4$:

  - Si $\kappa_1 c_4 > 0 \Rightarrow \frac{1}{2}\kappa_1 c_2 - b_1^2 > 0 \Rightarrow \kappa_1 c_2 > 0$. Therefore, $\kappa_1(c_2 + c_4) > 0$ and the sign on the right-hand side of the expression is always negative. Thus, for a sufficiently small $t > 0$, no red parabolic loop is generated.
  - If $\kappa_1 c_4 < 0$, the sign of the right-hand side can become positive for some types of surfaces, which would result in red parabolic loops.

The first case refers to when a hyperbolic zone appears or disappears within an elliptical region, while the other is the opposite assumption. Therefore, under this flow no hyperbolic regions can originate, although elliptic regions can be created.

- **Principal curvature flows:** We consider the K_2-flow, which we can express around the origin as:

$$K_2(x,y) = (\frac{c_2}{2} - \frac{b_1^2}{\kappa_1})x^2 + c_3xy + \frac{c_4}{2}y^2 + O((x,y)^3),$$

for let us remember that $\kappa_2 = 0$ being a parabolic point. As before, we can obtain the flow expression to give the parabolic set of S_t as:

$$0 = F_{xx}F_{yy} - F_{xy}^2 = (\frac{1}{2}\kappa_1 c_4 + O(x,y))t + Q(x,y) + O(t,(x,y)^2).$$

For a given t, the set of parabolic points must satisfy:

$$t = -\frac{Q(x,y)}{\kappa_1 c_4} + O((x,y)^2).$$

We see that in this case numerator and denominator always have the same sign, so that for $t > 0$ small, the isolated red parabolic point is always eliminated without generating a loop.

To summarise, we see that only parabolic loops (blue or red) could be generated under mean curvature flows. In particular, while hyperbolic regions cannot be generated inside elliptic regions, elliptic zones can be created inside hyperbolic areas.

4.2.2 On ridges

In this subsection we will confine ourselves to the study of ridges that are not umbilical points, as we will deal with that case immediately afterwards. As before, we will focus on the study of red-type ridges, the case of blue ridges being analogous.

Let K_2 be the minor principal curvature function and D_2 its associated principal direction. Thanks to this, we can define the condition that the red ridges fulfil, since they are maxima and minima of the curvature lines:

$$\nabla K_2(x,y) \cdot D_2(x,y) = 0.$$

As a consequence it follows that, for a sufficiently small neighborhood at the origin, the equation corresponding to these points is:

$$0 = b_3(\kappa_1 - \kappa_2) - (3b_1b_2 - (\kappa_1 - \kappa_2)c_3)x - (3b_2^2 - (\kappa_1 - \kappa_2)(c_4 - 3\kappa_2^3))y + Q(x,y) + O((x,y)^2),$$

where the function representing the quadratic terms is:

$$Q(x,y) = \alpha x^2 + \gamma xy + \left(\frac{1}{2}d_5(\kappa_1 - \kappa_2) - \frac{9}{2}b_2c_3 + \frac{6b_1b_2^2}{\kappa_1 - \kappa_2} - 9(\kappa_1 - \kappa_2)\kappa_2^2 b_3 - \frac{4b_2^2b_3}{\kappa_1 - \kappa_2}\right)y^2$$

in which we have only shown the coefficients relative to y^2 to lighten the representation, as they are the only ones we will use in the specific cases we consider for our analysis associated with the flows.

Generally, for a family of surfaces, ridges can only be created or destroyed by means of **Morse functions**[2] (for more information, see [11] and [13]). At the time of transition, there is (locally) an isolated ridge, which may disappear or become a ridge loop.

Suppose then that S_0 is the surface at the time of the transition and the origin is an isolated red ridge. Then, the linear terms of the above equation cancel out, allowing us to see that:

$$b_3 = 0, \quad 3b_1b_2 = (\kappa_1 - \kappa_2)c_3, \quad 3b_2^2 = (\kappa_1 - \kappa_2)(c_4 - 3\kappa_2^3).$$

Therefore, this equality is reduced to simply:

$$Q(x, y) + o((x, y)^2) = 0,$$

where:

$$Q(x, y) = \alpha x^2 + \gamma xy + \frac{1}{2}(d_5(\kappa_1 - \kappa_2) - \frac{15b_1b_2^2}{\kappa_1 - \kappa_2})y^2,$$

being positive definite, or negative definite, around the origin.

Let us analyse the influence that the flows already presented can have:

- **Principal curvature flows:** We can describe the curve of red ridges on a surface S_t as:

  $$\nabla K_2(x, y, t) \cdot D_2(x, y, t) = 0,$$

  which, thanks to what we have seen above, is also expressed as:

  $$0 = Q(x, y) + (d_5(\kappa_1 - \kappa_2) - \frac{15b_1b_2^2}{\kappa_1 - \kappa_2})t + O(t, (x, y)^2).$$

  For a given t, these points satisfy:

  $$t = -\frac{Q(x, y)}{d_5(\kappa_1 - \kappa_2) - \frac{15b_1b_2^2}{\kappa_1 - \kappa_2}} + O((x, y)^2).$$

  The denominator and the coefficient of y^2 of the quadratic form will always have the same sign. Since $Q(x, y)$ is (locally) positive or negative definite, t will always be negative near the origin. Therefore, when $t > 0$ there are no ridges and the K_2-flow cannot then generate any red ridges. Analogously, the same is true for the K_1-flow and the blue type ridges. In short, they do not generate ridge loops.

- **Mean curvature flows:** The calculations of this assumption would be similar to those already seen for the case of principal curvature flows. For the sake of brevity, we will only mention that the mean curvature flow can move in any direction, which may or may not generate ridge loops.

[2] A **Morse function** is one that has no degenerate critical points.

4.2.3 On umbilical points

Lastly, we have the umbilic points, which we recall are those in which the ridges "change colour". Apart from this fact, the following alternative characterisation of umbilical points will be useful in this subsection.

Proposition 4.2. *A point is umbilic iff the coefficients of the first two fundamental forms are linearly dependent on each other.*

Proof. Expressed alternatively, the condition of linear dependence between the coefficients of the fundamental forms can be expressed as:

$$\operatorname{rg}\begin{pmatrix} E & F & G \\ e & f & g \end{pmatrix} = 0 \Leftrightarrow \begin{cases} gE - eG = 0, \\ fG - gF = 0. \end{cases}$$

The last two equations are immediately obtained thanks to the local expression of principal curvatures (Weingarten equations), since it is sufficient to consider the matrix of the Weingarten map expressed in diagonal form, so that both terms of the secondary diagonal cancel out. Moreover, the fact that the point is umbilic means that both principal curvatures (the elements of the diagonal) must also be zero. From these relations, we obtain the desired characterisation. □

The umbilical points are always created or vanish in pairs, which can occur when the family of surfaces undergoes a non-verse transition labelled in Arnold's terminology as D_4 [13]. Suppose that, at the time the transition occurs, the origin is a double umbilic point in S_0. Such a surface can be represented as:

$$z = f(x, y) = \frac{1}{2}\kappa(x^2 + y^2) + \frac{1}{6}(b_0x^3 + 3b_1x^2y + 3b_2xy^2 + b_3y^3) + O((x, y)^3)$$

where the coefficients satisfy:

$$\begin{vmatrix} b_0 - b_2 & b_1 - b_3 \\ b_1 & b_2 \end{vmatrix} = 0.$$

For the sake of simplicity, we can assume that $b_1 = b_2 = 0$ by simply rotating axes.

As we have seen in the proof of the previous proposition, we can characterise the umbilic points thanks to the relations obtained by means of the Weingarten equations. Moreover, since we can substitute the coefficients of the second fundamental form by the second order derivatives of F, we obtain a characterisation analogous to that of the previous subsections of the umbilic points in terms of the Taylor developments of these functions applied to the aforementioned equations. We will only present this representation for flows at a specific time t.

This time we will consider flows somewhat different from those previously analysed, due to the particularities caused by the umbilic points. To do so, what we will do is to consider a new term that replaces β in the approximation of the solution to give a curvature flow, which we will call **generalised mean curvature flow**:

$$H_n(x,y) = \left(\frac{K_1^n(x,y) + K_2^n(x,y)}{2}\right)^{1/n}$$

This function can be obtained from the mean and total (Gaussian) curvatures. Therefore, its Taylor development around the origin can also be obtained from those of these functions. Omitting these details, the final result is:

$$H_n(x,y) = \kappa + \frac{1}{2}(b_0x + b_3y) + (-\kappa^3 + \frac{1}{4}c_0 + \frac{1}{4}c_2 + \frac{(n-1)b_0^2}{8\kappa})x^2 +$$
$$+(\frac{1}{2}c_1 + \frac{1}{2}c_3 - \frac{(n-1)b_0b_3}{4\kappa})xy + (-\kappa^3 + \frac{1}{4}c_2 + \frac{1}{4}c_4 + \frac{(n-1)b_3^2}{8\kappa})y^2 + O((x,y)^2).$$

Returning to the characterisation of umbilical points in terms of the flow, for a specific instant t, we would obtain:

$$t = -\frac{2\kappa(2b_0b_3c_2 + b_0^2c_3 + b_3^2c_1 - 2\kappa^3b_0b_3)}{b_3^2(2\kappa c_1 + 2\kappa c_3 - (n-1)b_0b_3)}x^2 + O(x^2).$$

For a generic surface, the right-hand term of this equality can be either positive or negative, so the flow could move in both directions. This means that pairs of umbilical points can both be created and destroyed.

Thanks to this new flow, we can obtain the flows we have been analysing throughout the chapter:

- **Mean curvature flows:** Case $n = 1$. Although the previous calculations were performed for $n > 1$, they are also valid for the case of the usual mean curvature flow. Hence, pairs of umbilical points can be created or destroyed.
- **Main curvature flows:** At the umbilic points, neither K_1 nor K_2 are functions of class C^infty at the umbilic points, so we cannot give their representation as a Taylor series development. Anyway, we see that the K_1-flow is the limiting case when $n \to \infty$ of the H_n-flow defined previously. The K_2-flow also behaves identically. As before, both flows can move in either direction.

4.3 Principal curvature flows over the face

Let us now look at the effect of principal curvature flows on real data of a human face. The experiment is based on data obtained by range devices (lasers) from the face of a young woman, which have first been smoothed to remove possible noise accumulated during data acquisition. These data describe in cylindrical coordinates $r = r(z, \theta)$ the whole head. However, we will focus only on the face and impose Neumann-type boundary conditions ($\frac{\partial r}{\partial \theta} = \frac{\partial r}{\partial z} = 0$), in order to obtain a well-defined boundary value problem.

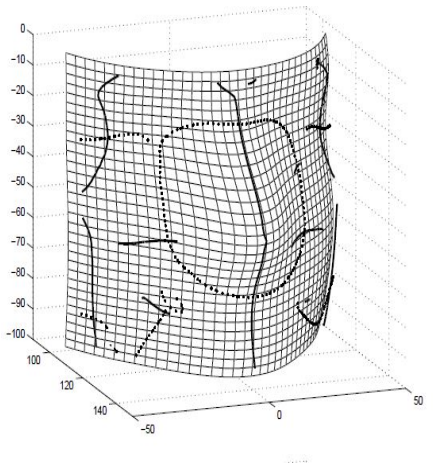

Figure 4.2: 3D map of the scanned face, showing the blue (thick lines) and red (dotted lines) ridges. **Source:** [31]

To better understand the experiment, it should be noted that the curvature lines corresponding to κ_1 are usually horizontal due to the choice of the type of coordinates. As the smoothing process proceeds, the face becomes closer to an ellipsoid with κ_1 maximum at the ridge corresponding to the nose and curvature lines perpendicular to it, crossing both sides of the face. In a fully formed face, these lines encircle around the nose, the eyes and the ends of the mouth. On the other hand, the lines corresponding to the minimum curvature κ_2 tend to be vertical in the soft parts of the face.

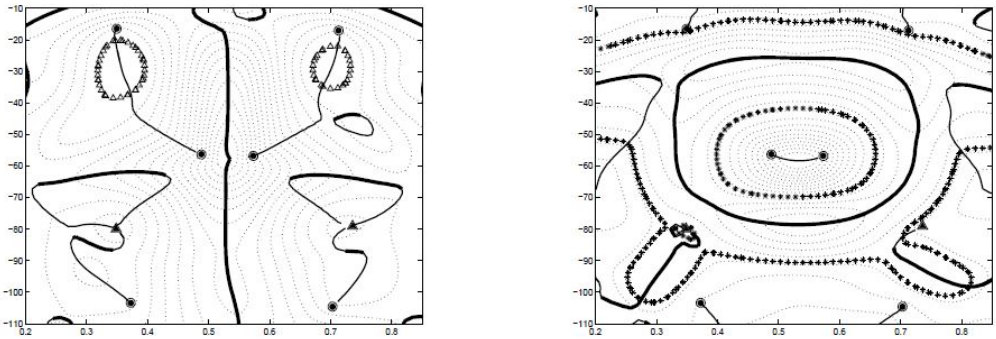

Figure 4.3: Ridges, parabolic lines and level sets of K_1 (left) and K_2 (right). **Source:** [31]

From Figures 4.2 and 4.3 we can better understand what are the different singularities present in the face, which we intend to simplify through the flows already presented.

In particular, the idea is that the flows corresponding to the principal curvatures simplify the surface through their associated principal directions. In fact, under the K_1-flow the face in the horizontal direction tends to adopt a more circular shape, while in the vertical direction it retains the original wavy curve caused by the eyes, nose and mouth;

reminiscent of the basic sketches used by artists to start their drawings. In contrast, with the K_2-flow, the face tends to flatten vertically, while horizontally there is a single peak along the nose, so that after a while the face will end up resembling a folded piece of paper. The effect of both can be seen in Fig. 4.4.

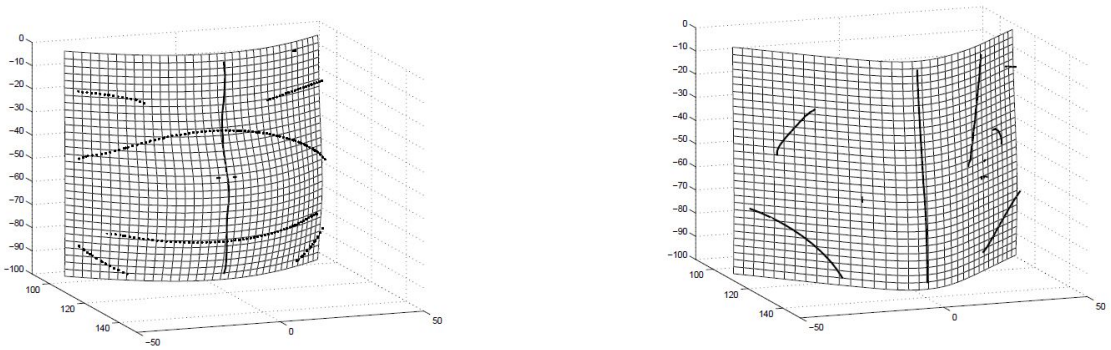

Figure 4.4: The face after passing through the K_1 (left) and K_2 (right) flows at the instant $t = 1000$. **Source:** [31]

Both flows end with parabolic loops. We also observe that the K_2-flow originates a blue parabolic loop near the boundary of the face. Although this is certainly a new structure, it is created on a practically flat part of the face, where the cheek interacts with the imposed Neumann boundary conditions, so it is not a new structure as such. Furthermore, in both principal curvature flows, a pair of umbilical points can be created or removed. All these facts can be seen in Figs. 4.5 y 4.6.

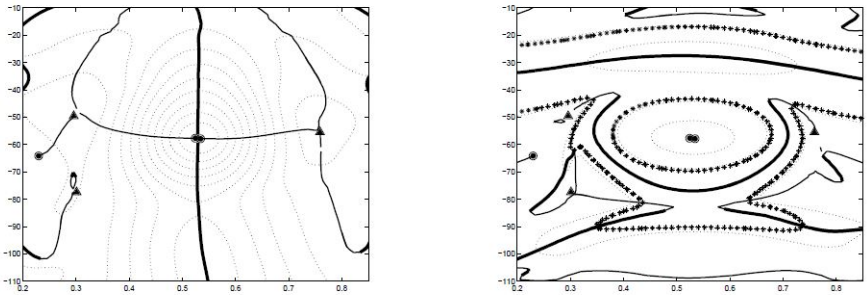

Figure 4.5: The face after passing through the flow K_1 at time $t = 100$. **Source:** [31]

Focusing on this last phenomenon, concerning the behaviour of the umbilical points, we can see in the figure 4.5 that the pair of umbilical points of the nose has come very close after passing through the flow corresponding to the maximum curvature. Although this could be interpreted as a result of the numerical simulation, we will show that this behaviour is common to singularities of this type.

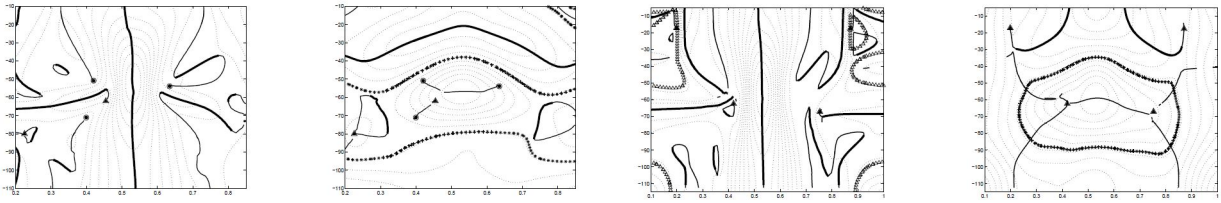

Figure 4.6: The face after passing through the K_2 flow at $t = 100$ (left) and $t = 250$ (right). **Source:** [31]

Proposition 4.3. *Given a pair of symmetric umbilical points on a ridge, both will approach each other after passing through the flow corresponding to the maximum principal curvature. In particular, they will eventually evolve into a single degenerate umbilical point.*

Proof. To simplify the calculations, we assume that the surface $z = f(x, y)$ is symmetric on both axes; $(x, y) \to (-x, y)$ and $(x, y) \to (x, -y)$. Therefore, the x and y axes are each a red and blue ridge, respectively. Moreover, thanks to this symmetry we see that in Monge's form only even-order terms are preserved:

$$z = f(x, y) = \frac{1}{2}\kappa_1 x^2 + \frac{1}{2}\kappa_2 y^2 + \frac{1}{24}(c_0 x^4 + 6c_2 c^2 y^2 + c_4 y^4) +$$

$$+\frac{1}{6!}(e_0 x^6 + 15e_2 x^4 y^2 + 15e_4 x^2 y^4 + e_6 y^6) + ...$$

Therefore, the two main directions are these axes. Having seen this, let us return to the idea of the proof. Suppose there are two umbilic points near the origin on the x-axis. We have then the following condition:

$$c_2 - c_0 + 2\kappa_1^3 > 0$$

In this case, the coordinates of the umbilical points are $(\pm\sqrt{\frac{2(\kappa_1-\kappa_2)}{c_2-c_0+2\kappa_1^3}} + ..., 0)$ If we pass both points through the flow of principal curvature major, we obtain:

$$F(x, y, \Delta t) = F(x, y, 0) + F(x, y, 0)\Delta t + o(\Delta t) = f(x, y) + K_1(x, y)\sqrt{1 + f_x^2 + f_y^2}\Delta t + o(\Delta t) =$$

$$= \kappa_1 \Delta t + \frac{1}{2}(\kappa_1 + (c_0 - 2\kappa_1^3)\Delta t)x^2 + \frac{1}{2}(\kappa_2 + c_2\Delta t)y^2 + \frac{1}{24}(c_0 + (e_2 - 20c_0\kappa_1^2 + 24\kappa_1^5)\Delta t)x^4 +$$

$$+\frac{1}{4}(c_2 + (e_4 + c_0\kappa_2^2 + 2c_2\kappa_1^2 - 4\kappa_1^5 - 4\kappa_1^4\kappa_2 + \frac{4(c_2 - \kappa_1^3)^2}{\kappa_1 - \kappa_2})\Delta t)x^2y^2 + \frac{1}{24}(c_4 + e_6\Delta t)y^4 + O(\Delta t, x^4, y^4).$$

Thus,

$$\frac{\partial(\kappa_1 - \kappa_2)}{\partial t} = c_0 - c_2 - 2\kappa_1^3 < 0,$$

which brings umbilical points closer together over time. We can also look at the second derivative, for which we will consider the denominator of the first component of the coordinate of each umbilical point:

$$\frac{\partial(C_2 - C_0 + 2K_1^3)}{\partial t} = b(x, y) + \frac{4}{\kappa_1 - \kappa_2}(c_2 - \kappa_1^3)^2,$$

where the function:

$$b(x, y) = e_4 - e_2 + 26c_0\kappa_1^2 + c_0\kappa_2^2 + 2c_2\kappa_1^2 - 40\kappa_1^5 - 4\kappa_1^4\kappa_2,$$

we see that it is bounded by the coefficients of z. Therefore, when $\kappa_1 - \kappa_2$ is small enough:

$$\frac{\partial(C_2 - C_0 + 2K_1^3)}{\partial t} > 0.$$

Thanks to the two conditions we have indicated, we see that, if we apply the K_1-flow, both umbilical points will approach the origin over time[3]. □

[3]In the limiting case they will eventually become a single degenerate umbilic point with index $+1$ or -1, depending on the type of initial umbilic point pair.

Chapter 5

Variational approach

Having seen the global evolution of the face surface over time through the use of curvature flows, in this chapter we will give an alternative and complementary view to that approach in terms of "characterisation of sphericity" and "lack of sphericity" as responsible for variations in shape. This view is based on analysing the similarity or difference of the surface (in our case, the face) to facilitate its modelling in these terms.

This approach is based on segmenting the face as a set of PS-models associated with it. Such model identification can be reformulated as an optimization problem. A first classification distinguishes between convex and non-convex optimization. In the former case, linear-type strategies provide general methods; the latter is much less tractable and often only approximate solutions are available. The adjustment of their spatio-temporal evolution and the "persistence" of appearances is an extension that is dealt with in terms of Variational Analysis. The initial problem consists of identifying the most appropriate functional, imposing natural constraints, characterising the structural equations and developing methods for exact or approximate resolution while minimising error.

The relationship between Differential Geometry and Variational Calculus is ancient and develops initially in the 18th century with the Bernouilli brothers, L. Euler and J. Lagrange as consecutive central figures. The first general formulation is due to Euler; while the adaptation to problems of Analytic Mechanics is due to Lagrange and Legendre, giving rise to the integral formulations of Classical Mechanics associated with the minimisation of a quadratic functional. The classical "examples" correspond to the minimisation of length (geodesics), area (minimal surfaces) or some energy functional (from Newton to Yang-Mills).

5.1 Willmore energy

The Wilmore energy flow allows to evaluate the "lack of sphericity" of a PS-surface. It is therefore well suited to evaluate the variation of the radii of curvature in osculating spheres to the surface, as defined after Meusnier's Proposition. The first step is to characterise the sphericity of a piece of surface.

The initial motivation for introducing the Wilmore energy flow comes from the work of S. Germain (1821-1826), where he models the elasticity of a surface in 3D space in terms of (twice) the average curvature $2H = \kappa_1 + \kappa_2$ (the trace of the curvature matrix at each point). Elastic models for the dynamic analysis of gestures motivate the introduction of a global version of this result: the Willmore energy and the corresponding associated flow. Although there are several equivalent definitions of these concepts, which we will see throughout the chapter, we will begin with one that involves the mean and total (Gaussian) curvatures.

Definition 5.1. *The **Willmore energy** of a surface S is defined as:*

$$\mathcal{W}(S) = \int_S (H^2 - \mathbf{K})\, dA = \frac{1}{4}\int_S (\kappa_1 - \kappa_2)^2\, dA$$

5.1.1 Gauss' theorem for spherical mappings

The above definition involves two terms that can be separated into two integrals. For the calculation of the flow, it would be most useful to reduce this expression as much as possible, so that one of the two parts does not vary. This reduction can be applied in a simple way to the particular case of the human face. If we ignore the most relevant "holes" for facial gestures (corresponding to eyes and mouth), the simplest topological model of the head is a topological sphere $\mathbb{S}^2$. This will allow us to simplify the part defined by the total curvature. For this purpose, we recover the characterisation of the fundamental forms defined in Chapter 3.

Definition 5.2. *The **third fundamental form** of a surface S in the basis of T_pS is defined as:*

$$(III) \equiv \langle L^2 r_u, r_v\rangle = \langle Lr_u, Lr_v\rangle = \langle r_u, L^2 r_v\rangle = \begin{pmatrix} n_u \cdot n_u & n_u \cdot n_v \\ n_v \cdot n_u & n_v \cdot n_v \end{pmatrix}$$

and is usually represented as $n_u^2 du^2 + n_u n_v du dv + n_v^2 dv^2$.

In particular, given a point $p \in S$ and $u_p, v_p \in T_pS$, we can express it in terms of the shape operator as $(III)(u_p, v_p) = d_pN(u_p)d_pN(v_p)$. It is then evident that the third fundamental form of the surface is the **first fundamental form of the Gauss map**. Expressed in terms closer to those of Figure 5.1, it is equal to the principal linear part of the angle growth between the normal vectors to two considered points of the surface. This formulation shows the connection with the Conformal Geometry approach.

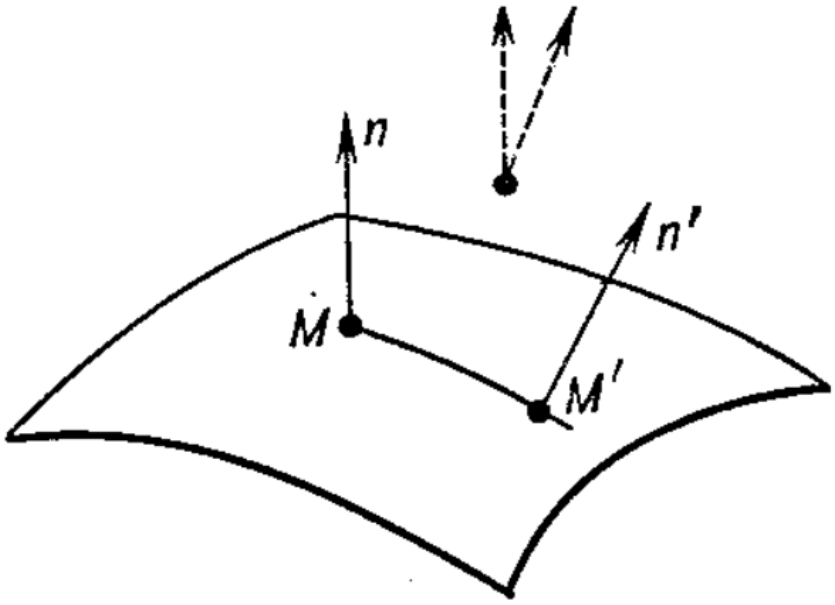

Figure 5.1: Interpretation of the third fundamental form. **Source:** [21]

However, the third fundamental form is completely determined by the first and the second, as the following proposition demonstrates[1].

Proposition 5.1.

$$\mathbf{K}(I) - 2H(II) + (III) = 0$$

Proof. Given $p \in S$, we will choose the parametrization $r(u, v)$ where r_u, r_v are parallel to the principal directions (eigenvectors corresponding to the eigenvalues κ_1 and κ_2 of the curvature matrix). Then,

$$\langle r_u, r_v \rangle = 0, \quad n_u = -\kappa_1 r_u, \quad n_v = -\kappa_2 r_v.$$

On this basis, we can rewrite, for $a = (a_1, a_2) \in T_pS$, the terms of the previous expression in a simpler way:

$$(I)(a, a) = E(a_1^2) + G(a_2^2), \quad (II)(a, a) = -\langle a, L_a n \rangle = \kappa_1 E(a_1^2) + \kappa_2 G(a_2^2)$$

$$(III)(a, a) = -\langle L_a n, L_a n \rangle = \kappa_1^2 E(a_1^2) + \kappa_2^2 G(a_2^2).$$

We can then develop the calculation of the elements of the formula:

$$\mathbf{K}(I) - 2H(II) + (III) = \kappa_1\kappa_2(E + G) - 2\frac{\kappa_1 + \kappa_2}{2}(\kappa_1 E + \kappa_2 G) + \kappa_1^2 E + \kappa_2^2 G = 0$$

□

[1]This proposition is a particular case of another more general result; **Cayley's Theorem**.

Corollary 5.1.

$$n_u^2 = 2He - \mathbf{K}E, \quad n_u n_v = 2Hf - \mathbf{K}F, \quad n_v^2 = 2Hg - \mathbf{K}G$$

Although this dependence may lead to the idea that (III) has no meaning of its own, this is incorrect. As we have seen, being the first fundamental form of the Gaussian application, we can use it to find the area of a spherical image on the Gaussian sphere in a simple way.

Definition 5.3. *Let $D \subset S$ be a surface domain. The **integral curvature** of D is defined as $\omega(D) = \iint_D \mathbf{K}\, dA$. In particular, if D is contained in a coordinate neighborhood of the local chart (U, φ):*

$$\omega(D) = \iint_D \mathbf{K}(u,v)\sqrt{EG - F^2}\, dudv$$

Theorem 5.1 (Gauss' theorem for spherical mappings)**.**

Suppose that $D \subset S$ has a one-to-one correspondence with a region $D^* = N(D)$ under the Gauss map $N : S \to \mathbb{S}^2$ and the Gaussian curvature has the same sign at every point of D. Then,

$$|\omega(D)| = \iint_{D^*} d\sigma,$$

with $d\sigma$ being the area element of the sphere.

Proof. We consider a parametrization of $\mathbb{S}^2$ given locally by the normal mapping $r(u,v) = N(u,v)$. The area is calculated as:

$$A(D^*) = \iint_{D^*} \sqrt{E_{\mathbb{S}^2} G_{\mathbb{S}^2} - F_{\mathbb{S}^2}^2}\, dudv,$$

where the coefficients of the first fundamental form are those corresponding to the sphere. These coefficients are also expressed in terms of the third fundamental form of the original surface:

$$E_{\mathbb{S}^2} G_{\mathbb{S}^2} - F_{\mathbb{S}^2}^2 = (2He - \mathbf{K}E)(2Hg - \mathbf{K}G) - (2Hf - \mathbf{K}F)^2 = ... =$$

$$= \mathbf{K}^2(EG - F^2) - 2H\mathbf{K}(eG - gE - 2fF) + 4H^2(ef - g^2) =$$

$$= \mathbf{K}^2(EG - F^2) - 2H\mathbf{K}2H(EG - F^2) + 4H^2\mathbf{K}(EG - F^2) = \mathbf{K}^2(EG - F^2)$$

From this, we can prove the requested result:

$$A(D^*) = \iint_{D^*} \sqrt{E_{\mathbb{S}^2} G_{\mathbb{S}^2} - F_{\mathbb{S}^2}^2}\, dudv = \iint_D |\mathbf{K}(u,v)|\sqrt{EG - F^2}\, dudv = |\omega(D)|$$

□

We then have a way of calculating the second term of the Willmore energy thanks to this theorem[2]. In fact, calculating this integral by means of **Stokes' Theorem**, we obtain that this integral is the area of the sphere of unit radius: 4π. Therefore, to study the flow of this energy, this constant term can be ignored.

As a final remark, note that the classical approach to calculating the second part of the integral is usually done by applying the **Gauss-Bonnet theorem**[3]. However, the presentation and development of such a result would require the introduction of topological notions such as the **Euler-Poincaré characteristic**[4] and the **genus**[5].

The above concepts and results facilitate the topological representation of the face using properties of triangulations and their symbolic representations (graphs), which are used in face recognition systems based on elastic gluing of graphs to find the "closest" faces to a given one. The limitations inherent in the length of the paper prevent us from going into further details.

5.1.2 Willmore functional

The classical interpretation of the Willmore energy is that of a measure of the smoothness of a surface, in the sense of determining the energy associated with it, analogous to the area functional. This can be seen more clearly if we return to the definition of the Willmore energy given earlier:

$$\mathcal{W}(S) = \int_S (H^2 - \mathbf{K})\, dA = \frac{1}{4}\int_S (\kappa_1 - \kappa_2)^2\, dA,$$

where at each point we have a first quadratic functional decoupled in terms of the principal curvatures. In particular, if $\kappa_1 = \kappa_2$ (as is the case for the sphere) the Willmore energy is zero. This observation justifies why the Willmore energy measures the "sphericity deffect" of a surface immersed in $\mathbb{R}^3$.

However, since the second term is a topological invariant both for the sphere (Theorem 5.1) and for general surfaces (Gauss-Bonnet), we can simplify this definition, always considering regular, compact and orientable surfaces.

Definition 5.4. *The **Willmore energy functional** of a surface S is:*

$$\mathcal{W}(S) = \int_S H^2\, dA.$$

More generally, if we denote by $SCO(\mathbb{R}^3)$ the set of compact and oriented surfaces in $\mathbb{R}^3$, we can define the prior functional as $\mathcal{W} : SCO(\mathbb{R}^3) \to \mathbb{R}$.

[2]The proved theorem can be seen as a particular case of the **General Stokes Theorem**, which generalises theorems such as the Riemann-Green or Gauss-Ostrogradski theorems to arbitrary manifolds.

[3]For an exhaustive version of the result with its proof, see [16].

[4]The **Euler-Poincaré characteristic** is a topological invariant calculable in terms of the triangulation of a surface. For more details, consult [16].

[5]Intuitively, the **genus** or **topological genus** is the "number of handles" or "holes" of a surface. This invariant is key to describe the types that appear in the topological classification of compact surfaces in $\mathbb{R}^3$.

Definition 5.5. *A **Willmore surface** is a critical point of the functional $\mathcal{W}$.*

The next step is to use variational calculus to see the essential characteristics of these types of surfaces. In particular, we will see that this functional has a global minimum that is already familiar to us. Although this proof has already been carried out by Willmore himself in texts such as [19], [56] or [57]; in this document we will stick to the presentation given in [2]. In that paper, the desired result is proved by making use of the following two lemmas, the proof of which can be found in the document itself.

Lemma 5.1. *Let S be a regular, orientable, connected and totally umbilical surface. Then, S is either a piece of a sphere or a piece of a plane.*

Lemma 5.2. *Let $S \in SCO(\mathbb{R}^3)$, we define the slice of surface with non-zero total curvature to be $S^+ := \{p \in S \mid \mathbf{K}(p) \geq 0\}$. Then, the Gauss map $N : S \to \mathbb{S}^2$ restricted to S^+ is surjective.*

Once we have these results at our disposal, we can give the result for obtaining the global minimum we have previously discussed.

Theorem 5.2. *Let $S \in SCO(\mathbb{R}^3)$; then, it is verified,*

$$\mathcal{W}(S) \geq 4\pi.$$

In particular, equality is given iff $S = \mathbb{S}^2$

Proof. Let S^+ be the part of S with total non-negative curvature. On the one hand,

$$\mathcal{W}(S) = \int_S H^2 \, dA \geq \int_{S^+} H^2 \, dA.$$

Moreover, analogously to how we defined the Willmore energy at the beginning, it is verified that:

$$H^2 - \mathbf{K} = \left(\frac{\kappa_1 + \kappa_2}{2}\right)^2 - \kappa_1\kappa_2 = \frac{\kappa_1^2 - 2\kappa_1\kappa_2 + \kappa_2}{4} = \frac{(\kappa_1 - \kappa_2)^2}{4} \geq 0,$$

so $H^2 \geq \mathbf{K}$ and we can increase the chain of inequalities to:

$$\mathcal{W}(S) = \int_S H^2 \, dA \geq \int_{S^+} H^2 \, dA \geq \int_{S^+} \mathbf{K} \, dA.$$

This last term would be analogous to the one defined in Gauss theorem for spherical mappings if the application considered were a diffeomorphism. However, thanks to the previous lemma, we can guarantee that the Gauss map restricted to this part of the surface ($N|_{S^+}$) is surjective. Therefore, we have the inequality:

$$\int_{S^+} \mathbf{K} \, dA \geq A(N(S^+)) = A(\mathbb{S}^2) = 4\pi,$$

which proves the first part of the theorem.

The concrete case in which the equality $\mathcal{W}(S) = 4\pi$ is given will be given only and exclusively if $H^2 = \mathbf{K}$ in all S or, equivalently, if $\kappa_1 = \kappa_2$ in all S. The latter is analogous to asking for the surface to be totally umbilical. By virtue of Lemma 5.1, fully umbilical surfaces are pieces of plane or sphere. However, since the latter is compact, it must necessarily be a complete sphere. □

As an example, see [2] to see how to compute the Willmore functional of the sphere directly using its usual parametrization.

5.1.3 Application to facial modelling

The above calculations are applicable in the case of considering the modelling of the face as a sphere. In fact, most of the work on the Willmore flow is applied to spherical topological models. A common strategy consists of the following steps:

1. Perform spherical remapping using a robust discretization of the Willmore flow;
2. Decompose the domain of spherical harmonics[6] (radial functions) using an orthonormal basis;
3. Coarse classification on energy descriptors.

However, spherical modelling can be somewhat simple, especially when facial gestures need to be modelled due to the high expressiveness and subtle variations that occur across the entire facial surface. In the simplest possible case, three holes corresponding to both eyes plus the mouth should be considered. These parts are considered because it has been detected that more variations occur in gestures of joy and sadness (wrinkles around the corner of the lips or under the eyelids).

The extension of the methodology previously explained for the spherical case to surfaces with holes has only been addressed in the framework of Riemannian geometry for tori. In fact, considering these three holes, the new model of the face would be the connected sum $\mathbb{T}^2\#\mathbb{T}^2\#\mathbb{T}^2$ of three tori $\mathbb{T}^2 := \mathbb{S}^1 \times \mathbb{S}^1$. The choice of this manifold is justified by the behaviour of analytical functions on the topological support and is reminiscent of simple models of humanoid figures (such as aliens) used in animation projects, as can be seen in Fig. 5.2.

However, the extension of the analysis on a sphere or on a torus to the connected sum of three tori presents significant difficulties (unless one adopts the framework of Conformal Geometry which is beyond the domain of this document). To understand the difficulty, let us look at the steps to be taken to develop an analysis analogous to that of the sphere case on the Willmore functional to the new model.

[6] **Spherical harmonics** are harmonic functions representing the spatial variation of an orthogonal set of solutions of the Laplace equation, expressed in spherical coordinates.

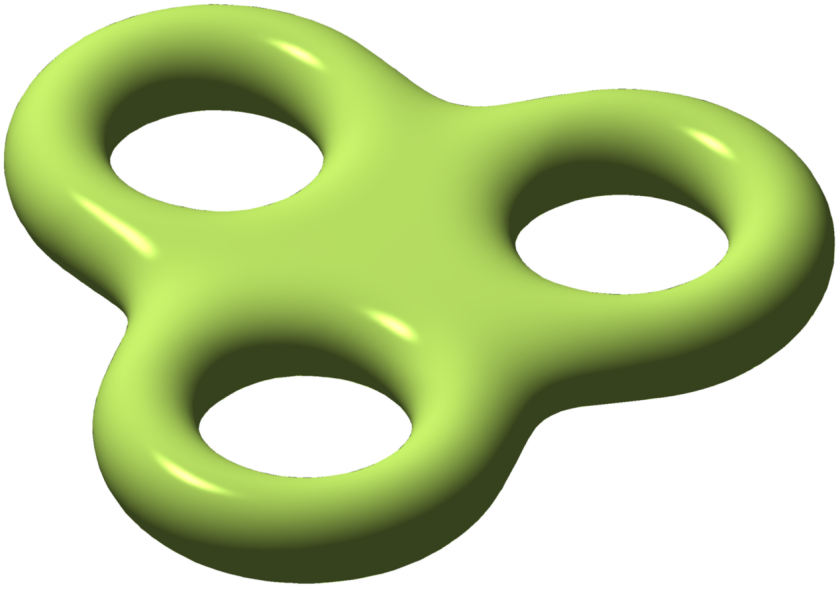

Figure 5.2: Matlab representation of the triple torus generated by Oleg Alexandrov

The general case of the connected sum $\#^g\mathbb{T}^2$ presents a high difficulty for $g \geq 2$. Even for $g = 1$ it gives rise to the famous **Willmore conjecture**, which gives the value of the lower bound of the Willmore energy $\mathcal{W}(M) = \int_M H^2 dS$ of a torus; that is, $\mathcal{W}(M) \geq 2\pi^2$ for $M = \mathbb{T}(r, \sqrt{2}r)$ [33]. For this reason, we will focus only on presenting the results for the torus $\mathbb{T}^2$. For the sake of brevity, we will omit the detailed calculations, all of which can be found at [2].

Proposition 5.2. *The Willmore functional for a torus of revolution $\mathbb{T}(r, R)$, where $r, R \in \mathbb{R}_{>0}$ are the respective minor and major radii of the torus, depends on the ratio between its two radii. Specifically, if we call this ratio $a = \frac{r}{R}$,*

$$\mathcal{W}(\mathbb{T}(r, R)) = \frac{\pi^2}{a\sqrt{1-a^2}}.$$

This functional depends on the ratio between the two radii of the torus, so it is worth asking whether there is an ideal value by which we obtain the "best" torus of revolution (the one that minimises the Willmore functional).

Proposition 5.3. *Among all the tori of revolution $\mathbb{T}(r, R)$, where $r, R \in \mathbb{R}_{>0}$, those that minimize the Willmore energy functional are those that verify $a = \frac{r}{R} = \frac{1}{sqrt2}$. Moreover, the value of this minimum is $2\pi^2$.*

The proof of this result is based solely on finding the minimum of the function defined in Proposition 5.2. The precise calculations can be found in [2].

5.2 Conformal invariance of the Willmore functional

The previous analysis may be too complex to solve the problem to be tackled, especially if we consider that some of the results presented have remained unproven until relatively recently. For this reason, it is convenient to resort to more flexible approaches, such as that of **Conformal Computational Geometry**[7]. **Computational Geometry** combines geometric models, data structures and algorithms to solve problems that arise in different Geometries.

Most of the approach developed in this paper can be adapted to the framework of Conformal Computational Geometry. Throughout the first decade of the 21st century, Gu has introduced and implemented algorithms that simplify initial static models and facilitate their extension to character animation. **Conformal geometry** provides support for modelling facial gestures beyond the initial Euclidean framework that is inappropriate for gestures. The key is that conformal transformations preserve the angles between the most expressive components of the face. In this section we show that not only are angles preserved through conformal applications, but that the Willmore functional is also preserved.

By virtue of the characterisation given in Definition 3.11, conformal applications preserve the angles between curves contained in the starting and arrival surfaces, as an extension of the isometries between metric spaces. An alternative, more explicit version is to use the local parametrizations of the surfaces to redefine it in those terms.

Definition 5.6. *Let $W_1, W_2 \subset \mathbb{R}^3$ be open and connected. A map $\Phi : W_1 \to W_2$ of class C^∞ is a **conformal map** if, for all $p \in W_1$, $d\Phi_p : \mathbb{R}^3 \to \mathbb{R}^3$ is a conformal linear mapping between vector spaces. That is, there exists a differentiable function $\lambda : W_1 \to \mathbb{R}_{\neq 0}$, such that:*

$$\langle d\Phi_p(u), d\Phi_p(v)\rangle = \lambda(p)^2 d\Phi_p\langle u, v\rangle,$$

*for any $u, v \in \mathbb{R}^3$. The function λ is called **conforming factor**.*

Proposition 5.4. *Conformal mappings are local diffeomorphisms.*

Proof. We will use the equivalence that $F : W_1 \to W_2$ is a local diffeomorphism iff dF_p is a vector isomorphism, for all $p \in W_1$. Given a conformal mapping Φ, we compute the kernel of its differential; $\ker(d\Phi_p)$. If $d\Phi_p(v) = 0$. Then

$$0 = ||d\Phi_p(v)||^2 = \langle d\Phi_p(v), d\Phi_p(v)\rangle = \lambda(p)^2 ||v||||^2,$$

and since $\lambda(p) \neq 0$, for all p, then it must be $v = 0$. See, $\ker(d\Phi_p) = \{0\}$, $d\Phi_p$ is a vector isomorphism and Φ a local diffeomorphism. □

[7]For more information on this sub-area, please refer to [24].

Conformal transformations can be understood as a "relaxation" of Euclidean transformations with a large number of applications in Physics and Engineering. Once we have seen their definition in terms of vector spaces, we show three examples of them, to finish by proving that any conformal mapping can be reduced to a combination of them.

Definition 5.7.

- *A map* $M : \mathbb{R}^3 \to \mathbb{R}^3$ *of class* C^∞ *is a* ***rigid motion*** *if, for all* $p \in \mathbb{R}^3$*, it is (composition of transformations) of the form*

$$M(p) = Ap + b,$$

  $where A \in \mathcal{M}_3(\mathbb{R})$ *is a special orthogonal matrix (corresponding to a rotation) and* $b \in \mathbb{R}^3$ *the translation vector.*

- *A map* $I : \mathbb{R}^3_{\neq 0} \to \mathbb{R}^3_{\neq 0}$ *of class* C^infty *is an* ***inversion*** *of centre* 0 *and radius* r *if, for all* $p \in \mathbb{R}^3$*, it can be written as*

$$I(p) = r^2 \frac{p}{||p||^2}.$$

- *A map* $H : \mathbb{R}^3 \to \mathbb{R}^3$ *of class* C^infty *is a* ***homothecy*** *of factor* $\lambda \in \mathbb{R}^3$ *if, for all* $p \in \mathbb{R}^3$*, it is of the form*

$$H(p) = \lambda p.$$

Observation.

- *A rigid motion consists simply of the composition of a rotation and a translation. Moreover, they generate the Euclidean group* $SE(3) := SO(3) \ltimes \mathbb{R}^3$ *and are isometries of ordinary three-dimensional space; that is, they preserve the Euclidean metric and, in particular, angles and volumes.*

- *An inversion makes a reflection of all points through the defined centre, i.e. it is like fixing a sphere of radius* r *and "swapping" its interior and exterior.*

- *A homothecy is a scaling of factor* λ*.*

Proposition 5.5.

a) Rigid motions are conformal mappings, with conformal factor constantly equal to 1*.*

b) The inversions of centre 0 *and radius* r *are conformal mappings, with conformal factor* $\lambda(p) = \frac{r^2}{||p||^2}$*.*

c) Homothecies are conformal mappings with constant factor equal to the ratio λ *of the homothecy.*

Proof. In all cases the proof is based on calculating the differential of the corresponding application, calculating the scalar product of the differential on two different vectors and extracting the value of the conformal factor. We will only prove case c), corresponding to homothecy. The rest can be seen in [2].

Let us calculate the differential of the homothecy $H : \mathbb{R}^3 \to \mathbb{R}^3$ at $p \in \mathbb{R}^3$ for $v \in \mathbb{R}^3$. To do so, we consider a curve $\alpha(t) : (-\epsilon, \epsilon) \to W_1$ that verifies $\alpha(0) = p$ and $\alpha'(0) = v$. Then,

$$dH_p(v) = \frac{d}{dt}|_{t=0}(H(\alpha(t))) = \frac{d}{dt}|_{t=0}(\lambda\alpha(t)) = \lambda\alpha'(0) = \lambda v.$$

Therefore, for any $u, v \in \mathbb{R}^3$, it is verified:

$$\langle dH_p(u), dH_p(v)\rangle = \lambda^2\langle u, v\rangle,$$

so H is a conformal mapping of conformal factor constantly equal to λ. □

Having seen these three types of conformal mappings, we will see that, from them, it is possible to define any type of conformal map as a composition of these. This theorem is very useful for proving the invariance of the Willmore energy functional for conformal transformations.

Theorem 5.3 (Liouville's Theorem)**.**
Every conformal and injective application $\Phi : W_1 \to W_2$, being $W_1, W_2 \subset \mathbb{R}^3$ open, is a composition of rigid motions, inversions and homothecies.

The proof of this result is far from trivial, requiring a solid background in Complex Analysis. The detailed proof can be found at [40] or [48].

With the above tools, we can tackle the proof of the theorem establishing the invariance of the Willmore energy functional by conformal applications.

Theorem 5.4 (Conformal invariance of Willmore functional)**.**
Let $S \in SCO(\mathbb{R}^3)$ and Φ be a conformal and injective map. Then,

$$S' = \Phi(S) \in SCO(\mathbb{R}^3) \text{ and } \mathcal{W}(S) = \mathcal{W}(S').$$

Proof. First, since the surface is compact, we can cover it with a finite number of charts $\{(U_i, X_i)\}_{i=1}^n$ such that

$$\cap_{i=1}^n X_i(U_i) = \emptyset, \quad \overline{\cup_{i=1}^n X_i(U_i)} = S \quad \text{y} \quad \partial \cup_{i=1}^n X_i(U_i) \quad \text{has null measure.}$$

It is therefore sufficient to prove that the functional is conserved for a given parametrization.

Let us see that the image by a conformal and injective map of a compact and orientable surface on $\mathbb{R}^3$ is also conformal and injective. Since Φ is a conformal map, by Proposition 5.4 it is a local diffeomorphism. Moreover, by being injective we also have that it is a global diffeomorphism. Since S is compact, its image by a global diffeomorphism will also be compact, since the mapping is necessarily continuous. In particular, S and S' are diffeomorphic, so this is in turn a surface.

To prove the invariance of Willmore functional, thanks to Proposition 5.5 and Liouville's Theorem, it is sufficient to prove the invariance for each of the types of conformal applications defined above. The proof is straightforward for each of the assumptions, requiring in turn the computation of curvatures and fundamental forms for this operation. In order not to extend the length of the document even further, these calculations are omitted here and can be consulted at [2]. □

5.3 Variational analysis of Willmore functional

Our next objective would be to use Willmore functional to show an effective way of modelling gestures. The strategy is similar to the one presented in the previous chapter: to define a flow that shows how the face varies throughout each gesture. Our approach will be to consider the face as a connected sum of Willmore surfaces, which will always allow us to analyse its state. Therefore, the aim of this section is to characterise the face during gestures as Willmore surfaces.

To do this, we will first give an alternative definition of flow in terms of the normal variation of the parametrization of a surface in terms of local charts.

Definition 5.8. *Let $S \subset \mathbb{R}^3$ be a surface not necessarily compact and a parametrization of S, (U, X). Given $\varphi : U \to \mathbb{R}$ a differentiable function with compact support defined on U, we take the normal variation of X determined by the chart as $\Phi : U \times (-\epsilon, \epsilon) \to \mathbb{R}^3$ given by*

$$\Phi(u, v, t) \equiv \Phi_t(u, v) = X(u, v) + t \cdot \varphi(u, v) \cdot N(X(u, v)),$$

being $N(X(u, v))$ the normal vector to the surface at that point, taking ϵ small enough so that $S_t = \Phi_t(U) \subset \mathbb{R}^3$ is a surface, where $\Phi_t(u, v)$ is a parametrization of it for all $t \in (-\epsilon, \epsilon)$.

Under these conditions, we can consider the region $R = X(V) \subset S$, where $V = \text{sop}(\varphi)$, which verifies $\overline{R} \subset X(U)$ (R is a connected and relatively compact open). Therefore, we can define

$$R_t := \Phi_t(V) \subset S_t.$$

Definition 5.9. ***Willmore's energy flow*** *is defined as the function*

$$w(t) = \mathcal{W}(R_t) = \int_{R_t} H_t^2 \, dA_t,$$

where H_t is the mean curvature of the surface S_t and dA_t the area element of the surface. Moreover, the initial value condition $w(0) = \mathcal{W}(R)$ is satisfied.

We see then that this flow is the gradient introduced in Definition 5.4, whose flow lines satisfy the differential equation already mentioned.[8]. The energy extreme values corresponding to the Willmore functional allow the modelling of "exaggerated gestures", such as those seen in the animation, compatible with the original geometry of the human face.

In particular, our goal will be to compute $w'(0)$ to find out whether R is a Willmore surface in terms of the **Euler-Lagrange characterisation**[9] characterising Willmore surfaces. In order to present such a characterisation, a prior theorem is required, the proof of which requires the following result.

Proposition 5.6 (Jacobi's formula)**.** *Given $A : \mathbb{R} \to \mathcal{M}_2(\mathbb{R})$ of class C^∞, it holds*

$$\frac{d}{dt}(|A(t)|) = \operatorname{tr}\left(\operatorname{adj}(A(t))\frac{dA(t)}{dt}\right),$$

where $\operatorname{tr}(A)$ *and* $\operatorname{adj}(A)$ *are the trace and adjoint matrix of A, respectively.*

Both the proof of this equality, and the prior lemma needed to give such a proof, can be found in [2]. Thanks to this result, we can now give the following theorem, based on the terminology presented in this section.

Theorem 5.5 (First variation formula of the Willmore functional)**.**

$$w'(0) = \int_R \phi(\Delta H + 2H(H^2 - 2\mathbf{K}))\, dA$$

Proof. The proof of this formula is based on the progressive computation of $w(t)$, $w'(t)$ and $w'(0)$. The computation of these integrals would be very lengthy, as it requires obtaining the fundamental forms of the surfaces, as well as their curvatures. During this process, use is made of the previously defined Jacobi Formula to find the area element. The explicit calculations can be found in [2]. □

Once this variation formula has been presented, we can give the desired characterisation of the Willmore surfaces.

Theorem 5.6 (Euler-Lagrange equation for Willmore surfaces)**.** *Let $S \subset \mathbb{R}^3$ be a surface not necessarily compact. We say that S is a Willmore surface iff it verifies the equation*

$$\Delta H + 2H(H^2 - 2\mathbf{K}) = 0.$$

[8]Its corresponding geometric version is the evolution problem **steepest descend**.

[9]In variational calculus and classical mechanics, the **Euler-Lagrange equations** are a system of second-order ordinary differential equations whose solutions are stationary points of a given functional. They were discovered in the 1750s by the homonymous authors. In particular, the application of the E.L. equations is based on considering them as a dynamical system on the considered manifold (surface), in terms of its tangent bundle. For an adaptation of Variational Analysis to this problem, consult [35].

Proof. Suppose that S is a Willmore surface. Being a critical point of the Willmore functional, we have that the derivative of the associated flow is zero, i.e. $w'(0) = 0$. Suppose that $\Delta H + 2H(H^2 - 2\mathbf{K}) \neq 0$. Then,

$$\exists p_0 \in S \quad \text{such that} \quad (\Delta H + 2H(H^2 - 2\mathbf{K}))(p_0) \neq 0.$$

We may assume, without loss of generality, that $(\Delta H + 2H(H^2 - 2\mathbf{K}))(p_0) > 0$ and, by continuity, there will be a neighborhood $V \subset S$ of p_0 where $\Delta H + 2H(H^2 - 2\mathbf{K}) > 0$. But then, taking a smaller neighborhood of that point and multiplying the given positive function by a proper plateau function f, we can choose ϕ such that $\phi = f(\Delta H + 2H(H^2 - 2\mathbf{K}))$ and we have

$$w'(0) = \int_R f(\Delta H + 2H(H^2 - 2\mathbf{K}))\, dA \geq \int_{\mathrm{sop}(f)} f(\Delta H + 2H(H^2 - 2\mathbf{K}))\, dA > 0,$$

which is a contradiction. Hence, $\Delta H + 2H(H^2 - 2\mathbf{K}) = 0$.

Reciprocally, if $\Delta H + 2H(H^2 - 2\mathbf{K}) = 0$, necessarily $H^2 = \mathbf{K}$. Therefore, such a surface is a critical point of the Willmore functional, applying the equivalent definition 5.1. □

This new characterisation makes it possible to extend Willmore's concept of surface even further. In particular, to those surfaces which are not compact, as is the case of planes. In fact, every minimal surface of $\mathbb{R}^3$ is a Willmore surface since $H = 0$. The most striking case is that of the open pieces of spheres, since they are the only Willmore surfaces in $\mathbb{R}^3$ with constant non-zero mean curvature (see [2]).

5.4 Geometric flows

Throughout this chapter we have only analysed the variation of the Willmore energy flow to study the variations suffered by the human face. However, there are other flows whose variation allows us to extract information about the geometry of the face. In this section we will present two of them, without going into the details of how to study their evolution.

5.4.1 Optical flow in video sequences

A gesture is a spatio-temporal succession of postures or configurations of data. Sampling in a video sequence allows each image to be analysed separately, detecting the most significant "facts" as outliers of a functional. A basic strategy for tracking "facts" uses the "Optical Flow", which is based on the "constancy" of the intensity function $I(x, y; t)$ in the grey scale and is expressed as $\nabla I = 0$. To do so, as we will see below, we have to minimize a quadratic functional associated with a "generic perturbation" of the gradient field.

In this section we will only give a first approximation to this study, being able to resort to analysis through works such as [9] and [39]. First of all, let us define the basic concepts and notions to carry out this study.

An object evolving in a video sequence is represented by a spatio-temporal surface. In essence, a video sequence is a succession of images called "frames". The discrete spatial domain representation of each 8-bit greyscale image is given by a **Intensity function** $I : R \to [0, 255]$, where the domain R is a rectangle $[a, b] \times [c, d]$ and $256 = 2^8$ is the number of values the function can take. However, since we are dealing with video sequences, a succession of images must be considered, so it is necessary to include a time dimension in the intensity function.

Definition 5.10. *The **Intensity function** for a video sequence can be defined as*

$$I : R \times [0, D] \to [0, 255],$$

resulting in the intensity (in greyscale) for a particular pixel of an image ($p \in R$) at a given time $t \in [0, D)$; where D is the duration of the video sequence.

The most common information processing strategies are either "dense", "semidense" or discrete, depending on processing capacity and the need for real-time or non-real-time response. However, they are all based on the extraction of "significant facts" isolated over a sampling of 4 or 5 fps (frames per second). The usual significant facts are corners or intensity maxima. Once event localisation and extraction is performed, matching is performed and homologous event tracking is carried out to estimate the trajectories carried out by moving events. All these processes are subject to uncertainty, including errors arising from environmental conditions (e.g. poor lighting), motion characteristics (e.g. of the possibly moving agents or camera) and from the initial phases of video sequence processing and analysis. Therefore, it is necessary to implement **optimization strategies** in each of the phases.

For two images sampled close together, the intensity function I is ideally assumed to be constant, as it is assumed that a pixel can move temporally or spatially between frames, but without changing its intensity during the process.

For this reason, its time gradient $\nabla_t I$, which we rewrite more explicitly as

$$\nabla_t I = \frac{dI}{dt} = v_x \frac{\partial I}{\partial x} + v_y \frac{\partial I}{\partial y} + \frac{\partial I}{\partial t},$$

is taken to be null; see, $\nabla_t I = 0$. In the above expression, $v = (v_x, v_y)$ is a two-component vector field containing the relevant information to estimate the motion.

Definition 5.11. *The **optical flow** is given by the integral curves associated with the cancellation of the gradient field of the intensity function in the grey scale.,*

$$\int_{\Omega} \nabla_t I = 0.$$

To adapt the analysis to discrete data, vector fields are initially assumed to be piecewise linear. Therefore, topological patterns are a deformation of linear patterns of planar ODEs that may have a singularity of source, sink or saddle point type. Each moving region in a video sequence can have a different linear pattern of motion. More realistic topological patterns are described in terms of (generally non-linear) deformations of the linear patterns mentioned above. The movement of moving agents in the scene or of the camera itself gives rise to blurring effects that need to be modelled and corrected. For the adjustment to smooth models, optimisation techniques or, in more advanced models, Variational Calculus are used. We will only consider basic Optimization strategies.

Optimization for optical flow

If $\Delta I := I_2 - I_1$ is the subtraction of two consecutive images, once the outliers have been removed (using the distance L^1, e.g.), the functional to be minimised is given at each point $p_0 = (x_0, y_0)$) by

$$\rho(p_0) = \sum_{p \in R(p_0)} [v_x \frac{\partial I(p)}{\partial x} + v_y \frac{\partial I(p)}{\partial y} + \Delta I(p)]^2 \ ,$$

where usually $R(p_0)$ is a region of 5×5 pixels centered at p_0.

To calculate the vector v representing the optical flow, or at least an estimate of it (in the discretization of the equation), we must solve a system $Wv = -b$ where

$$W = \begin{pmatrix} \sum \partial_x I^2 & \sum \partial_x I \cdot \partial_y I \\ \sum \partial_x I \cdot \partial_y I & \sum \partial_y I^2 \end{pmatrix} \quad \text{y} \quad b = \begin{pmatrix} \sum \partial_x I \cdot \Delta I \\ \sum \partial_y I \cdot \Delta I \end{pmatrix},$$

which is solved by the diagonalization of the matrix W. This is a basic singular value decomposition problem, as presented in Subsection 6.3.1.

Observation. *The optical flow condition can be overly restrictive, as it assumes that the pixel intensity remains constant at all times. To relax this assumption, the previous estimate can be extended by adding an additional term that takes into account temporal variations in illumination, the weight of which is controlled by a parameter β.*

$$\rho(p_0, u) = \sum_{p \in R(p_0)} [v_x \frac{\partial I(p)}{\partial x} + v_y \frac{\partial I(p)}{\partial y} + \Delta I(p)]^2 + \beta u,$$

where u is a scalar field containing the illumination variation.

Optical flow for point clouds

For 3D point clouds from Stereo Vision (spatial or temporal) or 3D laser scans, a similar method is developed using cylindrical coordinates (h, φ). In this case, the matrices appearing in the functional $\rho(p_0)$ are now given by:

$$W = \begin{pmatrix} \sum \|\partial_h I^2\|^2 & \sum \partial_h I \cdot \partial_\varphi I \\ \sum \partial_h I \cdot \partial_\varphi I & \sum \|\partial_\varphi I^2\|^2 \end{pmatrix} \quad \text{y} \quad b = \begin{pmatrix} \sum \partial_h I \cdot \Delta I \\ \sum \partial_\varphi I \cdot \Delta I \end{pmatrix}$$

Tracking 3D point clouds is more complex than tracking significant events in video sequences. Unlike images, the data contained in 3D point clouds are very sparse. The absence of a continuous model as a support suggests a combination of statistical methods and PL-structures associated to chunks (patches) with similar geometrical and kinematic characteristics (modulo a tolerance threshold). This requires a volumetric segmentation into changing regions using both metric criteria (Wasserstein's distance[10]) as well as topological (rough provisional grouping in PL-regions to be refined in later phases).

The generation of continuous volumes from discrete range information supported by point clouds is carried out using a PL-approximation based initially on simplicial structures.[11]. The automatic generation of these grids is carried out using nearest neighbour search algorithms (NN search[12]) with constraints associated with scalar (depth, height) or vectorial (orientation, e.g.) criteria. In the presence of motion, it is necessary to add kinematic constraints (Symplectic and Contact Geometries, e.g.).

To facilitate the application of Differential Geometry models and tools it is necessary to apply a "smoothing" of the information. This is carried out by a relaxation of classical regularization techniques (Tykhonov[13]) to facilitate its computational treatment. The methods and results presented above can be applied to the surface bounding the resulting PS-model.

5.4.2 Volume flows

The objective of 3D video is the generation of moving volumes that can be viewed in real time from a virtual camera managed by each user in an interactive way. Despite the advances made in the first decades of the 21st century, we are still far from achieving this goal from a computational point of view.

[10]The **Wasserstein distance**, also known as the **Kantorovich-Rubinstein metric**, is a distance defined between probability distributions of a given metric space. It is initially introduced to answer optimal transport problems.

[11]A **symplectic manifold** is a pair (M, ω) where M is a differentiable manifold and ω is a closed non-degenerate 2-form (for every non-zero vector u at a point of the tangent space there exists another vector v such that $\omega(u, v) = 0$) in the manifold, called **symplectic form**.

[12]**NN-search** is an optimization problem that consists of finding the point in a given set that is closest (or most similar) to a given one.

[13]See [9] for more details on **Tykhonov's regularization**.

The consideration of moving surfaces as three-dimensional manifolds requires the automatic generation of PL-models, their fitting by algebraic manifolds initially given by T-splines (product of three snakes or rational curves), and the analysis of their spatio-temporal evolution by modification of the control points (extending the active contour[14] approach for curves to the case of deformable surfaces and solids).

The resulting models provide the support for the reprojection of images or video sequences, which must be refined to obtain acceptable results. This requires the application of different criteria (hybrid approach) of topological (pasting and decomposition), metric (to minimise errors), conformal (to maintain consistency of support), kinematic (for compatibility with motion features) and dynamic (to support interaction). The variational approach provides the framework for a unified treatment of all the above issues, although there are open problems in each of these topics.

The most relevant advances at present are related to the synthesis (complementary to analysis) of video sequences based on Artificial Intelligence models and tools. In the framework of Deep Neural Networks (DNN) during the second decade of the 21st century, TensorFlow (PyTorch implementation under Python) has been developed, which provides a multilinear computational approach to the calculation of tensors (estimated by Tensor-Voting), from which trajectories and "heavy" constraints can be incorporated in a natural way.

DNNs provide support for more sophisticated techniques (e.g. Transformers and Stable Diffusion) that facilitate the incorporation of content (following similar principles to those used in EDO and EDP, respectively). The basic idea is to remap the moving three-dimensional reconstructions from 3D Reconstruction and Motion Analysis in Computer Vision. For this, it is necessary to perform a fusion of both sub-areas using Artificial Intelligence tools that facilitate the automatic recognition of "significant facts", from which to propagate the 3D and 2D+1d visual contents to be merged into a 3D+1d volumetric model that evolves in space-time. The analysis and synthesis of facial or body gestures provides a test-bed for integrating models and tools.

The high computational cost of these developments suggests the introduction of coarse-fine optimization criteria to help reduce this cost. This requires the development of elements of Differential Geometry and Variational Calculus for varieties of dimension three that extend the limits of this project, including the appropriate extension of the Willmore flow and its solutions. Except for some partial theoretical aspects, this extension is not yet available and is a challenge for the coming years, both for the mathematical modelling and for a computationally efficient implementation of the corresponding algorithms.

[14] An **active contour**, commonly called a **snake**, is an approximate elastic curve which, when superimposed on an image, deforms from an initial shape in order to conform to incidence and tangency conditions to delimit regions of interest adaptively. For more information, see [3].

Chapter 6

Data-driven strategies

Having presented the model-based approach for the characterisation of the human face, we will now present an alternative approach, which takes as its starting point data obtained from imaging devices (single or multiple digital cameras) or range devices (scanning devices, spatial or temporal stereo vision systems), including extension to the dynamic case (based on video sequences or changing 3D representations). In all cases, the development of continuous models from the discrete digital information provided by the imaging or range devices is required. The availability of individual images of human or animal faces allows the application of interpolation techniques with applications to morphing (gradual transition between images), including interpretation, simulation and animation of facial gestures.

Data-driven strategies are the most popular today and are usually referred as **bottom-up**. The availability or generation of PS-models decreases the computational cost for the management and modification of facial gestures. Therefore, a feedback is needed between the previously presented data-driven strategies and the ones based on mathematical models (which are referred to as **top-down**). One of the current challenges is to develop approaches that can exploit and combine the strengths of both approaches.

6.1 Data capture

The first stage prior to human face recognition is the acquisition of information using imaging or range devices. Image-based capture typically uses an RGB-D (Depth) camera, or two cameras for the capture of volumetric information. We assume that the cameras are **calibrated**, i.e. the internal camera parameters (focal length, camera centre coordinates and related distortions) are known to minimize biases in the interpretation of the data.

In the static case, a geometric pattern (usually given by regularly spaced lines) can be projected onto the human face giving curves contained in a plane (usually orthogonal), which are useful for the estimation of the sectional curvatures already mentioned when presenting Figure 3.4, where the maximum and minimum values at each point are the principal curvatures. The latter method is labelled as **structured light** and the actual capture of the information is based on the use of laser scanning tools (optical-mechanical devices capable of emitting electromagnetic pulses and receiving the reflected signal).

From the difference in position, phase or elapsed time interval, the distance between the instrument and each detected point is calculated. From this information, a dense depth map is generated that allows the curvature to be evaluated from the deformation of the projected pattern. However, it is important to note that the quality of the extracted model depends on the global illumination conditions, which limits the use of these systems to environments with controlled illumination.

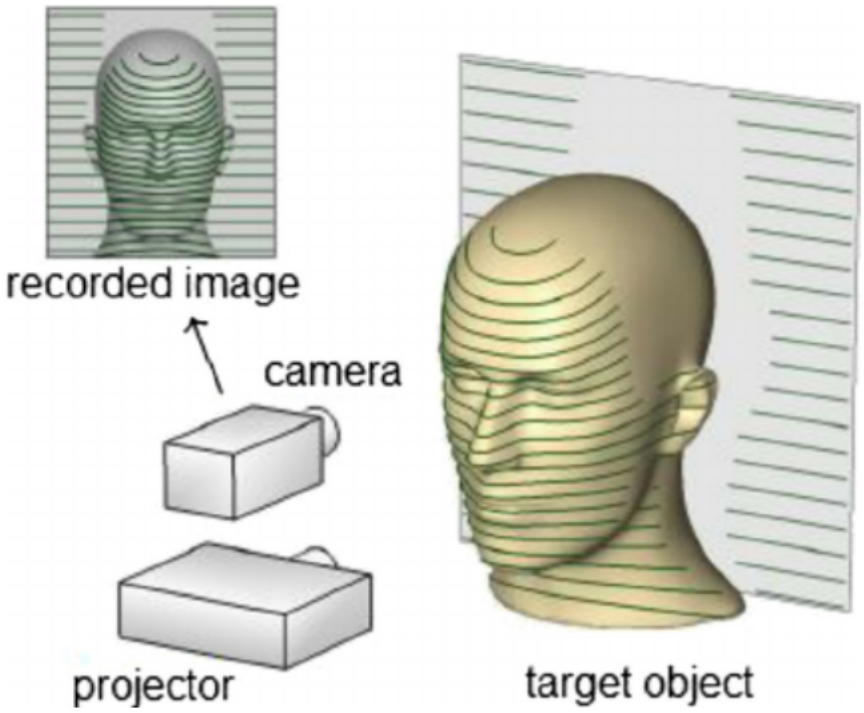

Figure 6.1: 3D scanner based on a structured light system. **Source**: [20]

Stereo Vision, based on two or more simultaneously captured views, allows a depth map to be generated from the comparison between homologous data contained in pairs of neighbouring views (depth is approximated by the inverse of disparity). The underlying principle is the **automatic matching of homologous point pairs** associated with pairs of images and the approximation of depth by the inverse of spatial disparity (difference in location of homologous points).

A digital image can be thought of as a map of coloured pixels or as the projection of a "scene slice" onto the image plane. The latter is called the **geometric image model**. Each capture device provides "lines of sight" that connect each spatial point $\mathbf{P}_i$ with its projection onto the image plane Π_j from the centre $\mathbf{C}_j$ of the j-th camera, $\mathbf{p}_i^j = \pi_{C_j}(\mathbf{P}_i) = \overline{\mathbf{P}_i\mathbf{C}} \cap \Pi_j$. Ideally, the intersection of each pair of lines $\ell_i^1 \cap \ell_i^2$ corresponding to a pair of homologous points $(\mathbf{p}_i^1, \mathbf{p}_i^2)$ provides the 3D coordinates of the points of interest. The homologous lines corresponding to pairs of homologous points verify structural relationships expressed by a matrix which becomes the object to be estimated[1].

The approach based on pairs of views provided by synchronised cameras extends Spatial Stereo Vision to Temporal Stereo. In this approach, pairs of views taken simultaneously are replaced by close pairs extracted from a sampling in the video sequence. In this case, the comparison of homologous data must take into account the apparent distortion associated with the change in the relative location (position and orientation) of the camera with respect to the object. The video-based strategy is often called as **Dynamic Stereo Vision**, as opposed to the strategy based on pairs of simultaneously captured views, which is labelled as **Static Stereo Vision**.

Dynamic Stereo Vision uses a sampling rate of approximately four or five frames per second (fps). The output is a collection of irregularly distributed points to which a PL-strain of an initially triangular mesh is fitted. **Delaunay triangulations**, commonly used in Computational Geometry, provide optimal meshes that maximise the minimum angle (Figure 6.2). Alternatively, structured light-based procedures provide plane curves (usually orthogonal sections), from which the principal curvatures κ_1 and κ_2 are calculated.

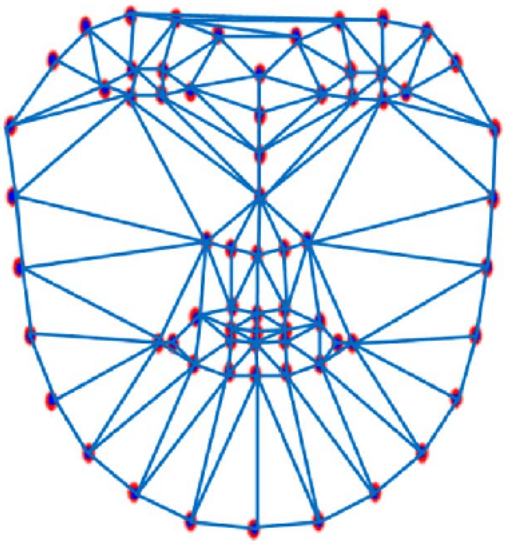

Figure 6.2: Delaunay triangulation of points of interest on the face. **Source**: [36]

[1]For three or more views, it is necessary to replace the matrix by a structural tensor associated with the scene or movement.

Complete coverage of a volumetric object requires several data captures for complex objects and subsequent pasting from the partial overlapping of local data. This strategy is a discretization of the change of charts used in Geometry to move from a local to a global approach. The major advantage of laser scanning devices is that the metric distortion is very small (less than 0.1 mm for laser triangulation devices), and faithfully reproduces a discrete approximation to the object.

6.2 Facial recognition methods

Most face recognition applications focus on the use of static facial images to perform recognition or identification tasks. These images are usually given as greyscale, as the consideration of the colours present in the image implies a higher added computational cost that does not usually compensate for the negligible improvement obtained in the final geometrical results. On the other hand, video sequences are more complex to analyse, due to the fact of having to consider an additional dimension such as time evolution.

In general, volumetric object recognition systems are based on a combination of principles from photogrammetry[2] and Projective Geometry. This combination is called **beam calibration**, as it incorporates metric aspects from photogrammetry, on the one hand, and projective transformations between projective line beams contained in the planes Π_j of the cameras C_j, on the other.

After obtaining the necessary data to carry out the recognition and identification tasks, the next step is to adapt them to models with structural topological constraints such as the human face. Therefore, in this section we will present the main statistical approaches for face recognition, focusing on performing such work on images, due to the higher complexity of the 3D case or 2D+1d moving images associated to video sequences.

While there are a wide variety of methods and approaches for face and gesture recognition in images today, the vast majority of these techniques can generally be placed in one of the following two groups:

- **Holistic representation:** Methods based on considering the whole face as an input element (input). These are the most widely used, as they preserve the configuration of the face (interrelation between the different parts that make it up). The idea behind these methods is to use information reduction techniques in order to give such a description. This leads to the creation of eigenfaces and fisherfaces using techniques such as Principal Component Analysis (PCA), Linear Discriminant Analysis (LDA) or Support Vector Machines (SVM). This will be discussed in more depth in the next section.

[2]**Photogrammetry** uses discrete and sparse information to describe the position, shape and size of an object from a photographic overlay of the object using metric information associated with the device or the environment. The method is based on a simultaneous optimization process associated with distance maps, or triangular grids associated with point clouds.

- **Local feature extraction:** Methods focusing on the identification and extraction of significant facts/features, also known as points of interest. The interest in these points lies in the fact that these local features do not vary, so that we can decompose the face into different components such as eyes, forehead, mouth... The ultimate goal is to represent these regions in a simple and understandable way from local statistics associated to the geometry of the appearance, which are then used to train a structural classifier such as Hidden Markov Models (HMM) or Convolutional Networks (CNN). There are a variety of methods for extracting and storing these significant facts, such as Gabor wavelets (well suited for textures), the Discrete Cosine Transform (DCT) or the use of histograms representing the gradient of location and orientation. A detailed analysis of these and even more methods can be found in [38].

Both methodologies can be combined to mitigate the shortcomings of the other, resulting in more robust methods. For example, holistic representation avoids the loss of information caused by the decomposition proposed by techniques based on the extraction of significant facts, but they do not enjoy the same level of detail as they are based on information reduction techniques such as PCA itself. Some of these mixed techniques are based on the creation of modular "eigenfaces" or a hybrid use of interest point extraction.

In a complementary way, 3D Computer Vision Reconstruction develops continuum-type models (covering the whole image) based on dense information combining basic ideas of Projective Geometry with propagation models. For simplicity, a **central projection model is adopted for each camera**; that is, projection from an ideal point $\mathbf{C}_j$ called the centre of the camera. The projective model of the central projection $\mathbb{P}^3 \to \mathbb{P}^2$ is represented, except for scale, by a matrix $M \in \mathcal{M}_{3\times 4}$; that is, it depends on 11 parameters corresponding to the 6 location coordinates (position and orientation) and the 5 parameters associated with the camera calibration. These are called **extrinsic** and **intrinsic parameters**, respectively.

6.3 Eigenfaces

After having seen the different ways of capturing data and some of the most common approaches for face recognition, we will now present one of the most common techniques for face detection from images; the **eigenfaces**. The idea of eigenfaces, which arises from considering an image as a set of pixels, can have two approaches:

- **Holistic:** Each of the face images obtained during data acquisition is represented as a vector containing all the pixels of the image, finally obtaining a matrix that refers to the set of faces.

- **Bag of features:** Decompose the face into different regions of interest and represent each of these regions as a vector, finally obtaining a matrix representing the whole face.

Both approaches are mutually compatible and backward compatible, since the faces obtained as a union of significant regions can also be represented vectorially and end up forming a matrix representing the set of all the images obtained. Therefore, in both cases we obtain either a matrix $M \in \mathcal{M}_{m\times n}$ or a vector v of size $m \times n$.

Because this information has considerable dimensions, we seek to compress this data in a concise way in order to handle it more easily. To do so, we will resort to calculating eigenvalues, which in turn represent some of its main characteristics. However, to carry out this task, given that the data obtained will most likely result in a matrix that is not square ($m \neq n$), we cannot apply a Jordan decomposition to the matrix, so we will have to resort to other techniques. In particular, rectangular matrices can be interpreted geometrically as elements of a Grassmann manifold[3], and the simplest models of the spatio-temporal evolution of matrices in terms of ODEs over matrix spaces (the simplest are of type Riccati[4]). In this section we restrict ourselves to the static approach only.

6.3.1 SVD

Given a matrix $M \in \mathcal{M}_{m\times n}$, we seek to give a factorization of it in what is known as a **singular value decomposition** (SVD). This factorisation is of the form:

$$M = U\Sigma V^t$$

where U and V are square matrices of order m and n, respectively; while $\Sigma \in \mathcal{M}_{m\times n}$ and its non-zero elements are located on the main diagonal. In addition, we will consider $m \geq n$.

Definition 6.1. *If the rank of a matrix $M \in \mathcal{M}_{m\times n}$, denoted as $\mathrm{rg}(M)$, is its number of linearly independent rows; the **nullity**, $\mathrm{nul}(M)$, is the largest set of linearly independent vectors $v \in \mathbb{R}^n$ for which $Mv = 0$; $\mathrm{nul}(M) = n - \mathrm{rg}(M)$.*

Proposition 6.1.

(I) The matrices M^tM and MM^t are symmetric.

(II) $\mathrm{nul}(M) = \mathrm{nul}(MM^t)$ y $\mathrm{rg}(M) = \mathrm{rg}(MM^t)$

(III) The eigenvalues of MM^t are real and non-negative.

[3] **Grassman manifold** $Grass(k, n)$ is a homogeneous space $GL(n)/(GL(k)timesGL(n-k))$ which parametrizes all linear subspaces L^k of an n-dimensional vector space V of fixed dimension k. For more details, see [1].

[4] A **Riccati equation** is a first order non-linear ODE of the form

$$y'(x) = q_0(x) + q_1(x)y(x) + q_2(x)y^2(x),$$

with $q_0(x), q_2(x) \neq 0$. It has a multitude of applications from engineering to financial mathematics, since it generalises other types of ODEs such as the Bernoulli equation (case $q_0(x) = 0$) or the linear case ($q_2(x) = 0$).

(IV) The non-zero eigenvalues of MM^t are equal to the eigenvalues of M^tM.

Proof.

We will only present the proof of the last statement, while the others can be consulted in [15]. Suppose v is an eigenvector corresponding to a non-zero eigenvalue λ of M^tM. Then, $MM^tv = \lambda v \Rightarrow (MM^t)Mv = \lambda Mv$.

If $Mv = 0 \Rightarrow M^tMv = M^t0 = 0$, but this contradicts the fact that λ was non-zero. Therefore, $MV \neq 0$ and Mv is an eigenvalue of MM^t related to λ. Reciprocally, if λ is a non-zero eigenvalue of $MM^t = (M^t)^tM^t$, it is also a non-zero eigenvalue of $M^t(M^t)^t = M^tM$. □

Thanks to this result we construct the SVD factorisation mentioned above. This process consists of the following steps:

1. **Construct the matrix Σ:** To do this, we first calculate the eigenvalues of the symmetric matrix M^tM, which is square of order n. All eigenvalues are non-negative real and are ordered as:

$$s_1^2 \geq s_2^2 \geq ... \geq s_k^2 > s_{k+1} = ... = s_n = 0$$

   Its positive square roots are called the **singular values** of M and allow us to construct the matrix $\Sigma \in \mathcal{M}_{m\times n}$, which is composed of null values except on the diagonal, where these singular values are found.

2. **Construct the matrix V:** The matrix $M^tM \in \mathcal{M}_n$ is symmetric, so we know that it has a factorization $M^tM = VDV^t$, where D is a diagonal matrix composed by these eigenvalues $d_i = s_i^2$ (ordered in decreasing order) and V is an orthogonal matrix whose i-th column is the eigenvector v_i associated to d_i.

3. **Construct the matrix U:** We consider the positive square roots of the non-zero eigenvalues s_i, as well as their associated eigenvectors v_i; $i = 1, 2, ..., k$. We define:

$$u_i = \frac{1}{s_i}Mv_i, \text{ para } i = 1, 2, ..., k.$$

   As the vectors used for the definition are eigenvectors, this implies:

$$u_i^tu_j = (\frac{1}{s_i}Mv_i)^t\frac{1}{s_j}Mv_j = \frac{1}{s_is_j}v_i^tM^tMv_j = \frac{1}{s_is_j}v_i^ts_j^2v_j = \frac{s_j^2}{s_i}v_i^tv_j = \begin{cases} 0 & \text{si } i \neq j \\ 1 & \text{si } i = j \end{cases}$$

   Thus, the first k columns of U form an orthonormal set of vectors in $\mathbb{R}^n$. However, $m - k$ additional columns are also necessary to finish constructing the matrix $U \in \mathcal{M}_m$. To obtain these columns, we apply the Gram-Schmidt method, since it guarantee that the matrix obtained is formed by m linearly independent vectors.

Proposition 6.2. *The matrices obtained give the factorisation $M = U\Sigma V^t$.*

Proof. We will prove that $MV = U\Sigma$, since the inverse of V is its transpose as this is an orthogonal matrix. The vectors $v_1, v_2, ..., v_n$ form a basis for $\mathbb{R}^n$, $Av_i = s_i u_i$ for i = 1, ..., k; and $Av_i = 0$ for $i = k+1, ..., n$. Only the first k columns of U give rise to non-zero entries in the product $U\Sigma$, so that:

$$AV = A[v_1...v_n] = [Av_1...Av_n] = [s_1u_1...s_ku_k0...0] = U\Sigma$$

□

6.3.2 PCA

Principal Component Analysis (PCA) is a statistical technique used to reduce the dimensionality of a dataset and identify new relevant underlying variables in the data[5].

The idea behind PCA is to project objects onto an orthogonal subspace for their compact representations. Specifically, it involves the mathematical procedure of transforming a number of correlated variables into a smaller number of uncorrelated variables, called **principal components**. Thus, the first of these represents the largest variance of the data, the second represents the second largest variance, and so on.

The procedure to obtain these values, as well as their associated eigenvectors, is based on encoding and decoding the matrix $M \in \mathcal{M}_{m\times n}$ containing the data, seeking to minimize the distance between both representations. This is calculated in terms of the **Frobenius norm** given by $||M||_F = \sqrt{\sum_{i=1}^{m}\sum_{j=1}^{n}|a_{ij}|^2} = \sqrt{\mathrm{tr}(M^tM)}$.

The searched matrix V will be found column by column, estimating the first of them, d^*, as an optimization problem:

$$d^* = \arg\min_d ||M - Mdd^t||_F^2 \text{ subject to } d^td = 1$$

We rewrite the optimization problem in terms of the trace, using its properties:

$$\arg\min_d ||M - Mdd^t||_F^2 = \arg\min_d \mathrm{tr}((M - Mdd^t)^t(M - Mdd^t)) =$$

$$= \arg\min_d \mathrm{tr}(M^tM - M^tMdd^t - dd^tM^tM + dd^tM^tMdd^t) =$$

$$= \arg\min_d \mathrm{tr}(M^tM) - \mathrm{tr}(M^tMdd^t) - \mathrm{tr}(dd^tM^tM) + \mathrm{tr}(dd^tM^tMdd^t) =$$

$$= \arg\min_d -2\,\mathrm{tr}(M^tMdd^t) + \mathrm{tr}(dd^tM^tMdd^t) = \arg\min_d -2\,\mathrm{tr}(M^tMdd^t) + \mathrm{tr}(M^tMdd^tdd^t)$$

Considering the constraint imposed on the optimization problem, we continue with this simplification:

[5]For stochastic processes this technique is known as the **Karhunen-Loève transform** and is based on the Fourier series representation of these processes. While PCA would be the terminology used for the discrete case, Karhunen-Loève would be the analogue for the continuous case.

$$\arg\min_d -2\,\mathrm{tr}(M^tMdd^t) + \mathrm{tr}(M^tMdd^tdd^t) = \arg\min_d -2\,\mathrm{tr}(M^tMdd^t) + \mathrm{tr}(M^tMdd^t) =$$

$$= \arg\min_d -\mathrm{tr}(M^tMdd^t) = \arg\max_d \mathrm{tr}(M^tMdd^t) = \arg\max_d \mathrm{tr}(d^tM^tMd)$$

and the optimization problem[6] is solved using the eigenvalue decomposition of the matrix M^tM, the optimal vector being the eigenvector associated to the largest eigenvalue. The rest of the principal components are found in an analogous way on the result of having subtracted those components already found. Therefore, the final decomposition of the matrix into principal components is $T = MV$.

Observation.

It is worth noting two salient facts that may have been overlooked in the above reasoning:

- *The matrix M^tM corresponds to the **covariance matrix** of the considered dataset, so at the end we are obtaining the aforementioned relationship between the different components (either those of all the scanned faces or those of the different regions that make up a face).*
- *While the optimization problem starts as an attempt to **minimize the distance** between the original data and the data obtained after going through the encoding and decoding process, by the time it changes to a maximization problem the objective becomes to **maximize the variance** between the two.*

We can give an alternative formulation of this principal component decomposition by simply applying the singular value factorization of M that we have previously presented:

$$T = MV = U\Sigma V^tV = U\Sigma$$

6.3.3 Eigenfaces

The eigenfaces approach was first introduced in [47], although it took a couple of years for Turk and Pentland to formalize it in [53]. In it, the generated autofaces are used to create a "base"[7] of what is known as "face space" from which to identify and even generate faces. One of the necessary conditions for applying this technique is that the images used must have been taken in almost identical conditions, both in terms of lighting and shadows (location of cameras and spotlights), as well as the location of the different parts of the face (nose, eyes, mouth, etc.). It should also be noted that this methodology can

[6] In the absence of the condition $d^td = 1$, the above optimization problem would be formulated in terms of what is known as the **Rayleigh quotient**; $\frac{\mathrm{tr}(d^tM^tMd)}{\mathrm{tr}(d^td)}$.

[7] Although the term "base" is used in the literature, the more accurate terminology would be "span", as more elements are taken to form it than the dimension of the space due to the fact that possible errors (human or mechanical) may have arisen during the initial data collection and must be prevented.

be extrapolated to other Computer Vision problems such as the recognition of written characters or lip-reading, which is why the terminology eigenimage is also used sometimes.

To generate the eigenfaces base on this eigenfaces space, it is necessary to follow the following procedure:

1. **Obtain the set of training images**, storing all of them in a matrix M whose columns are the different images (represented as pixels) that make up the total dataset.

2. **Calculate and subtract the average image** A from the total M in order to work with a normalized dataset[8].

3. **Calculate the eigenvalues and eigenvectors of the covariance matrix.** Each of the eigenvectors has the same dimension as the original images, so they can also be viewed as images: the **eigenfaces**. In addition, their associated eigenvalues indicate how much each varies from the average image calculated above.

4. **Choose the k principal components.** A threshold ϵ is set on the total variance $\sum_{i=1}^{n} s_i^2$ to delimit the exact number of principal components to consider, as the large amount of training data results in an exorbitant number of principal components. k is the smallest integer that satisfies $\frac{\sum_{i=1}^{k} s_i^2}{\sum_{i=1}^{n} s_i^2} > \epsilon$.

The eigenvalues and eigenvectors are obtained from the methods presented throughout this section. As an example, Figure 6.3 shows the result of decomposing the image of a face into principal components to obtain the representation of the face as an eigenface.

Figure 6.3: Image of a face (left) and its representation as an eigenface (right). **Source**: [53]

[8]This will ensure that a set of independent variables is obtained, as the correlation matrix to be obtained shows that they are uncorrelated (being diagonal) and follow a multivariate normal distribution. For more details, see [8].

6.3.4 LDA

Using PCA we obtain an eigenfaces span that would allow us to express any other face as a linear combination of the principal components obtained. Applying an approach such as the one used in Machine Learning, we can consider these principal components as groups in which to agglutinate the various data we have, which is known as a **clustering** problem. However, the format of the training data used (images represented as pixels in a single matrix) means that there is usually a greater amount of information per element (pixels per image) than the training data itself (number of images considered), which means that the final system obtained does not best represent the whole of the data, since with PCA the aim is to find components that maximize the variance with respect to the original data (**least squares**).

To solve this problem, it is common to use **Linear Discriminant Analysis** (LDA), also known as **Normal Discriminant Analysis** (NDA) or **Discriminant Function Analysis** (DFA)[9]. It is a method for classifying elements into groups or classes, the prerequisite being that the number of elements is known beforehand[10]. The underlying idea behind LDA is to maximize the distance between the groups or **clusters** created, while minimizing the variance between the elements of each class.

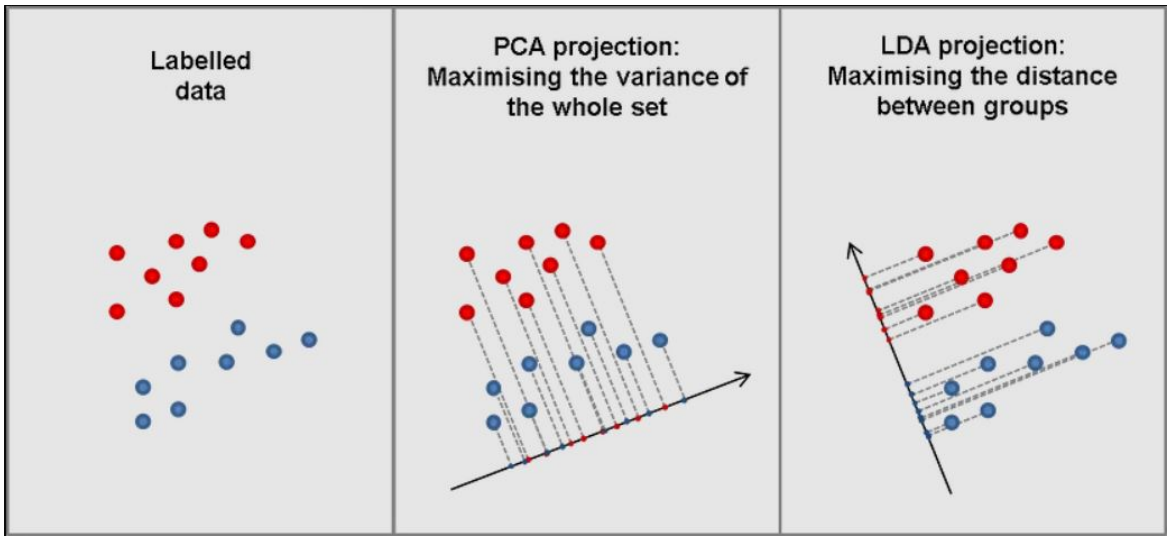

Figure 6.4: PCA vs LDA. **Source:** [37]

[9]Linear discriminant function methods allow the classification of data into classes by creating hyperplanes. Another common example of this type of method, whose application is widespread in Machine Learning, are **Support Vector Machines** (SVM).

[10]The simplest case is where there are only two classes and is known as **Fisher's linear discriminant**. In fact, this nomenclature is often used as a synonym for LDA, although the two terms are not entirely synonymous.

Let us see what is the formulation of the classification problem presented by LDA, whose details can be seen in [38] and [46]. Let S denote the total set of images, which we want to separate into q different classes $C_1, ..., C_q$, where we denote by l_i the number of points belonging to the class l_i and by $l = \sum_i l_i$ the total of these. The centroids of each class C_i are denoted by μ_i, where μ is that of the total training data set:

$$\mu_i = \frac{1}{l_i} \sum_{x_j \in C_i} x_j, \qquad \mu = \frac{1}{l} \sum_{x_j \in S} x_j.$$

Let A_i be the matrix associated to the class C_i whose columns consist of the normalized data of each image:

$$A_i = [x_1 - \mu_i, ..., x_{l_i} - \mu_i], \qquad x_i \in C_i.$$

Thus,

$$\frac{1}{l_i} A_i^t A_i$$

is the covariance matrix associated to the class C_i. We then define the **intra-class variance matrix** S_w (where "w" comes from the term "within") as the sum of these matrices:

$$S_w = \sum_i^q \frac{1}{l_i} A_i^t A_i.$$

Based on the underlying idea behind LDA, the aim is to **minimize** $d^t S_w d$, analogous to what had been done in PCA.

In addition, we also want to maximise the variance between the different classes, so we define the normalized centroid matrix $B = [\mu_1 - \mu, ..., \mu_q - \mu]$, which allows us to describe the **matrix of between-class variances** S_b (where "b" comes from the term "between") as:

$$S_b = \frac{1}{q} B^t B.$$

Thus, we want to maximize $d^t S_b d$. Both conditions can be unified in one as a Rayleigh quotient:

$$\max_d J(d) = \frac{d^t S_b d}{d^t S_w d}$$

whose necessary condition of optimality is:

$$\frac{\partial J}{\partial d} = \frac{S_b d(d^t S_w d) - S_w d(d^t S_b d)}{(d^t S_w d)^2} = 0$$

from which we obtain the generalised eigensystem:

$$S_b d = J(d) S_w d$$

where d is the largest absolute eigenvector of $S_w^{-1}S_b$ (assuming that S_w is invertible), analogously to what happened in PCA. As we mentioned at the beginning of this section, the number of training images is usually much smaller than the number of pixels contained in each image, so S_w may be singular and therefore not invertible, although it would be sufficient to take its pseudoinverse.

Another difficulty is the high number of training images and features to be found. To solve this problem, dimensionality reduction techniques (both PCA and LDA) are applied to obtain the optimal V matrix:

$$V = V_{FLD}^t V_{PCA}^t$$

where

$$V_{PCA} = \arg\max_V |V^t M^t M V|, \quad V_{LDA} = \arg\max_V \frac{|V^t V_{PCA}^t S_b V_{PCA} V|}{|V^t V_{PCA}^t S_w V_{PCA} V|}.$$

Thus, LDA is used to reduce the number of features to a more manageable number prior to performing classification tasks. Each of these new dimensions is a linear combination of pixel values, resulting in a span of the face space. This methodology is analogous to that of eigenfaces, only in this case the nomenclature used is **fisherfaces**.

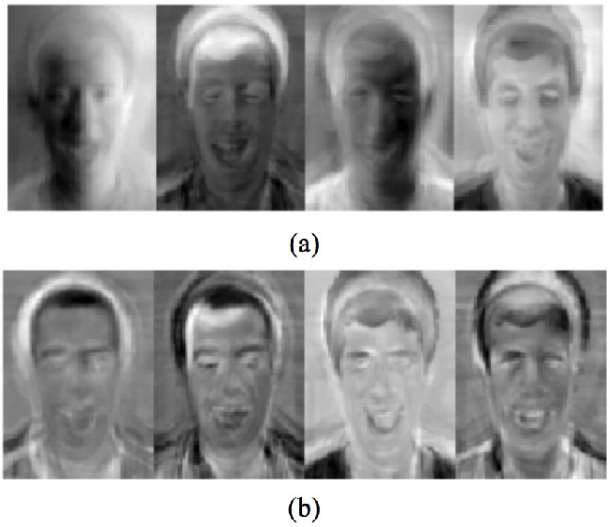

Figure 6.5: Eigenfaces (a) vs fisherfaces (b). **Sourcce**: [52]

As discussed in [38], fisherfaces usually give better results than eigenfaces. Primarily, this is because it is a robust approach with respect to variations in the illumination conditions or location of the training image set considered. This can be seen in Figure 6.5, where we see that eigenfaces have captured variations caused by illumination and/or head pose change; whereas fisherfaces reduce those variations not related to facial images. However, several studies show that, for a small sample of data, PCA performs better and is even less sensitive to different training datasets.

6.3.5 Implementation

Once the theoretical concepts have been presented, we will give a practical implementation of the eigenfaces method in Python. To carry out this development, [32] and [42] have been used as a guide. The final result can be downloaded and tested following the steps indicated in the Annex A.1.

The face images used are the so-called **Olivetti dataset** (Figure 6.6), which was obtained between April 1992 and April 1994 at AT&T Cambridge laboratories. In it, there are 10 different images of 40 different people, which have been taken under various conditions of lighting, facial expression and details such as the absence or not of glasses. However, all images were taken against a dark, homogeneous background, with the participants in an upright and frontal position (with tolerance for some lateral movement). It is necessary to separate this data into a test data set and a training data set, so that we are able to test the effectiveness of the model created.

Figure 6.6: A sample of the first 25 images from the Olivetti dataset.

After obtaining the principal components of these faces, we can visualize some of them (Figure 6.7). For this purpose, we have selected 106 data to obtain a p-value of 0.05 to obtain a final recognition accuracy of at least 95%. The resulting data have lower dimensionality and allow us to train the model for face classification to facilitate the identification of human faces.

After training the model, it is necessary to evaluate its performance to check the effectiveness of the model. To do this, the test dataset is used and various metrics are extracted from the results obtained, which are calculated according to whether or not the classification task has been performed correctly:

- **True Positive** (**TP**): Correctly predicted values (correct prediction).
- **False Positive** (**FP**): Incorrectly predicted values (incorrect prediction).
- **True Negative** (**TN**): Correctly rejected values (correct prediction).
- **False Negative** (**FN**): Incorrectly rejected values (incorrect prediction).

Figure 6.7: The first 25 eigenfaces obtained, ordered from highest to lowest variance

Although these values are particularly intuitive in the binary case, for the situation where there are n-classes it is sufficient to perform this analysis on a class-by-class basis. These results can be summarised using the technique known as the **confusion matrix**, which provides information on the hits and misses of the classification model, as well as the type of errors it makes. However, for our case, we will not use this technique, as we would obtain a matrix of size 40, which would not provide any advantage for the visualization in effective terms. In these cases, it is preferable to apply the dimensionality reduction techniques described above (extending SVD or PCA, for example), or to resort to the available metrics to assess the validity of the model obtained:

- **Accuracy**. Frequency with which the evaluated method makes the correct prediction. It is calculated as the sum of the true predictions divided by the total number of predictions.
$$\text{Accuracy} = \frac{TP + TN}{TP + TN + FP + FN}$$

- **Precision**. It represents the accuracy of the method. It is calculated as the proportion of cases that were predicted to be positive and were actually positive, divided by the total number of cases that were predicted to be positive.
$$\text{Precision} = \frac{TP}{TP + FP}$$

- **Recall**. Fraction of positive cases that were predicted to be positive.
$$\text{Recall} = \frac{TP}{TP + FN}$$

- **F-score**. A metric that combines recall and precision to determine the accuracy of the test. For n-class problems, this score is usually found for each class. It is calculated as:
$$\text{F-score} = 2 \cdot \frac{\text{precision} \cdot \text{recall}}{\text{precision} + \text{recall}}$$

- **Support**. Number of observations that are predicted in a given class.

If we look at the final results, we see that we have obtained an accuracy of 93%, so the generated model is able to detect these faces under these conditions with a high certainty. These results are not entirely consistent with the likelihood ratio obtained, as the accuracy is slightly lower than 95%. This is because the dataset is not particularly large, so when splitting the data into training and test sets there may be occasions when there is not enough data on a face to adequately train the model. To overcome this, we included the option **stratify**, which attempts to preserve the layout of the data when splitting the data (ensuring sufficient images of each face), but with only 10 images of each person it is not possible to make predictions with any greater accuracy. After running the program several times, the only thing that can be guaranteed is an accuracy of more than 90%.

Chapter 7

Conclusions and future work

7.1 Conclusions

In this report we have collected the theoretical concepts behind the techniques used for face modelling and recognition. Starting with the top-down strategies for modelling the human face from an appearance-based approach, we present the formal language of manifolds to build a final model described by the union of smooth submanifolds with curvature of constant sign. The analysis and evolution of such a model was performed in terms of curvature maps for the identification and separation into regions, allowing their characterization and reconstruction.

After performing the static modelling in terms of curvature maps, the terminology of flows has been presented both for the simplification of the features of the face and for controlling the deformations produced in the face during the performance of gestures. In the first case, in addition to considering the flows associated with the mean and total curvatures (as invariants of the differentiable structure at each point), we have characterised the notion of "good flow", looking at examples such as the maximal principal curvature flow, which allows us to simplify singularities such as the pair of umbilical points that occurs in the nose.

For gesture modelling, a strategy closer to Kinematics is adopted, where energy functionals play a fundamental role. In particular, the characterisation of sphericity through the Willmore energy flow is a very useful technique in combination with Variational Analysis and Conformal Geometry methods; although the use of other geometric flows to complement the information obtained should not be ruled out.

Finally, a brief introduction has been made to the bottom-up strategies, indicating the main methods for data capture and face recognition. The latter can be done simply and efficiently using methods such as eigenfaces or fisherfaces, which we have already seen can be implemented effectively. However, these techniques also have limitations such as the need for a large set of labelled data for training Machine Learning models, as well as the restrictions of variability in illumination or orientation conditions.

7.2 Future work

Due to the inherent limitations of the scope of the project, as well as the wide variety of disciplines involved in face modelling and recognition, many topics and lines of work have only been presented superficially. Some of the topics that have only been sketched in this report and that could be susceptible to future developments are the following:

- Incorporate the underlying geometry of both muscles and skeleton into the appearance-based model, using strategies typical in Computer Graphics CSG (Constructive Solid Geometry).
- Relate the piecewise smooth and piecewise linear approaches (PS vs PL) taking as support a discretization of the models based on "significant facts" associated with the map of parabolic curves separating regions of positive and negative curvature.
- Incorporate the relationships between the top-down (model-based) and bottom-up (data-driven) strategies typical of Computer Vision.
- Perform a simulation of facial gestures using curvature maps and their relationships in terms of the Willmore energy functional.
- Relate discrete models based on point clouds (e.g. from scans) to PS-models using PL-intermediate structures (simplicial vs. cuboidal complexes).
- Relate PS-models, sectional curvatures associated with appearances (Chapter 3); with those coming from structured light on the face, projection of linear patterns given by parallel line beams (Chapter 6).
- Develop software tools for interactive gesture control, including representation of natural vs. exaggerated gestures, and remapping of masks without using control points (as in the Gollum character, e.g.).
- Remapping radiometric models (associated with the behaviour of light) on face geometry and gestural dynamics for special effects.
- Adapting quasi-static strategies based on curvature maps to the dynamic framework of real characters to facilitate non-verbal Human-Computer Interaction (HCI).
- Train and validate Artificial Intelligence models for facial gesture recognition, tracking and simulation.

Appendix A

Software resources

A.1 Eigenfaces

This section shows the necessary steps to emulate the development environment for face detection using the eigenfaces method, in order to be able to execute the final development of the same. The development has been carried out on a computer with Windows 10 as operating system although, for other systems, the steps to follow are practically equivalent except for slight modifications depending on the operating system used.

1. **Install the Anaconda development platform**. To do this, simply download and run the installer provided in [4], keeping the default options it offers. **Anaconda** is a free and open source distribution of the Python and R programming languages, used for data science and Machine Learning. It provides a complete, ready-to-use environment that includes a large number of packages, libraries and tools that are commonly used in the field of data science, as well as an intuitive interface that makes it easy to use.

2. **Download all the packages and libraries required by the various notebooks**. Once the previous step has been completed, all you have to do is look for *Anaconda Prompt* among the available programs and run it. On opening it, a command console will appear from which the different modules downloaded to the system can be modified. The download of new packages is carried out by means of the command

   pip install <package_name>

   The following list shows all the commands needed to perform the download, so just copy and execute them one by one.

```
$ pip install numpy
$ pip install pandas
$ pip install matplotlib
$ pip install sklearn
```

3. **Open the interface that gives access to the notebook**. Access to the development notebooks can be done in a simple way by searching for the programme *Jupyter Notebook*. When running it, a browser must be selected on which the documents can be viewed (Google Chrome was used as the default option during development). Once this choice has been made, simply go to the location where the project is stored, which can be downloaded at the following Github page, and run the notebook. In fact, because the results of the last run are retained, it can be consulted as it is. In case you want to test it on the machine itself, the execution of each of the cells can be done thanks to the button *Run* (Figure A.1).

Figure A.1: Header of a file executed by Jupyter Notebook

Bibliography

[1] R. Abraham, J.E. Marsden, and T. Ratiu. *Manifolds, tensor analysis, and applications; Second edition*. Springer-Verlag, 1988.

[2] Jose Antonio Lorencio Abril. "Superficies de Willmore en el espacio euclídeo". TFG. Universidad de Murcia, 2022.

[3] Juan Gutiérrez Aguado. "Contornos activos: Bases teóricas, representación y minimización". TFG. Universitat de Valencia, 1999.

[4] *Anaconda Distribution: Free Download*. Anaconda. Accedido el 24/10/2023. URL: https://www.anaconda.com/download.

[5] V. I. Arnold, S. M. Gusein-Zade, and A. N. Varchenko. *Singularities of Differentiable Maps*. Vol. 1. Birkhäuser, 1985.

[6] Vladimir I. Arnold. *Catastrophe Theory*. Springer-Verlag, 1992.

[7] Thomas F. Banchoff. *Meusnier's Theorem*. Brown University, Accedido el 15/9/2023. URL: https://www.math.brown.edu/tbanchof/balt/ma106/lab8.html?dtext86.html.

[8] Patrick Billingsley. *Probability and Measure; Third Edition*. WI, 1995.

[9] Luis Llamas Binaburo. "Estimación online del flujo óptico a partir de una secuencia de vídeo". TFG. Universidad de Zaragoza, 2013.

[10] Nicolas Bourbaki. *Algebra I*. Elements of Mathematics. Springer-Verlag, 1989.

[11] J. W. Bruce and P. J. Giblin. *Curves and Singularities: A Geometrical Introduction to Singularity Theory*. 2nd ed. Cambridge University Press, 1992.

[12] J. W. Bruce, P. J. Giblin, and F. Tari. "Parabolic Curves of Evolving Surfaces". In: *Int. J. Comput. Vision* 17.3 (1996), 291–306. URL: https://doi.org/10.1007/BF00128235.

[13] J. W. Bruce, P. J. Giblin, and F. Tari. "Ridges, Crests and Sub-Parabolic Lines of Evolving Surfaces". In: *Int. J. Comput. Vision* 18.3 (1996), 195–210. URL: https://doi.org/10.1007/BF00123141.

[14] Theodor Bröcker and Klaus Jänich. *Introducción a la topología diferencial*. Editorial AC, 1977.

[15] Richard L. Burden, Douglas J. Faires, and Annete M. Burden. *Análisis numérico, 10ª edición*. CENGAGE Learning, 2016.

[16] Manfredo P. do Carmo. *Geometría diferencial de curvas y superficies*. Alianza Editorial, 1990.

[17] Yun Gang Chen, Yoshikazu Giga, and Shun'ichi Goto. "Uniqueness and existence of viscosity solutions of generalized mean curvature flow equations". In: *Journal of Differential Geometry* 33.3 (1991), pp. 749–786. URL: https://doi.org/10.4310/jdg/1214446564.

[18] Keenan Crane. *A Quick and Dirty Introduction to the Curvature of Surfaces*. Technische Universität Berlin, Accedido el 03/12/2023. URL: http://wordpress.discretization.de/geometryprocessingandapplicationsws19/a-quick-and-dirty-introduction-to-the-curvature-of-surfaces/.

[19] Franki Dillen and Leopold Verstraelen, eds. *Geometry and Topology of Submanifolds IV* (Conference on Differential Geometry and Vision). Katholieke Universiteit Leuven, Belgium. Leuven, Belgium: World Scientific, 1992, p. 296. DOI: 10.1142/1723.

[20] Fernando Manteca Fernández. "Generación de modelos 3D mediante luz estructurada". TFG. Universidad de Cantabria, 2018.

[21] *Fundamental Forms of a Surface*. Encyclopedia of Mathematics. Accedido el 23/11/2023. URL: http://encyclopediaofmath.org/index.php?title=Fundamental_forms_of_a_surface&oldid=47024.

[22] Christoph Garth. *Apuntes de la asignatura Computergrafik*. Technische Universität Kaiserslautern, 2022.

[23] Ian Goodfellow, Yoshua Bengio, and Aaron Courville. *Deep Learning*. http://www.deeplearningbook.org. MIT Press, 2016.

[24] Xianfeng David Gu and Shing-Tung Yau. *Computational conformal geometry (Advanced Lectures in Mathematics)*. International Press of Boston Inc, 2008.

[25] María de los Ángeles Hernández Cifre and José Antonio Pastor González. *Un curso de Geometría Diferencial*. Ediciones Doce Calles, S.L., 2010.

[26] David Hilbert and Stephan Cohn-Vossen. *Anschauliche Geometrie*. Grundlehren der mathematischen Wissenschaften. Springer Berlin, Heidelberg, 1932. DOI: 10.1007/978-3-662-36685-1.

[27] Ana Núñez Jiménez. *Apuntes de la asignatura Geometría de curvas y superficies*. Universidad de Valladolid, 2019.

[28] I. T. Jollife. *Principal Component Analysis, Second Edition*. Springer, 2002.

[29] Wilhelm Klingenberg. *A Course in Differential Geometry*. Graduate Texts in Mathematics. Springer New York, NY, 1978. DOI: 10.1007/978-1-4612-9923-3.

[30] John M. Lee. *Introduction to smooth manifolds*. Springer, 2013.

[31] Conglin Lu, Yan Cao, and David Mumford. "Surface Evolution under Curvature Flows". In: *Journal of Visual Communication and Image Representation* 13.1 (2002), pp. 65–81. URL: https://www.sciencedirect.com/science/article/pii/S1047320301904766.

[32] Hassan Id Mansour. *Face Recognition using Eigenfaces (Python)*. Medium. Accedido el 24/04/2023. URL: https://hassan-id-mansour.medium.com/face-recognition-using-eigenfaces-python-b857b2599ed0.

[33] Fernando C. Marques and André Neves. "Min-Max theory and the Willmore conjecture". In: *Annals of Mathematics (2)* 179.2 (2014), pp. 683–782.

[34] Fernando C. Marques and André Neves. "The Willmore conjecture". In: *Jahresbericht der Deutschen Mathematiker-Vereinigung* 116.4 (2014), pp. 201–222. DOI: 10.1365/s13291-014-0104-8.

[35] Jerrold E. Marsden and Tudor S. Ratiu. *Introduction to Mechanics and Symmetry. A Basic Exposition of Classical Mechanical Systems*. 2nd ed. Texts in Applied Mathematics. Springer New York, NY, 1999. DOI: 10.1007/978-0-387-21792-5.

[36] Hoda Mohammadzade, Amirhossein Sayyafan, and Benyamin Ghojogh. "Pixel-Level Alignment of Facial Images for High Accuracy Recognition Using Ensemble of Patches". In: *Journal of the Optical Society of America A* 35 (Feb. 2018). DOI: 10.1364/JOSAA.35.001149.

[37] Vivek Muraleedharan. *What is Linear Discriminant Analysis (LDA)*. Brown University, Accedido el 20/10/2023. URL: https://vivekmuraleedharan73.medium.com/what-is-linear-discriminant-analysis-lda-7e33ff59020a.

[38] Miloš Oravec. *Face Recognition*. IntechOpen, 2010.

[39] Roberto Pablo Pérez Palomares. "Optical Flow. Related Problems". PhD thesis. 2017. URL: http://hdl.handle.net/10803/403061.

[40] Robert Phillips. "Liouville's Theorem". In: *Pacific Journal of Mathematics* 28.2 (1969).

[41] Ian R. Porteous. *Geometric Differentiation*. Cambridge University Press, 2001.

[42] Dario Radečić. *Eigenfaces — Face Classification in Python*. Towards Data Science. Accedido el 24/04/2023. URL: https://towardsdatascience.com/eigenfaces-face-classification-in-python-7b8d2af3d3ea.

[43] Adrian Rosebrock. *OpenCV Eigenfaces for Face Recognition*. pyimagesearch. Accedido el 20/04/2023. URL: https://pyimagesearch.com/2021/05/10/opencv-eigenfaces-for-face-recognition/.

[44] Walter Rudin. *Análisis real y complejo*. McGraw-Hill, 1988.

[45] Eike Schling et al. "Design and Construction of Curved Support Structures with Repetitive Parameters". In: Sept. 2018.

[46] Amnon Shashua. *Introduction to Machine Learning*. The Hebrew University of Jerusalem, 2008.

[47] Lawrence Sirovich and M Kirby. "Low-Dimensional Procedure for the Characterization of Human Faces". In: *Journal of the Optical Society of America. A, Optics and image science* 4 (Apr. 1987), pp. 519–524.

[48] Mirjam Soeten. "Conformal maps and the theorem of Liouville". TFG. Rijksuniversiteit Groningen, 2011.

[49] Michael Spivak. *A comprehensive introduction to differential geometry*. Vol. 1. Publish or Perish, 1999.

[50] Michael Spivak. *A comprehensive introduction to differential geometry*. Vol. 2. Publish or Perish Inc, 1999.

[51] Alex Taylor. *Equivalent definitions of the tangent space*. URL: `https://art-math.github.io/files/tangentspace.pdf`.

[52] Ana Tsifouti. "Image usefulness of compressed surveillance footage with different scene contents". PhD thesis. May 2016. DOI: `10.13140/RG.2.1.2047.9609`.

[53] Matthew Turk and Alex Pentland. "Eigenfaces for Recognition". In: *Journal of Cognitive Neuroscience* (1991).

[54] Luis Alberto Tristán Vega. *Apuntes de la asignatura Análisis Matemático*. Universidad de Valladolid, 2019.

[55] Carlos Ruiz Vera. *Cartografía*. Universidad de Murcia, 2014.

[56] Thomas J. Willmore. "Note on Embedded Surfaces". In: *An. Sti. Univ. Al. I. Cuza Iasi Sect. I a Mat. (N.S.)* 11B (1965), pp. 493–496.

[57] Thomas J. Willmore. *Riemannian Geometry*. New York: Oxford University Press, 1996.